Biofuels and biochemicals from biomass
&
Carbon fiber reinforced composites

Dr Pulidindi

Email ID: pulidindi@sjtu.edu.cn

Research advisor: Professor Xinling Wang

Lecture dated 9th June 2020

SHANGHAI JIAO TONG UNIVERSITY

Renewable Energy Sources

Major problems: Energy insecurity, and environmental pollution
Challenge: Effective utilization of renewable resources

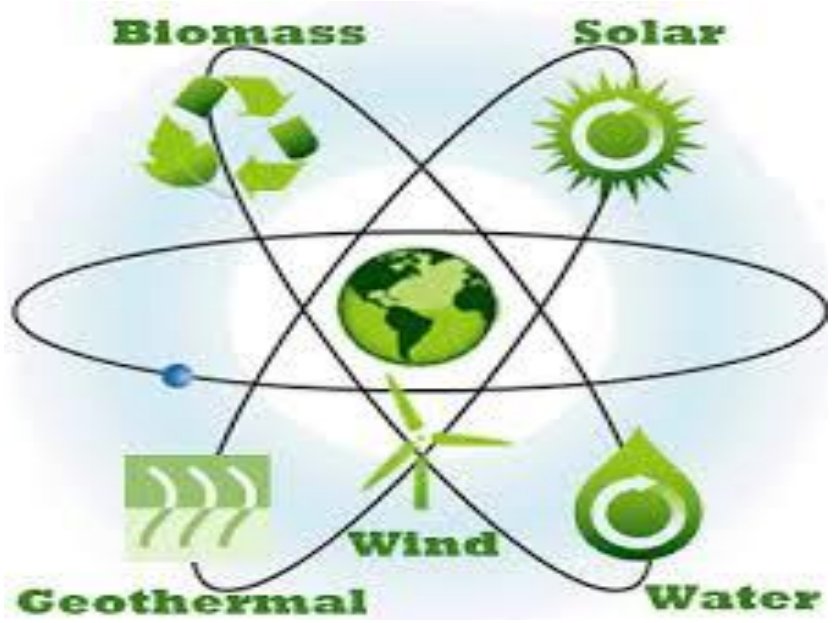

Alternate Energy Sources

Closed loop carbon cycle
Biofuels are carbon neutral

Paradigm shift - petroleum based to biomass based chemicals, fuels and materials production

Biomass – A Promising feedstock

- Terrestrial lignocellulose - major biomass source
- Marine and fresh water algae
- Animal remains (glycogen)
- CO_2

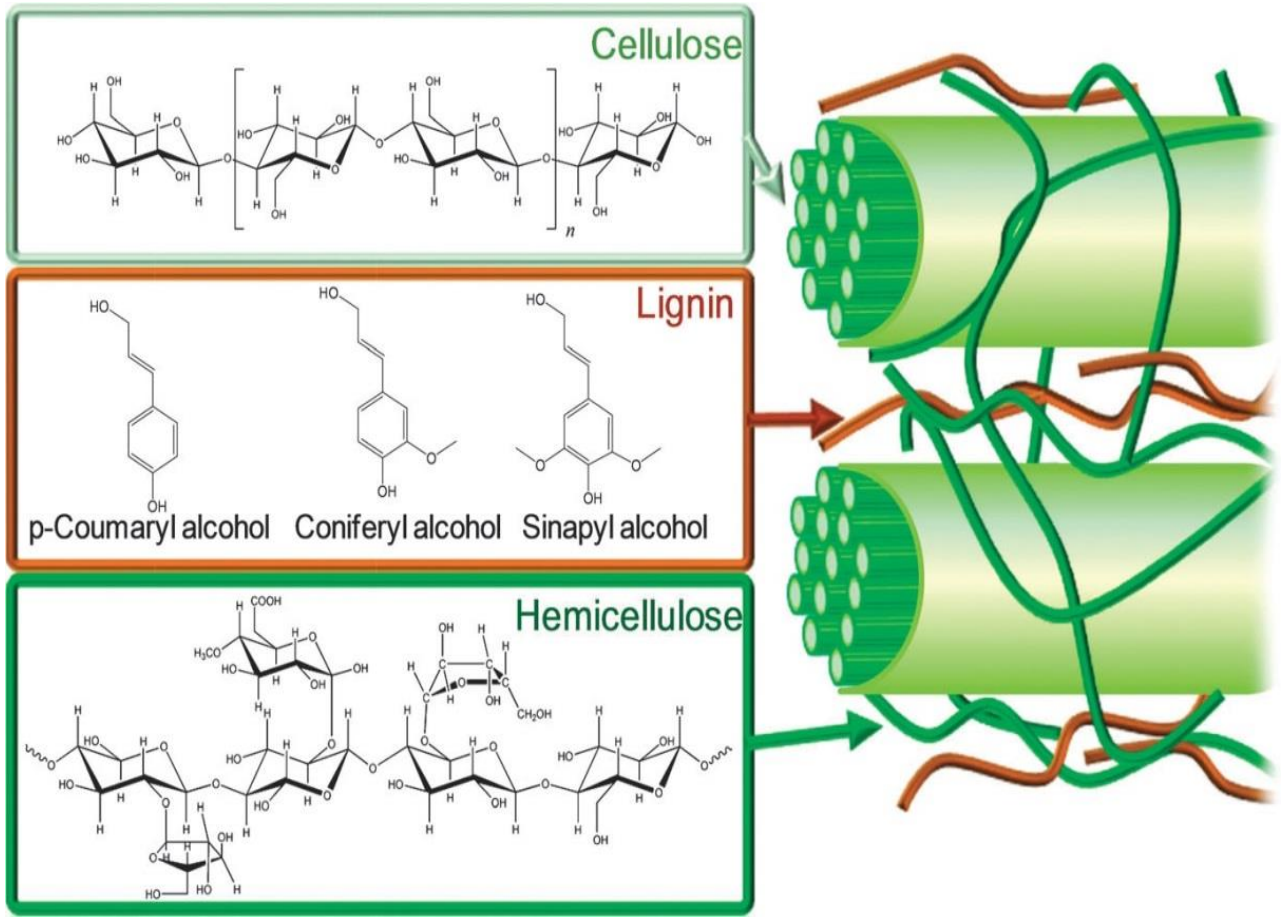

Structure

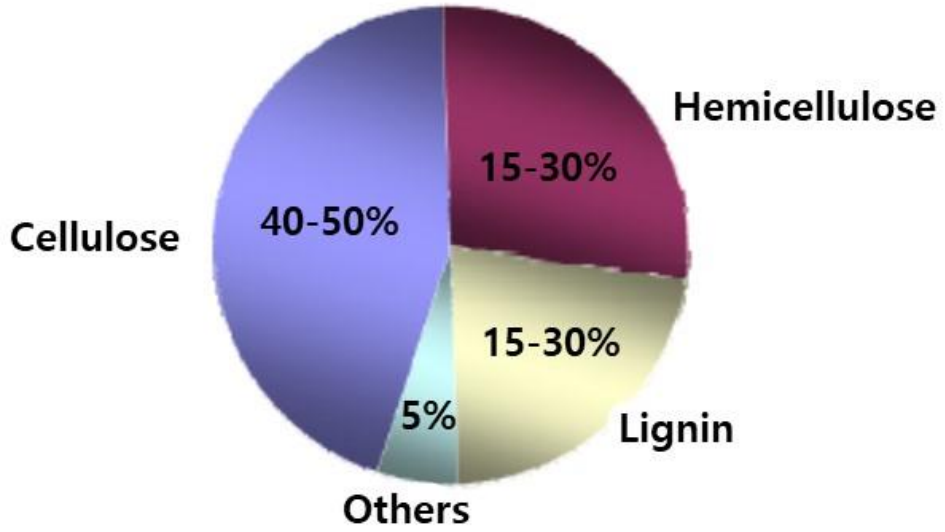

Composition

Biomass – Abundant
Renewable
Environmentally friendly
Biofuels - Compatible with existing fuel infrastructure

Concept of biorefinery

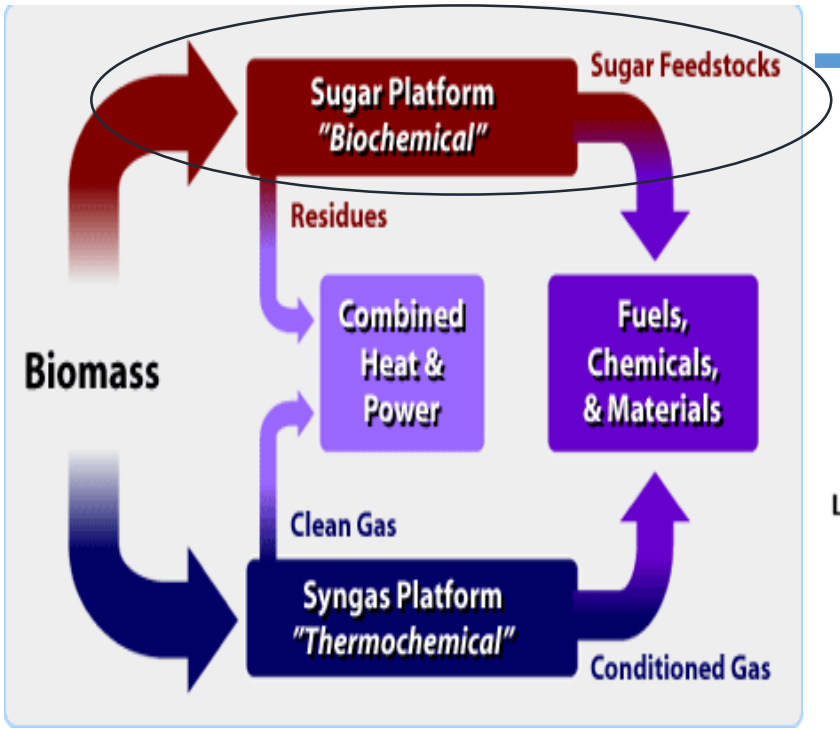

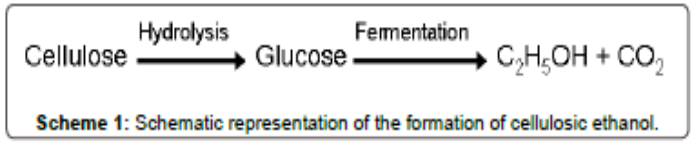

Scheme 1: Schematic representation of the formation of cellulosic ethanol.

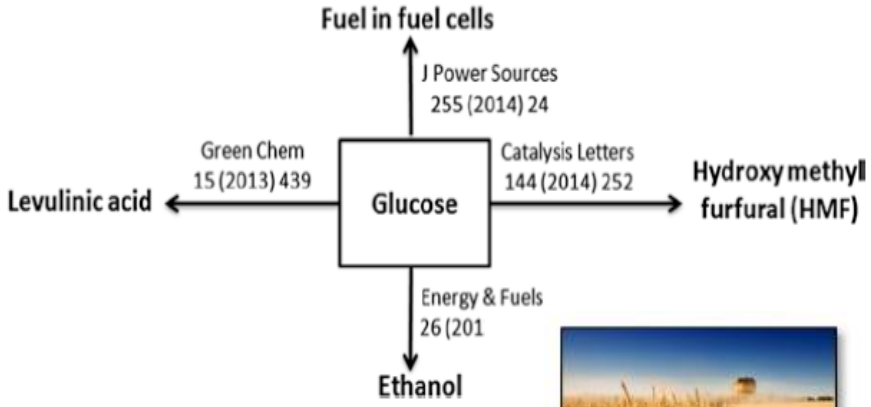

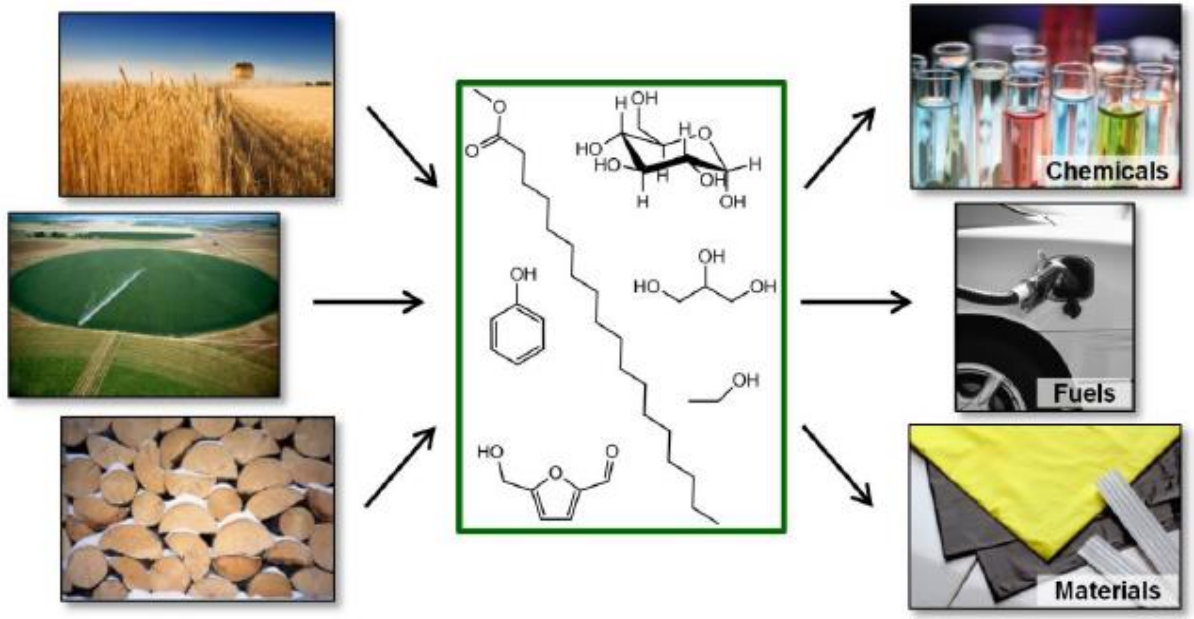

Sustainability of biorefinery

Productive use of cellulose, hemicellulose and lignin

Major biofuels - Bioethanol and Biodiesel

Bioethanol - promising substitute to conventional gasoline

Comparable energy density values

(Ethanol (24 MJ/L) Vs gasoline (34.3 MJ/L)

Bioethanol production from lignocellulosic biomass - several bottle necks

Focus:

Utilizing both the cellulose and hemicellulose for bioethanol

Lignin conversion to BTX chemical

Biodiesel production from non-edible feedstock

CO_2 and H_2 economy

Conversion of CO_2 to fuels and chemicals

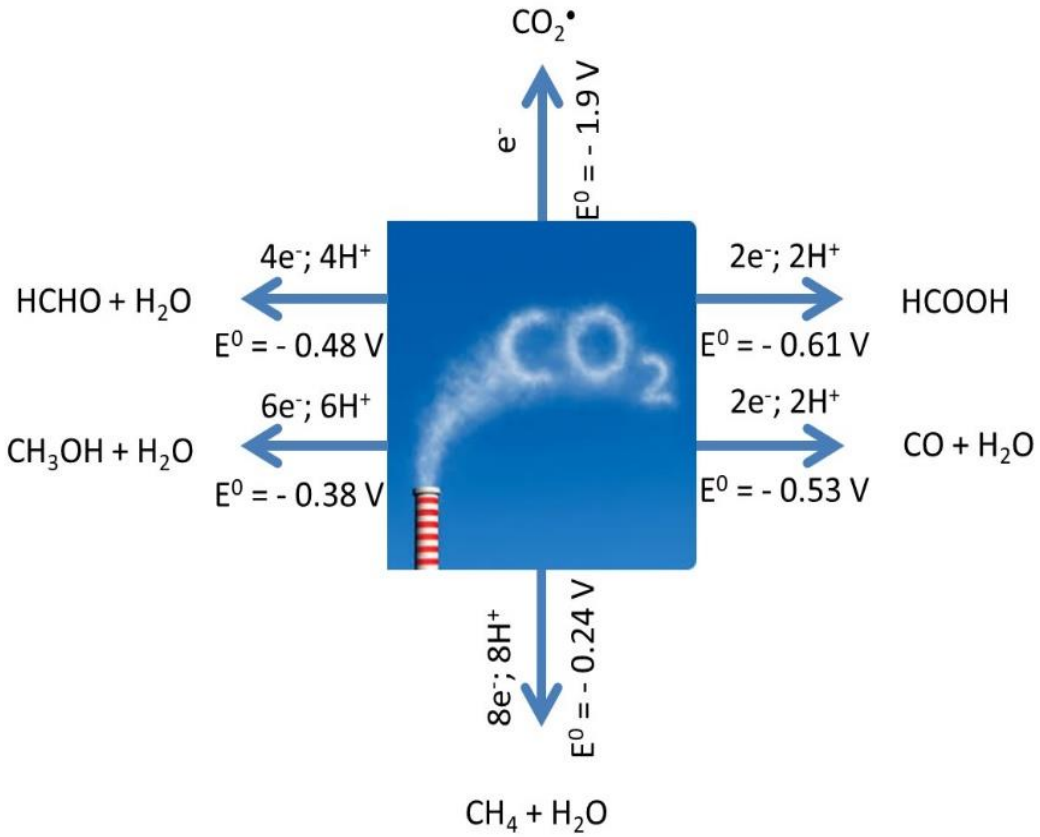

Known electrochemical pathways for the activaton and conversion of CO_2 to fuel precursors (CO, HCHO) and fuels (HCOOH, CH_3OH and CH_4).

$$CO_2 + H_2O + 2e^- \rightarrow HCOO^- + OH^-$$

$$CO_2 + H_2O + 2e^- \rightarrow CO + 2OH^-$$

$$CO_2 + 6H_2O + 8e^- \rightarrow CH_4 + 8OH^-$$

$$2CO_2 + 8H_2O + 12e^- \rightarrow C_2H_4 + 12OH^-$$

Electrochemical reduction of CO_2 to fuels on Cu electro catalysts

Reske et al.,, J. Am. Chem. Soc. 2014, 136, 6978−6986

Controlling the selectivity of electro reduction of CO_2 and reducing the over potential of the formation of methane and ethylene are major challenges towards the sustainability of the electro catalytic pathway for CO_2 conversion.

Can biofuels be carbon negative?

Selective and fast reduction of CO_2 to formate

$(NH_4)_2CO_3 + NaBH_4$ —(Microwave irradiation, 5 min; 90 °C)→ HCOONa ; 75 wt.% yield

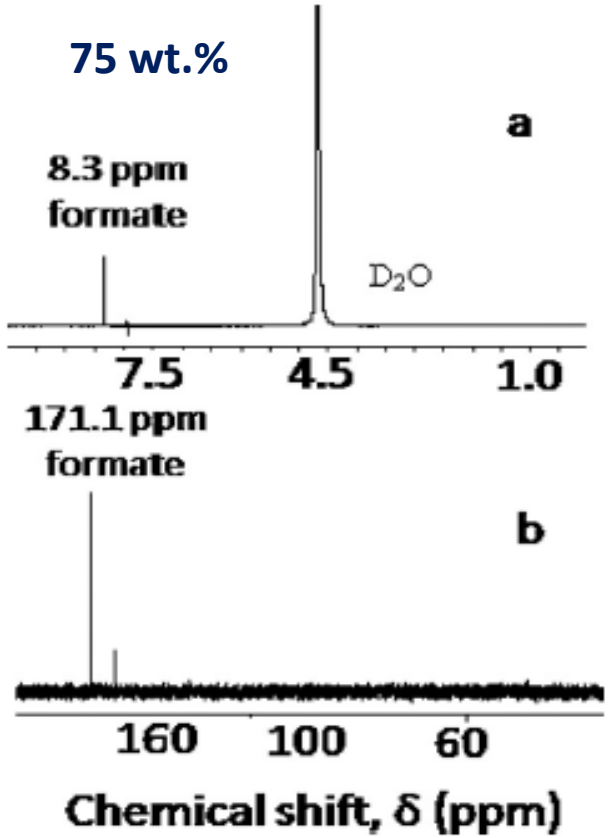

(a) ^1H and (b) ^{13}C NMR spectra of reduction product of CO_2 (from $(NH_4)_2CO_3$)

Gedanken et al., Journal of CO_2 Utilization, 7, 2014, 19

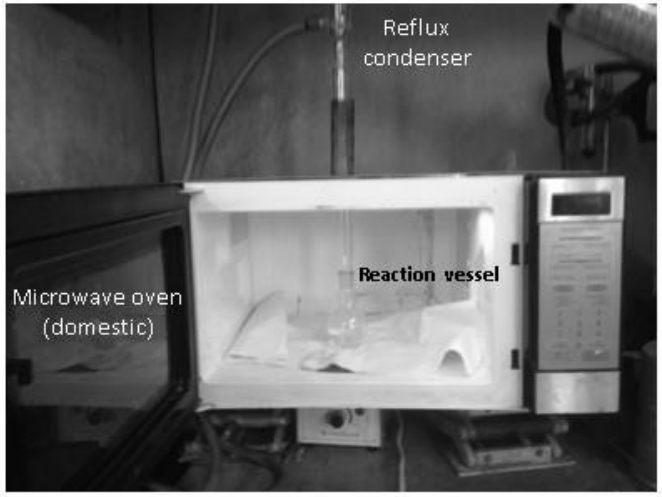

Experimental setup for the microwave assisted CO_2 reduction process

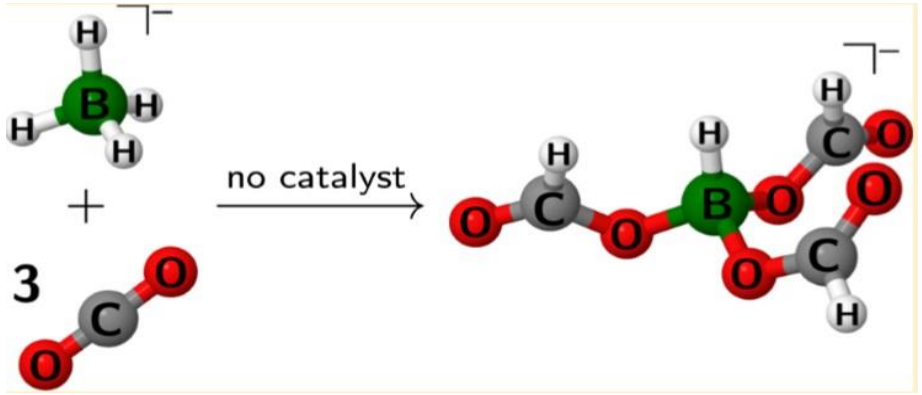

Uptake of 3 equivalents of CO_2 by $NaBH_4$ in the reduction of CO_2 to formate

$(OCHO)BPin \xleftarrow[\text{metal-catalyzed}]{HBPin} CO_2 \xrightarrow[\text{no catalyst}]{1/3\ NaBH_4} 1/3\ Na[HB(OCHO)_3]$

previous work — this work

Knopf and Cummins, Organometallics, 34(9), 2015, 1601-1603

Zhao et al., Fuel, 142, 2015, 1-8

Grice and Keith et al., Fuel, 150, 2015, 139-145

Heterogeneous Solid catalysts for CO_2 reduction are awaited!

Reducing agent, but not the catalyst, is key to success in CO_2 reduction

Focus to be shifted to hydrogen economy

Unconventional methods of activation of biomass for bioethanol production

Fermentation of carbohydrates to ethanol

Glucose fermentation to ethanol

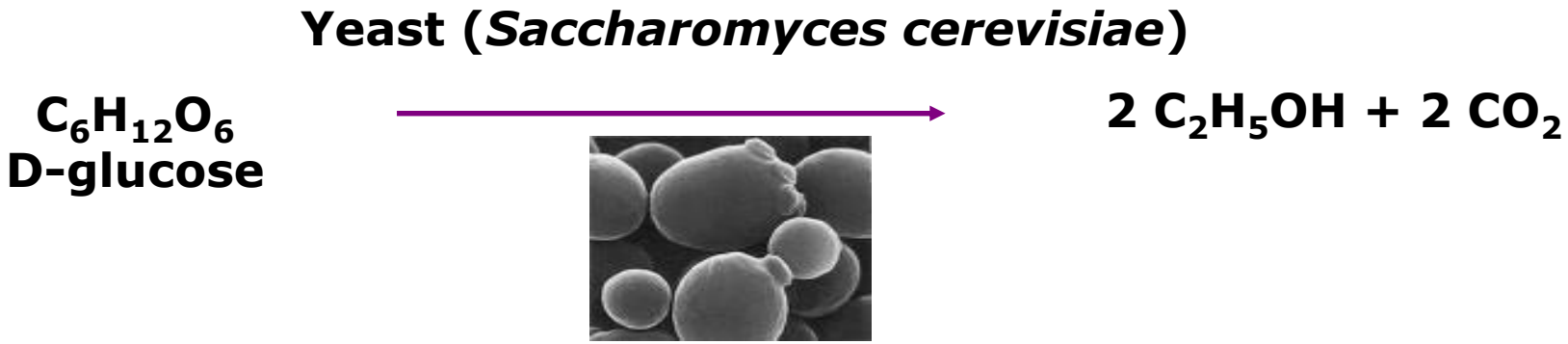

Theoretical yield of ethanol:
1 g glucose yields 0.51 g ethanol
1 g sucrose yields 0.54 g ethanol

Experimental ethanol yield is always lower than 50 wt.% because of the formation of glycerol as secondary metabolite

Yeast strain employed: Bakers yeast (Bravo brand)

How to make the fermentation faster?

Fermentation rate of glucose is accelerated using mild sonication (40 kHz)

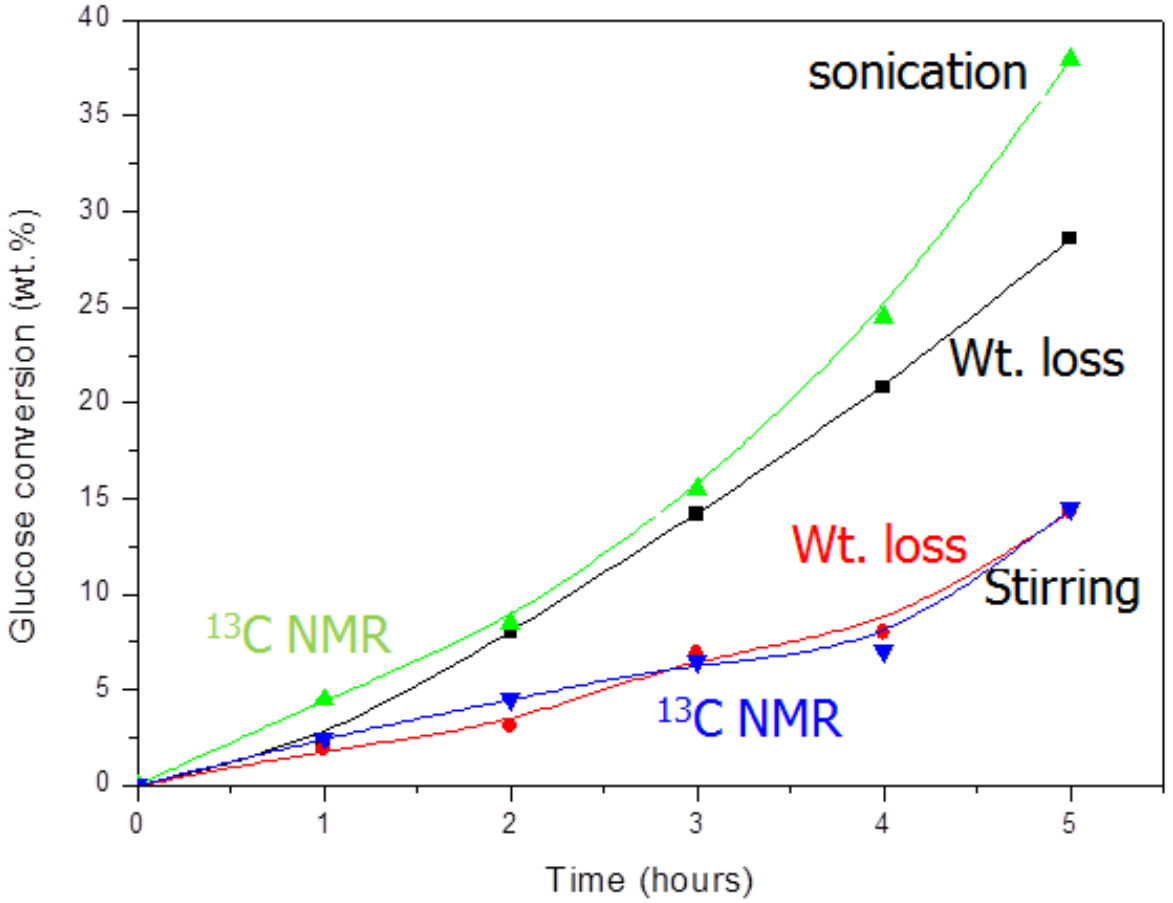

Kinetics from ^{13}C NMR and from wt. loss

- Glucose conc. - 20 wt.%
  Temp. - 30 °C
- sonication: 38 % conversion in 5 h
  stirring: only 14.5 % conversion in 5 h
- $k_{sonication} = 15.35 \times 10^{-6}$ sec^{-1}
  $k_{stirring} = 6.67 \times 10^{-6}$ sec^{-1}

Gedanken et al., Energy and Fuels, 26, 2012, 2352

Kinetics of glucose fermentation

$$C_6H_{12}O_6 \rightarrow 2C_2H_5OH + 2CO_2$$

conversion of glucose (wt %)

$$= (I_{E,16.8\ ppm}/2I_{G,95.8\ ppm}) \times 100$$

conversion of glucose (wt %)

= (observed decrease in weight

/total decrease in weight expected) × 100

$$k = (2.303/t)\log[a/(a - x)]$$

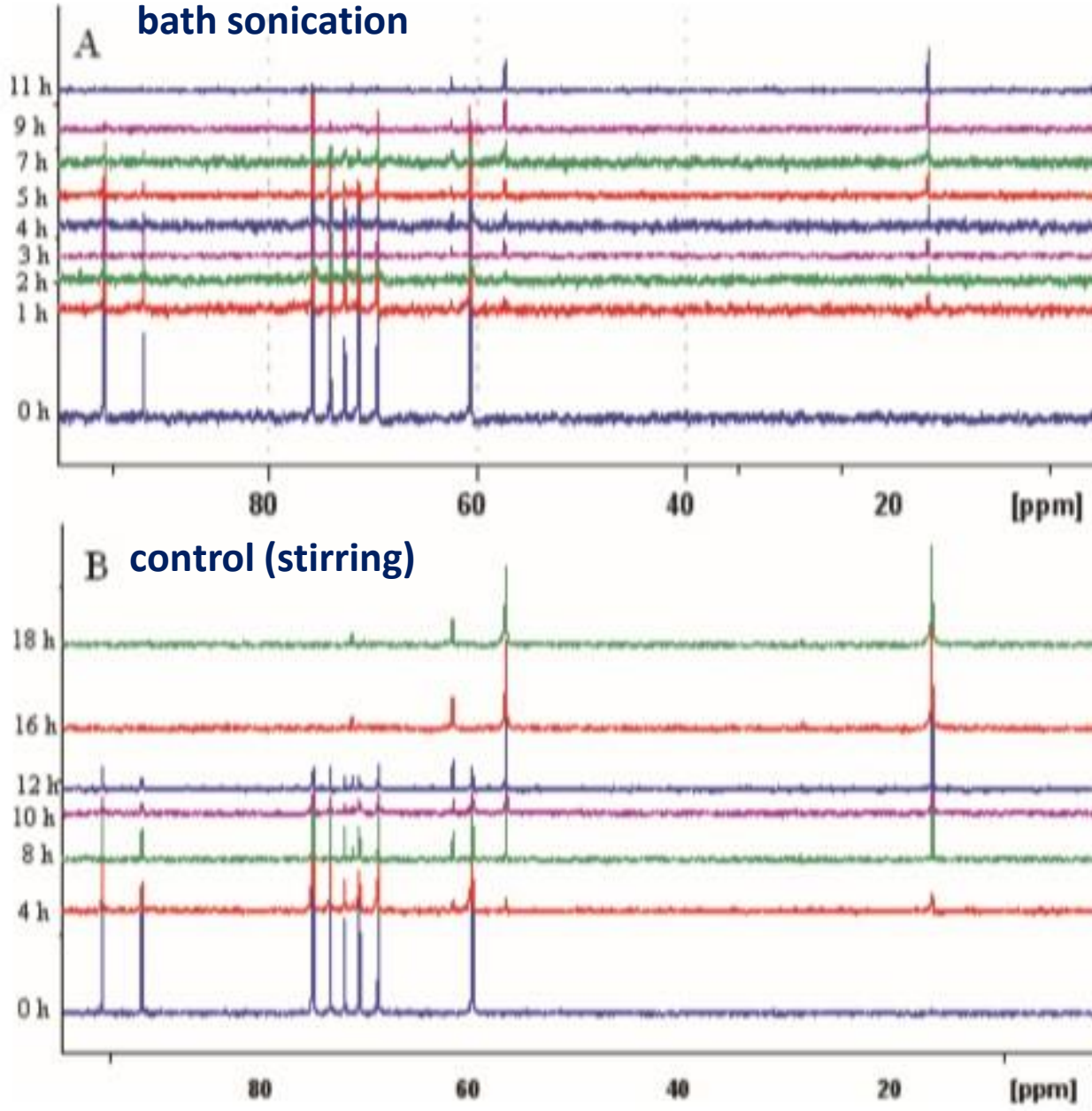

^{13}C NMR spectra of aliquots from the fermentation broth under (A) bath sonication and (B) control (stirring) conditions at 30 °C collected at regular time intervals.

Acceleration of fermentation with 40 wt.% glucose

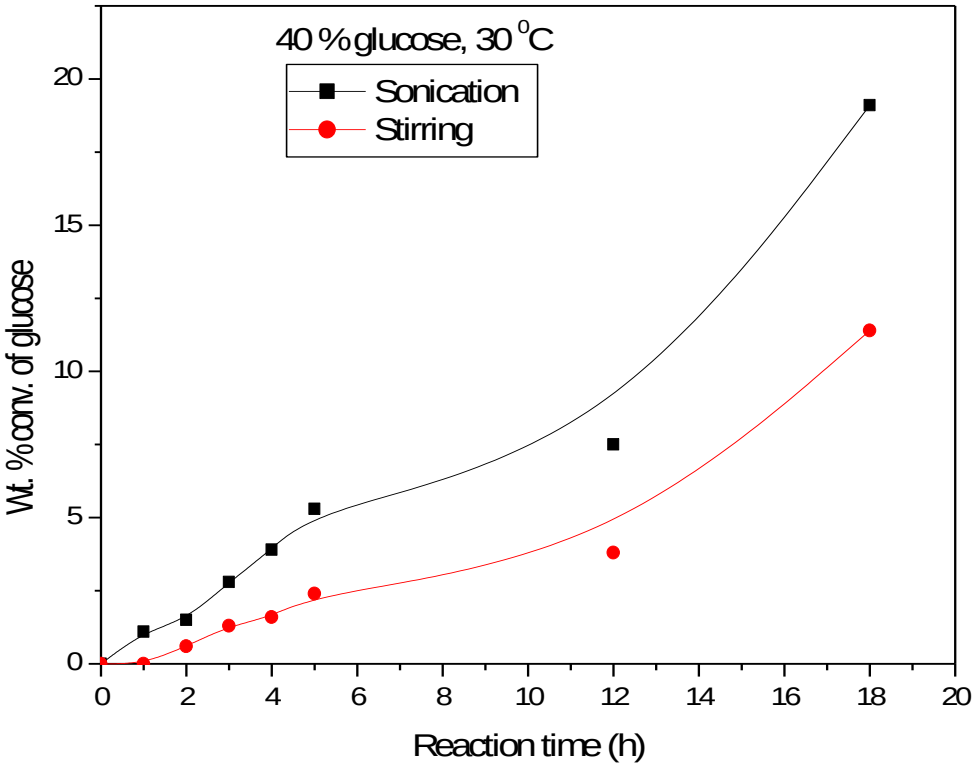

Glucose conversion with sonication Vs stirring

Sonication: 19 wt. % conversion in 18 h

Stirring: 11 wt. % conversion in 18 h

Yeast cells Stirring

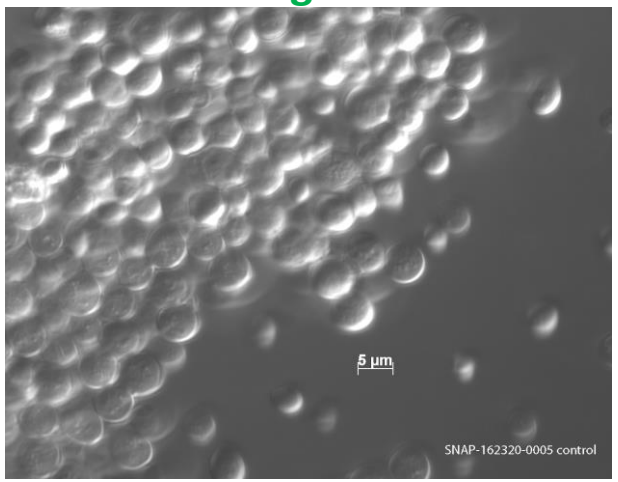

Yeast cells Sonication

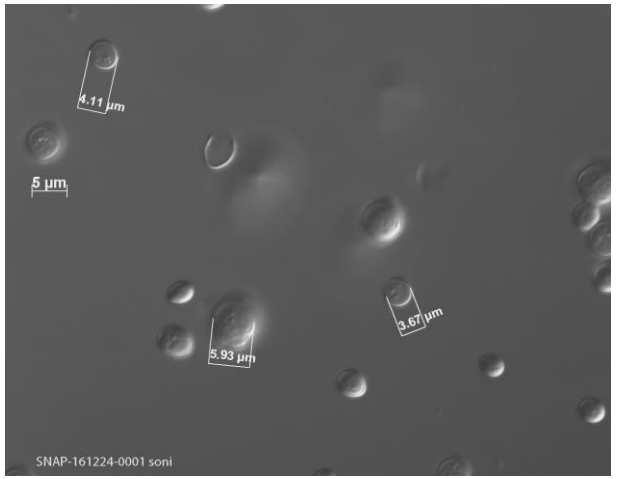

Sonication facilitated dispersion of yeast aggregates

Yeast is reusable even after sonication

What are the other avenues for improving bioethanol production process?

Production of bioethanol using *Pinus radiata* cones

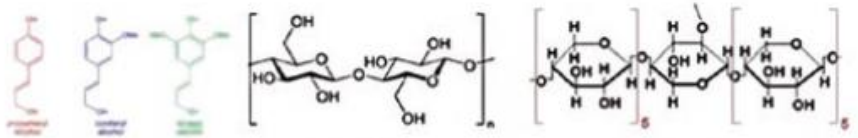

Biomass = Lignin + Cellulose + Hemicellulose

Delignification

Holocellulose (Cellulose + Hemicellulose)

Hydrolysis

Glucose + Xylose

Fermentation

Ethanol

Pinus radiata, 10 g

0.125 M NaOH, 100 mL, 70 °C, 1 h

delignification

Holocellulose
7.2 g

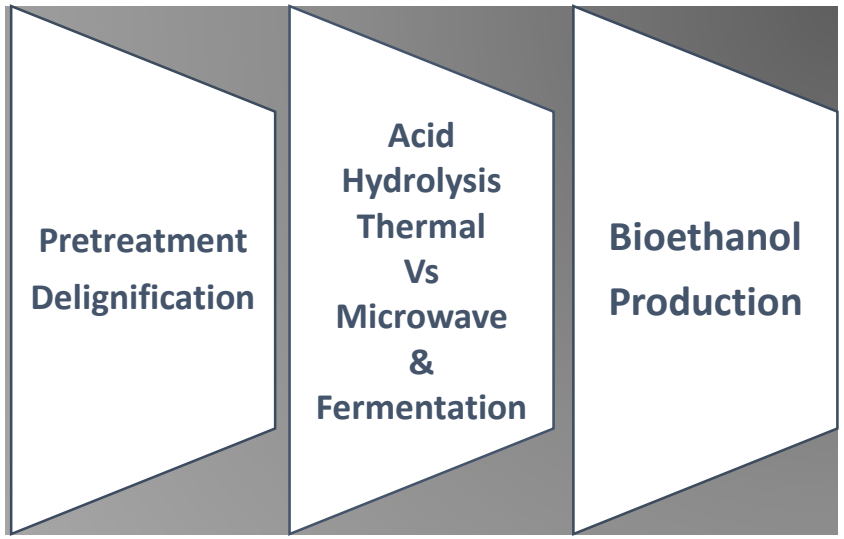

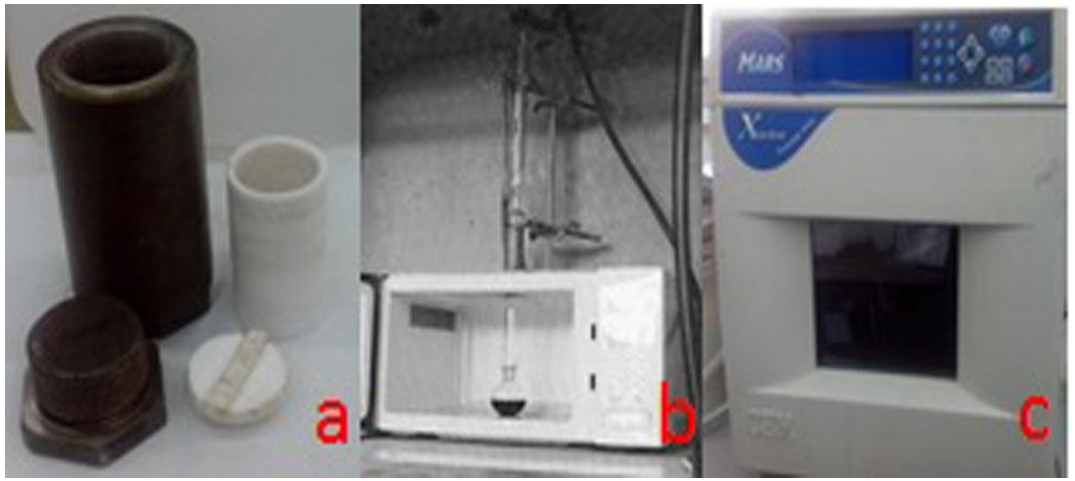

(a) teflon lined stainless steel autoclave
(b) modified domestic microwave oven
(c) commercial microwave oven, MARS, CEM

Qualitative analysis of sugars - ^{13}C NMR

Qualitative analysis of product ethanol - ^{1}H and ^{13}C NMR

Quantitative analysis of the fermentable sugars in the hydrolyzate and ethanol in the fermentation broth is carried out using HPLC analysis

Fermentation of glucose and xylose

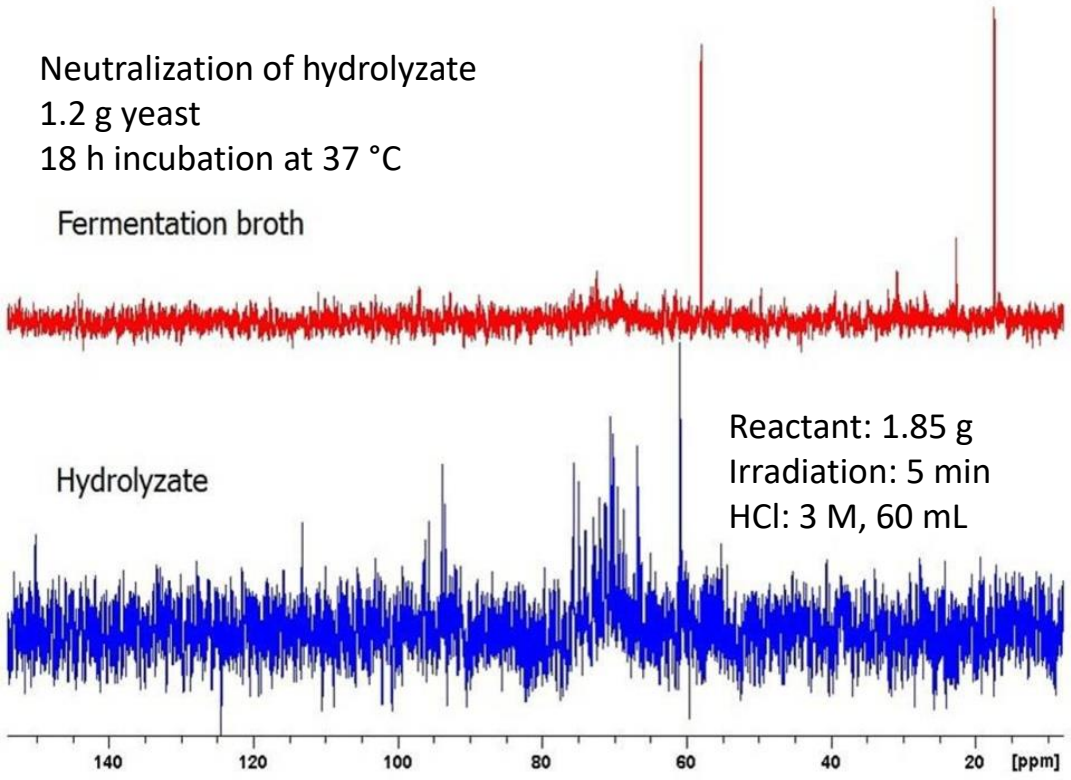

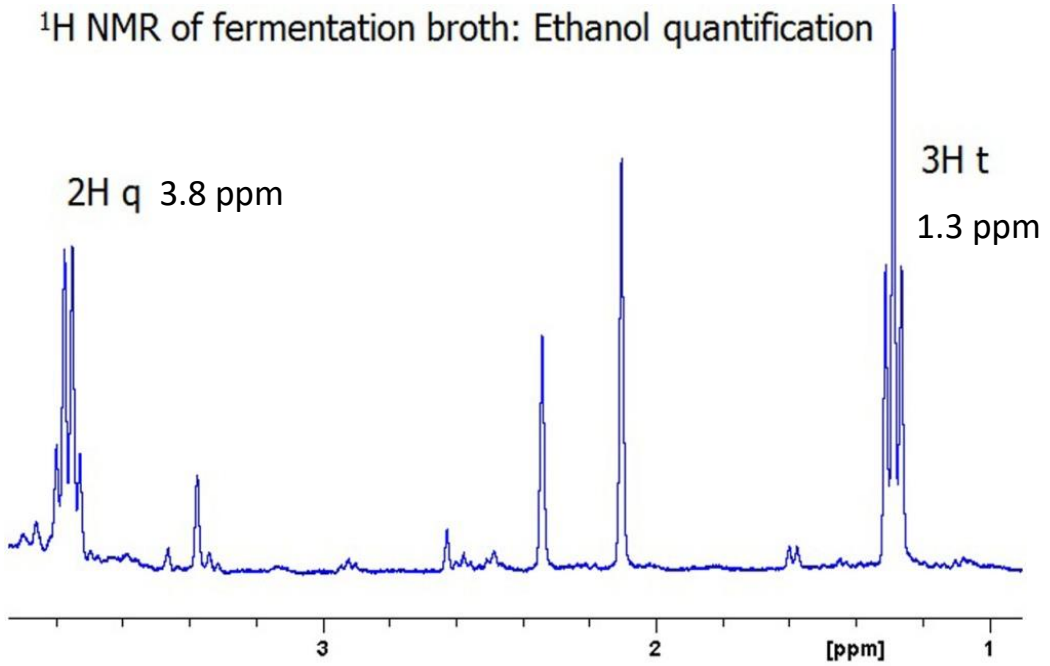

17.2 ppm -CH_3 of ethanol
58.0 ppm -CH_2O of ethanol

3H, t at 1.3 ppm -CH_3 of ethanol
2H, q at 3.8 ppm -CH_2O

Almost no trace of fermentable sugars after fermentation for 18 h
In addition to glucose, xylose was also metabolized by the Baker's yeast strain
^1H and ^{13}C NMR spectra confirm ethanol formation

Unique example of xylose metabolism by *Saccharomyces cerevisiae*

Compound	Hydrolyzate composition (mM)	Fermentation broth Composition (mM)
Xylose	27.8	0.62
Glucose	4.5	1.7
Ethanol	-	41.2

HPLC analysis of the aliquot from the pine cone hydrolyzate, and the fermentation broth at 18th h

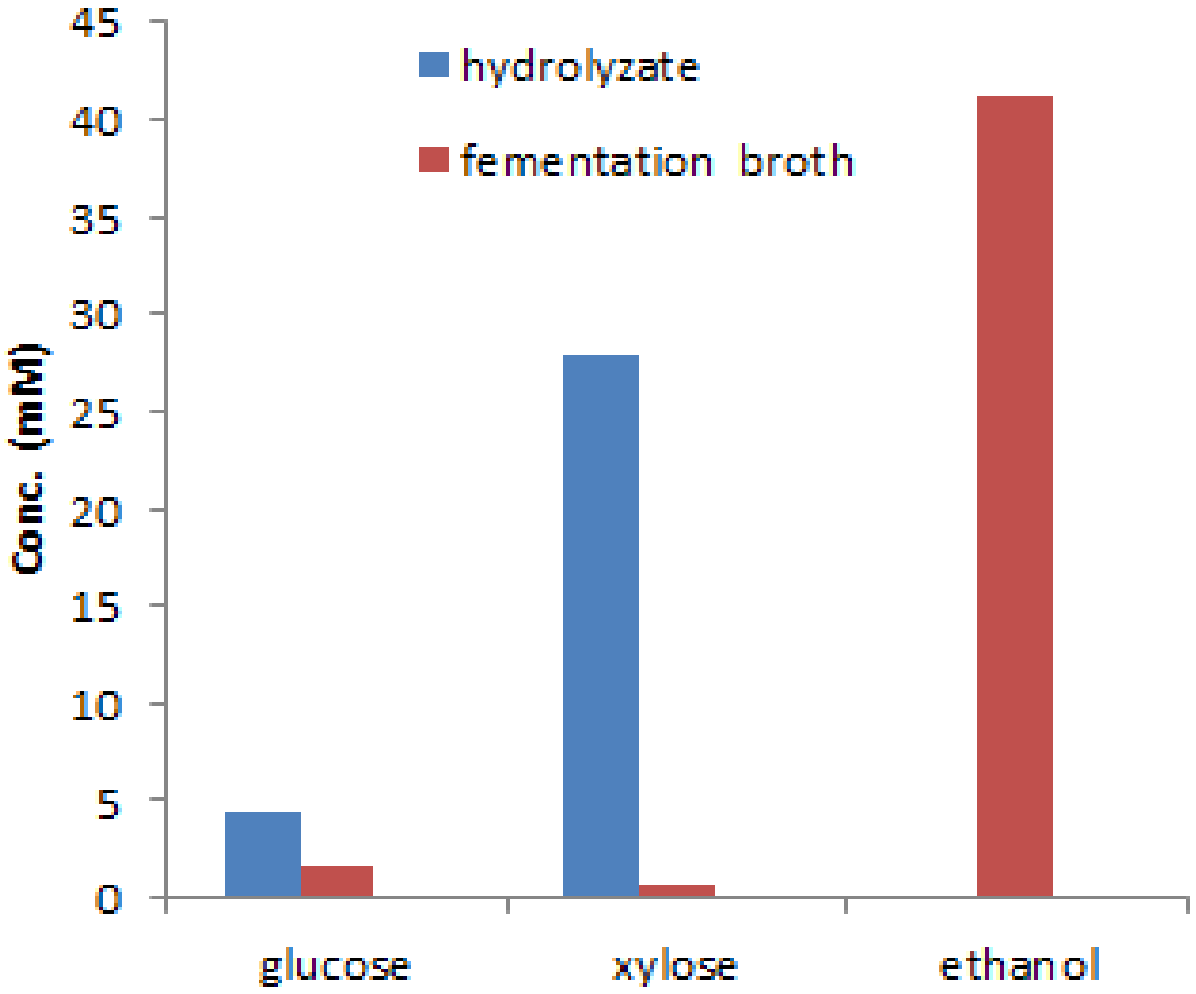

Xylose metabolism by the Baker's yeast strain is feasible
5.7 wt. % ethanol could be produced from raw pine cones

Gedanken et al., J. Environ. Management, 162, 2015, 215

Single step conversion of macroalgae to ethanol using sonication

Proximate composition	Relative % on dry weight basis
Carbohydrate	37±3.9
Cellulose	23.8 ±1.2
Starch	7.6±1.1
Protein	6.2±0.9
Carbon	28.1±1.2
Nitrogen	4.5±0.7
Hydrogen	5.5±1.3
Sulphur	2.3±0.4

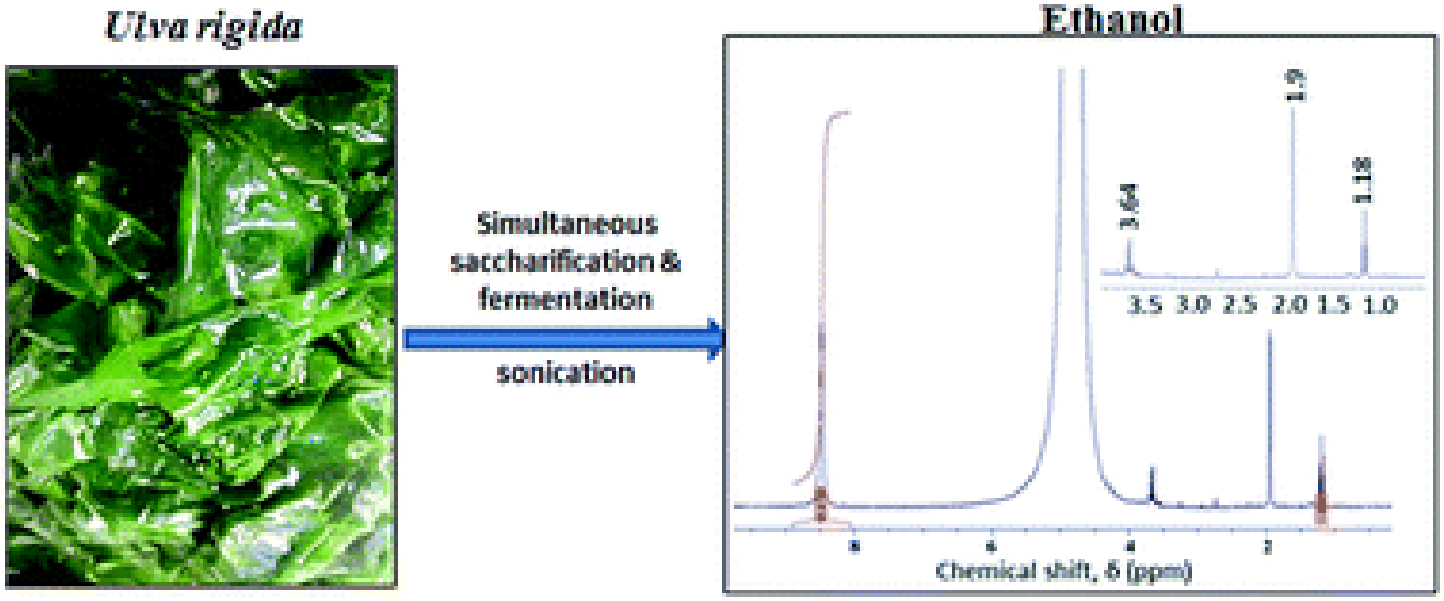

Cellulose & Starch constitute the major fraction (31.4 wt.%) of carbohydrates that could yield glucose upon saccharification

Objective - Selective and fast production of glucose from the cellulose and starch components of algae & conversion of glucose to ethanol under sonication in a SSF process

Gedanken et al., RSC Advances, 5, 2015, 16223

Enzymatic saccharification of *Ulva rigida* under sonication

Before carrying out the SSF process, the saccharification process is evaluated in isolation

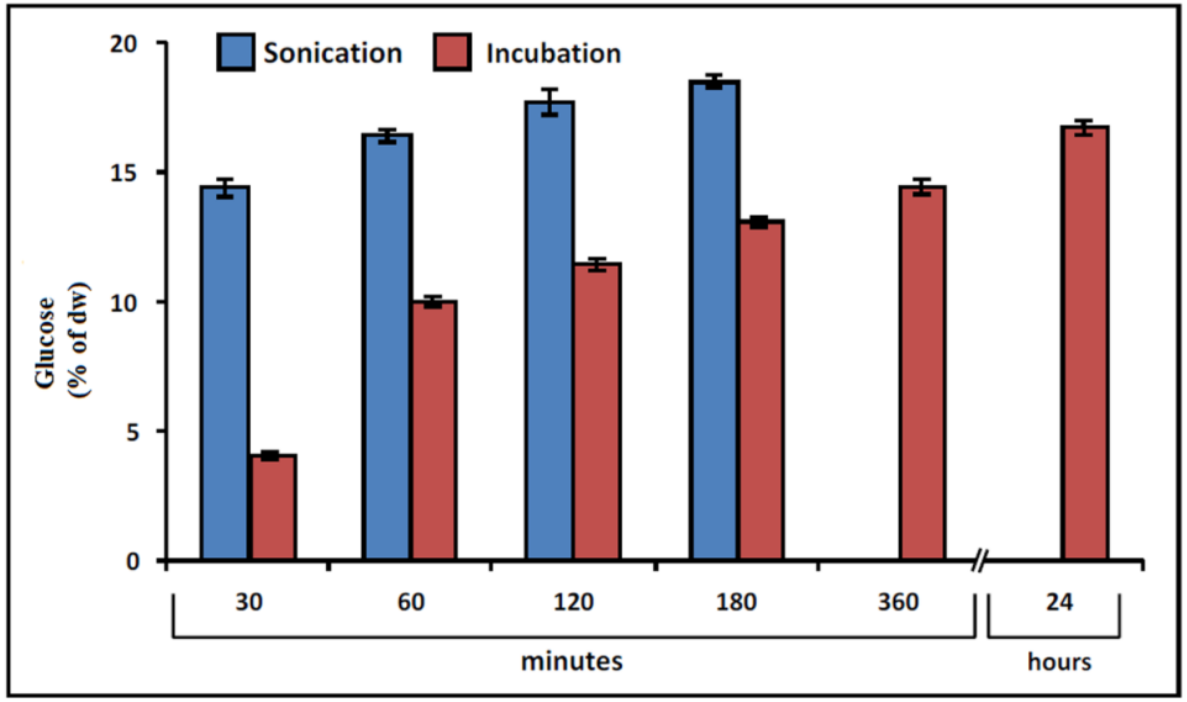

Algae hydrolysis, Sonication Vs incubation at 37 °C

1.68 g of dried *U. rigida* 40 mL of distilled water 40 mL of 200 µM sodium acetate (buffer) (2.1 % w/v), 100 µL amyloglucosidase 300units/mL, 40 µL α-amylase 250units/mL, 0.1 g cellulase, 0.3 units/mg
All the contents were taken in a 100 mL glass media bottles with cap

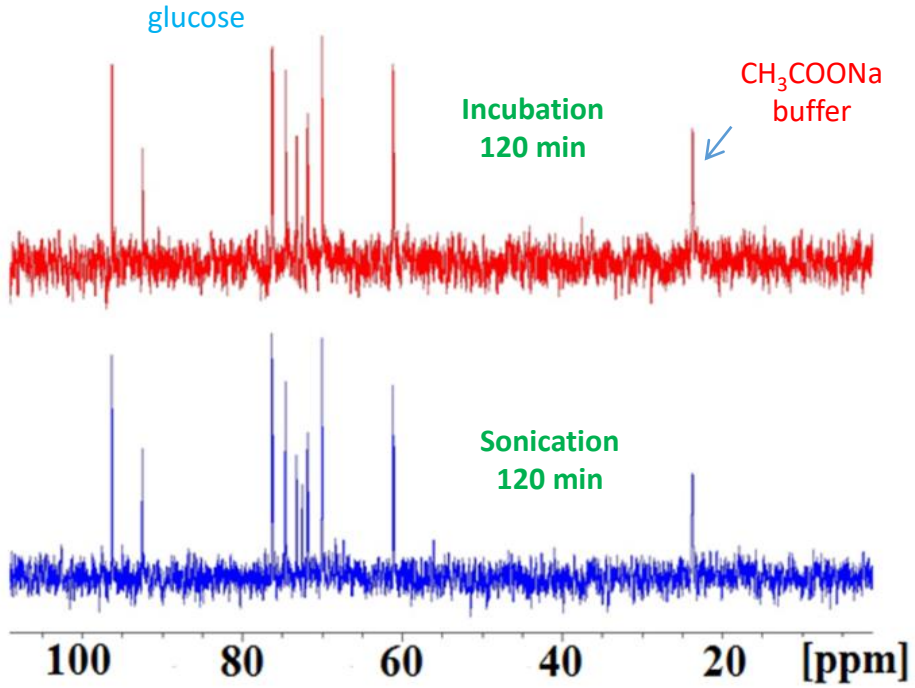

^{13}C NMR spectra of hydrolyzate

Use of cellulase and amylase selectively hydrolyzed cellulose and starch Fractions to glucose

- ✓ **3.6 times higher yield of glucose using sonication Vs incubation for hydrolysis process**
- ✓ **Enhancement in the release of glucose is attributed to mechanical and thermal effects**
- ✓ **Structural rigidity of the cellulose and starch components in the biomass reduced upon sonication**
- ✓ **Ultrasound irradiation reduced reaction time by improving mixing, phase transfer, and diffusion of enzymes across cell membranes (algae), so that enzymes can easily reach the bulk of the substrate**

Sonication based SSF process for bioethanol production

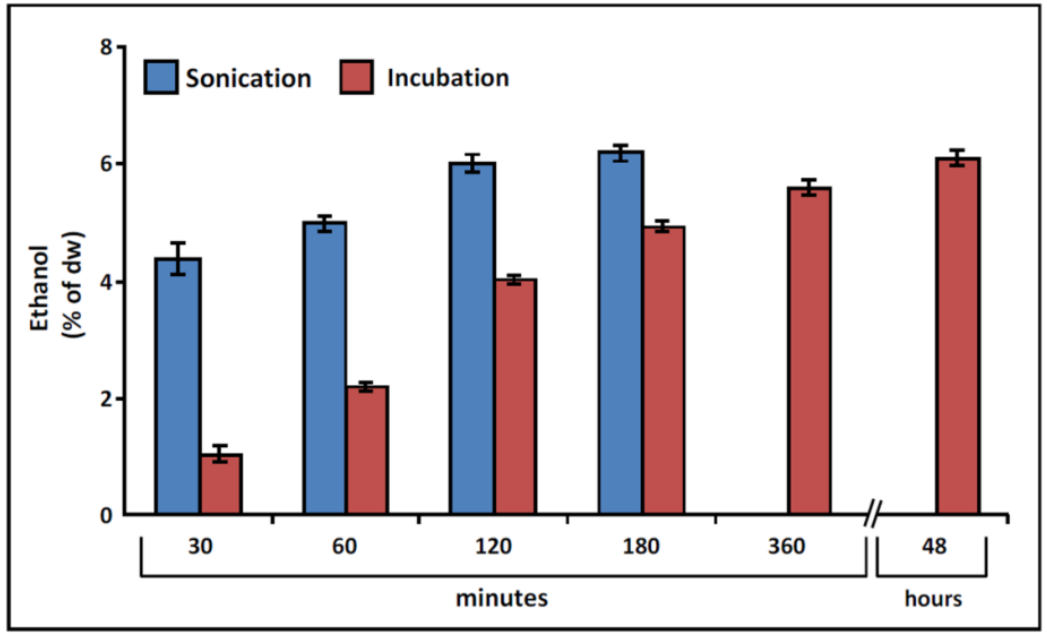

SSF process - Sonication Vs Incubation at 37 °C

1.68 g of dried *U. rigida* in 40 mL of distilled water
40 mL of 200 µM sodium acetate (buffer) (2.1 % w/v)
100 µL amyloglucosidase 300 units/mL, 40 µL α-amylase 250 units/mL,
0.1 g cellulase (0.3 units/mg), 0.5 g of Baker's yeast
100 mL glass media bottles with cap were used

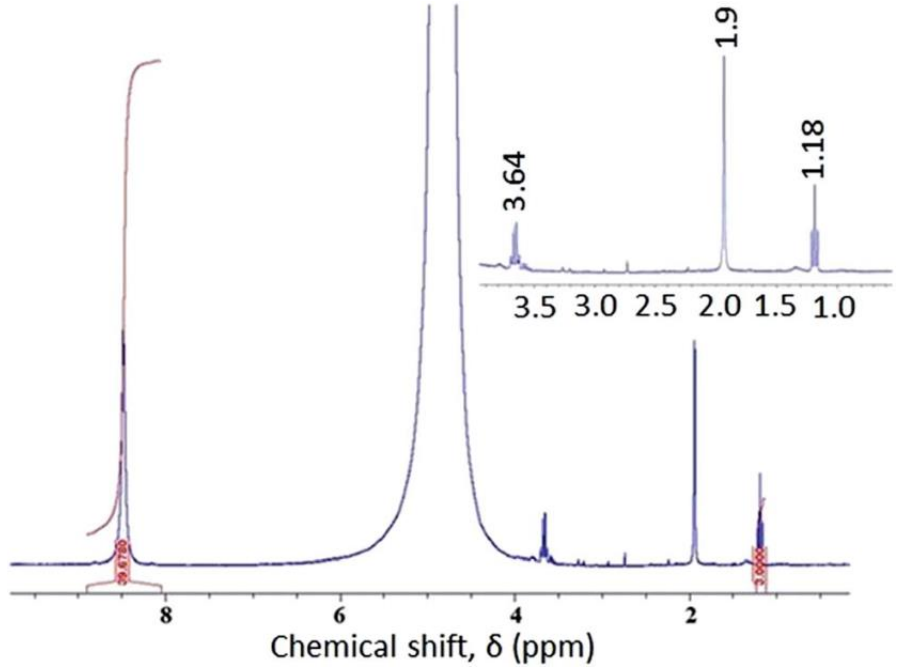

^{1}H NMR for ethanol quantification

3H (t, 1.18 ppm) and 2H (q, 3.64 ppm) - ethanol
3H, s, 1.9 ppm - sodium acetate (buffer)
1H, s, 8.5 ppm - internal standard (HCOONa)
Relative integral values of the internal standard and the ethanol peaks – measure of ethanol amount

- ✓ **SSF process was also faster under sonication relative to incubation**
- ✓ **In 30 min. the yield of ethanol under sonication is high (4.3±0.3 wt.% Vs 1.0±0.1 wt.% under incubation)**
- ✓ **Even after incubation for 48 h, the ethanol yield under incubation is only 6.1±0.1 wt.%**
- ✓ **Acceleration in the SSF process could be due to the possibility of generation of fresh surface on the yeast cells by the faster removal of ethanol and CO_2 formed during fermentation**

Cultivation of high carbohydrate *ulva rigida* for enhanced bioethanol production

Integrated multi-tropic aqua culture

High carbohydrate *Ulva rigida*

SSF

Ethanol yield 16 wt. %

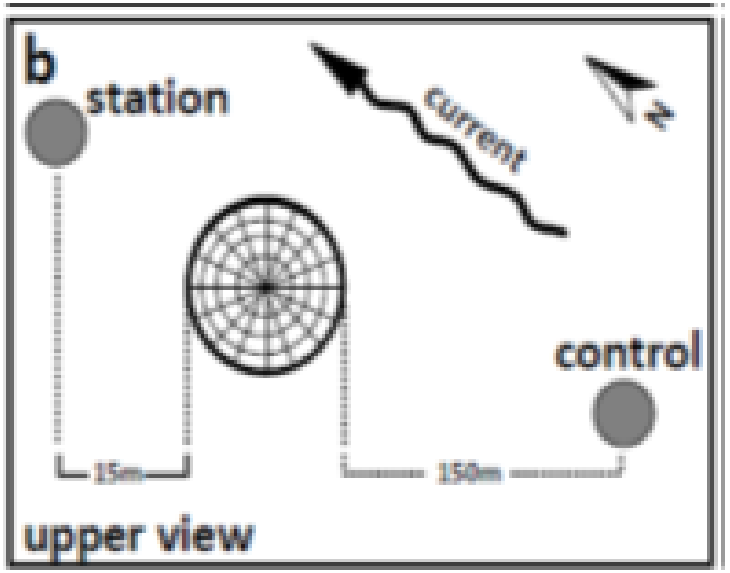

September trial

a

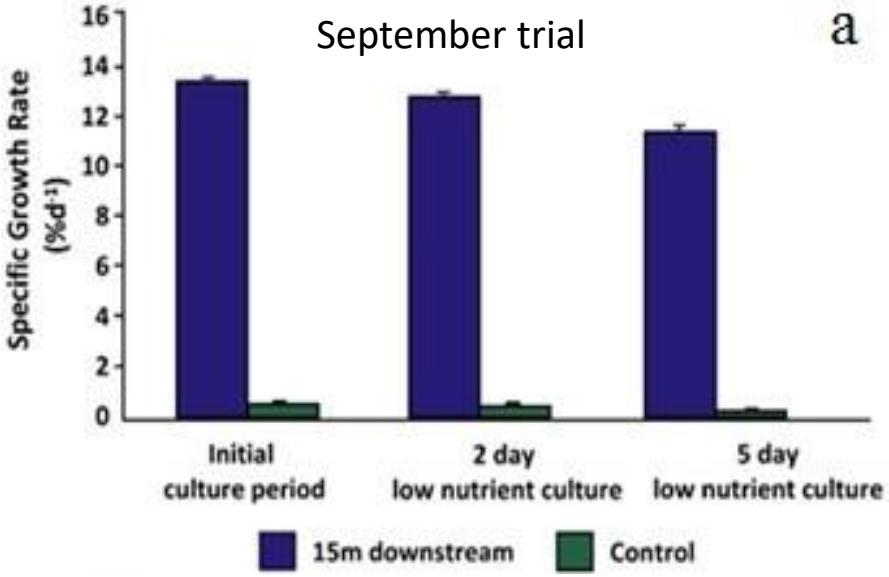

- ✓ Starch content was higher (31.5 % of DM) at the control station than downstream to the cages (24% of DM)
- ✓ High nutrient concentrations were found to alter the proximate composition in seaweeds and caused a shift to lower levels of carbohydrates such as starch
- ✓ After two days of culture manipulation at the low nutrient site, the starch contents bounced up and levelled with the values of the control site

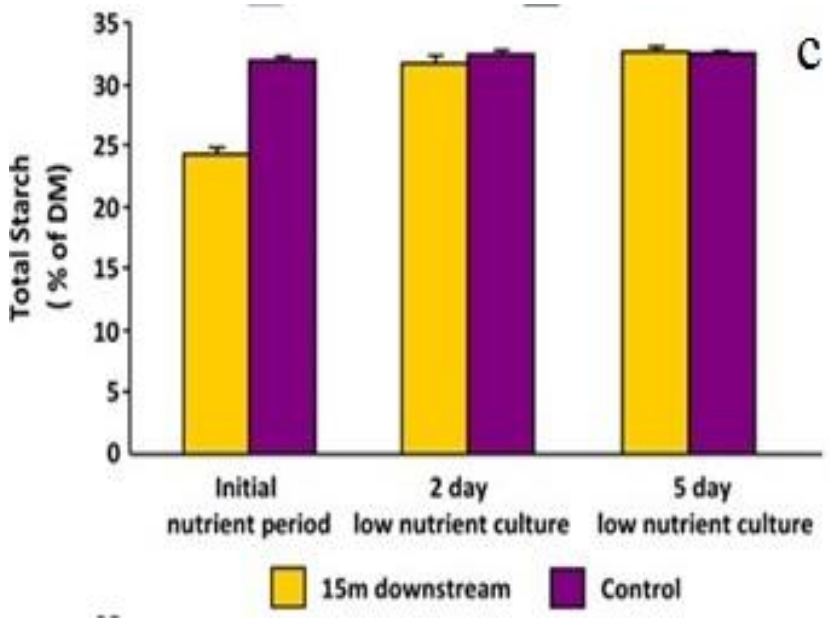

- ✓ 27 times higher specific growth rates (SGR) achieved under nutrient rich conditions
- ✓ Availability of inorganic nutrients - most important factor controlling the growth and productivity of seaweeds

Gedanken et al., RSC Adv., 2015, 5, 29251

Bioethanol yield – regular *Ulva* Vs high carbohydrate *Ulva*

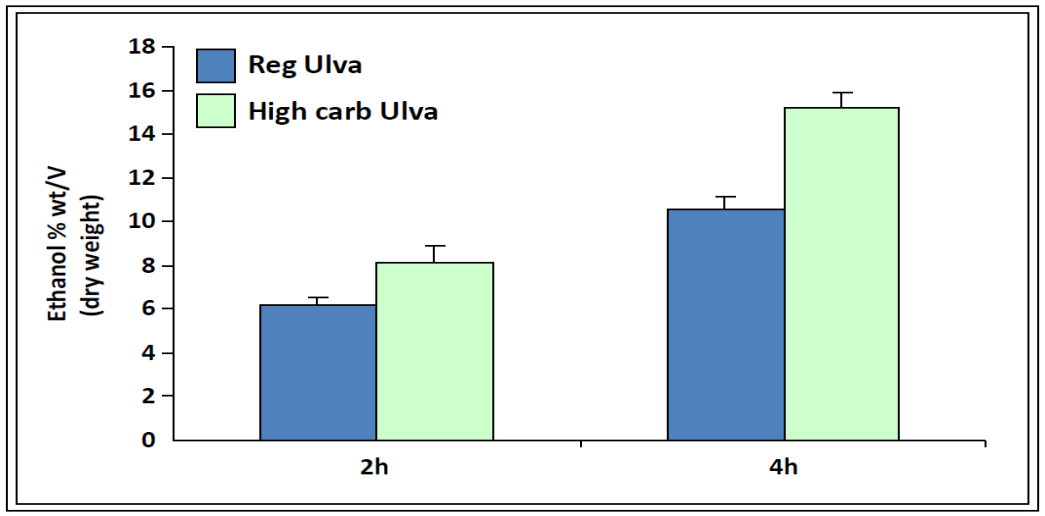

Effect of modulating the carbohydrate content of *ulva rigida* on the ethanol yield

Enhanced ethanol yield with high carbohydrate cultured algae (16 wt. %) Vs as regular *Ulva rigida* (8 wt. %) (15 wt.% solid consistency, middle enzyme loading)

Observed ethanol yield - 16 wt.%
Process efficiency – 89 %
Expected ethanol yield: 17.8 wt.%
31.5 wt.% starch yield 35 wt.% glucose
35 wt.% glucose should yield 17.8 wt.%

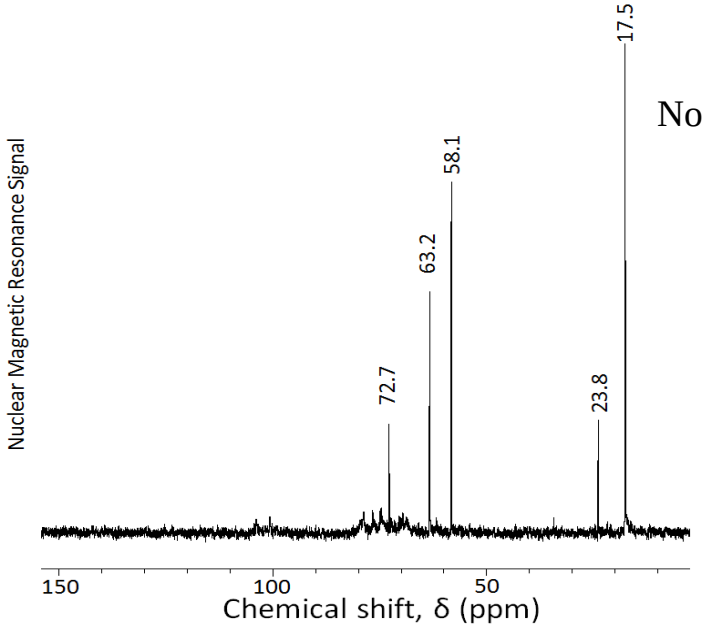

No fermentable sugars are detected (in the region of 60-100 ppm)

SSF process is effective for the conversion of *Ulva* to bioethanol with complete conversion of glucose

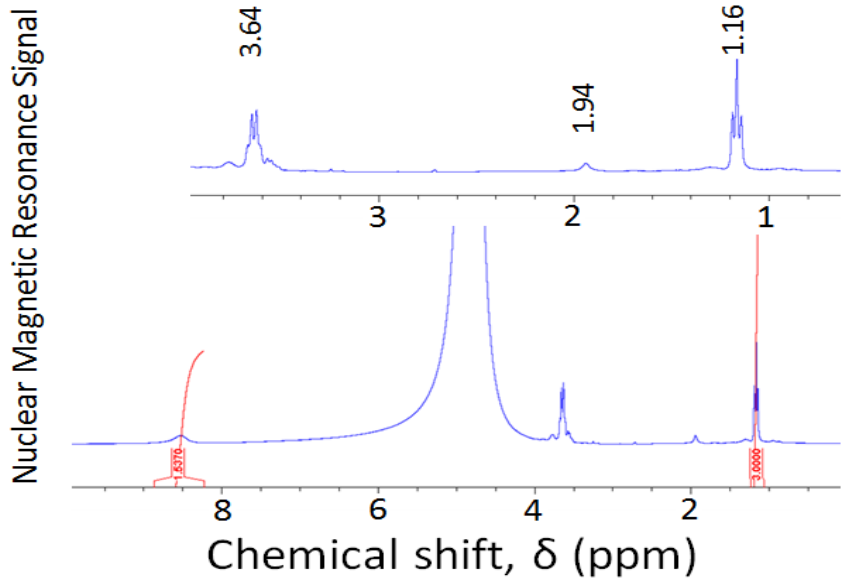

^{13}C and ^{1}H NMR spectra of aliquot of sample collected from the fermentation (SSF) broth under optimal reaction conditions

Process efficiency improved from 65 % to 89 % using high carbohydrate *ulva*

Solar energy driven SSF of starch

- The conversion of potato starch to ethanol in a single-step process

$$\text{Starch} \xrightarrow[\text{(α-amylase)}]{\text{Hydrolysis}} \text{Liquefied starch} \xrightarrow[\text{(glucoamylase)}]{\text{Hydrolysis}} \text{Glucose} \xrightarrow[\text{(microorganisms)}]{\text{Fermentation}} \text{Ethanol}$$

- Aqueous starch solution (5 wt %) and amylase mixture were charged into the reactor bed loaded with instant baker's yeast (*Saccharomyces cerevisiae*)
- Top flat glass surface allowed the solar radiation into the reactor
- Fermentation took place in the first chamber and the produced ethanol was continuously separated from the yeast bed by evaporation-condensation (at 30-35 °C) process
- The ethanol droplets condensed on the glass were collected into the second chamber

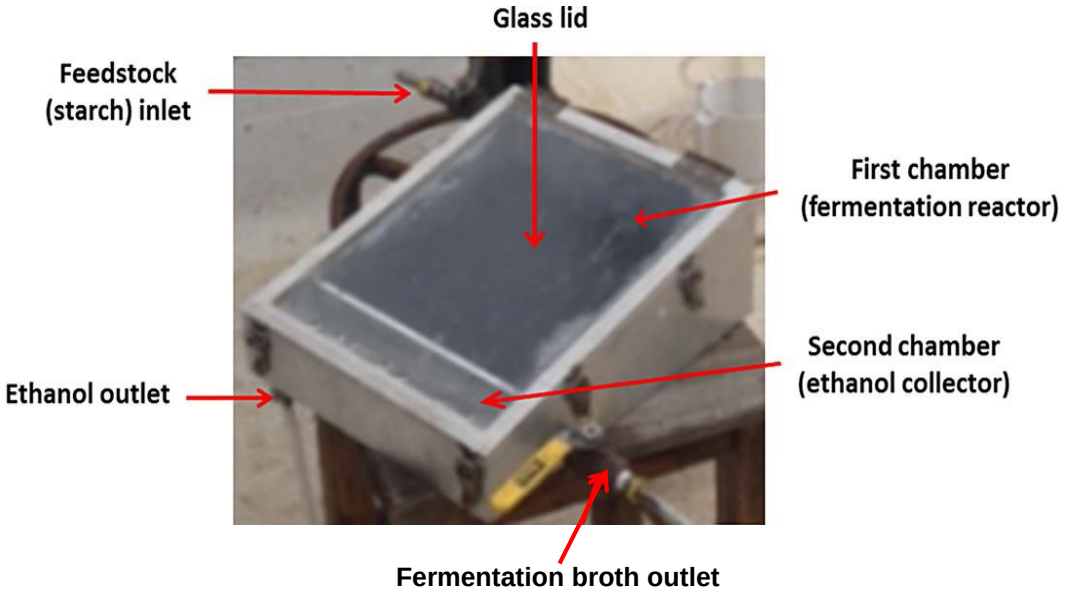

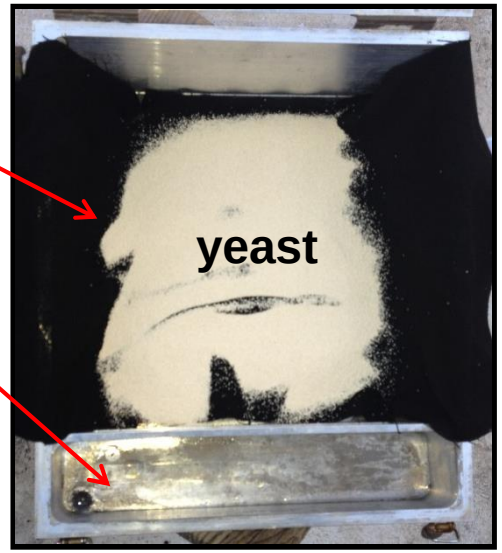

Gedanken et al., ChemSusChem, 8, 2015, 3497

Solar energy driven SSF of starch

SSF of starch
starch solution (1.6 L, 5 wt. %); Baker's yeast (75 g);
amylo glucosidase (2.5 mL), α-amylase (2.5 mL)

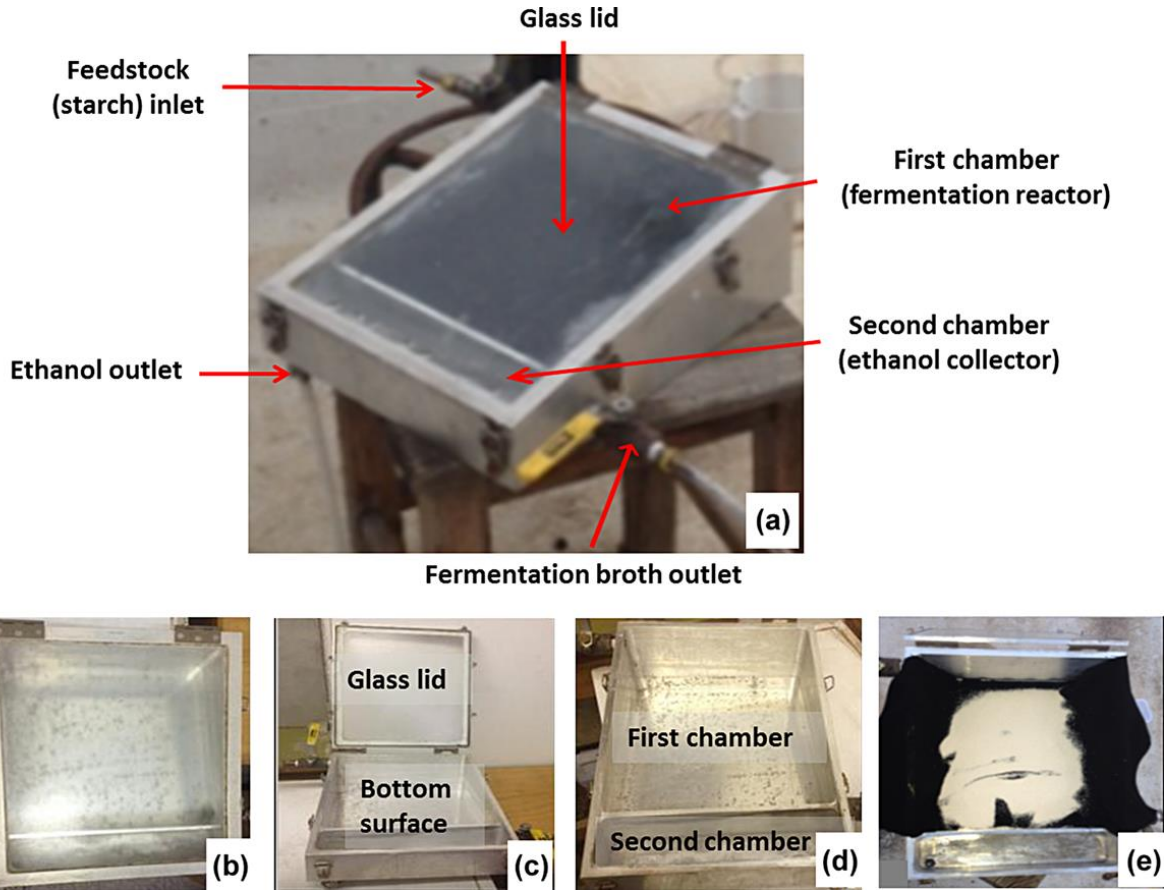

Solar reactor for conversion of starch to bioethanol

2.6 – 1.8 wt. % ethanol collected daily (ca. 25 mLday^{-1}
38 g ethanol was collected over 63 days from 80 g starch
Ethanol yield 84 wt. % of the theoretical yield

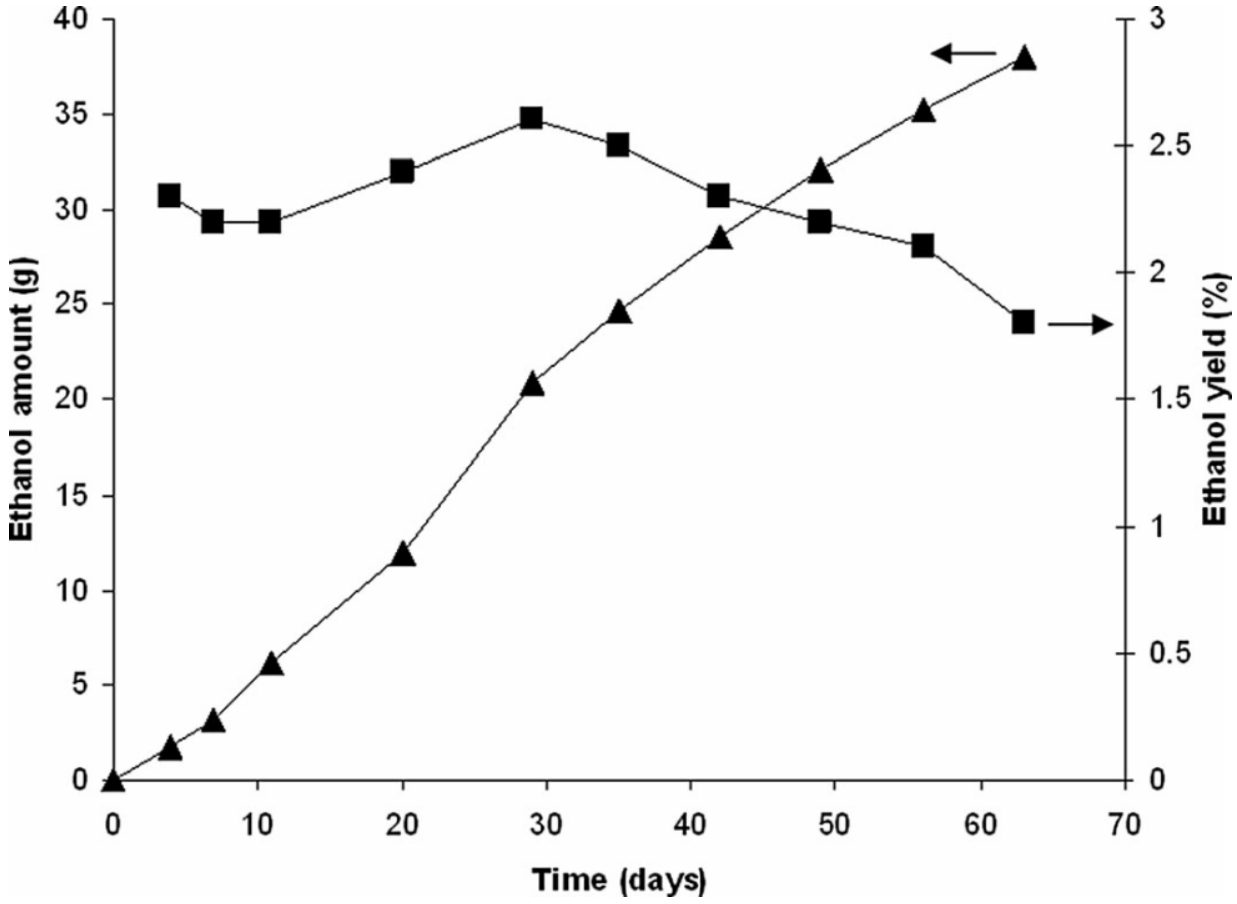

Solar energy driven bioethanol production from starch as a function of time

Analysis of products of SSF of starch

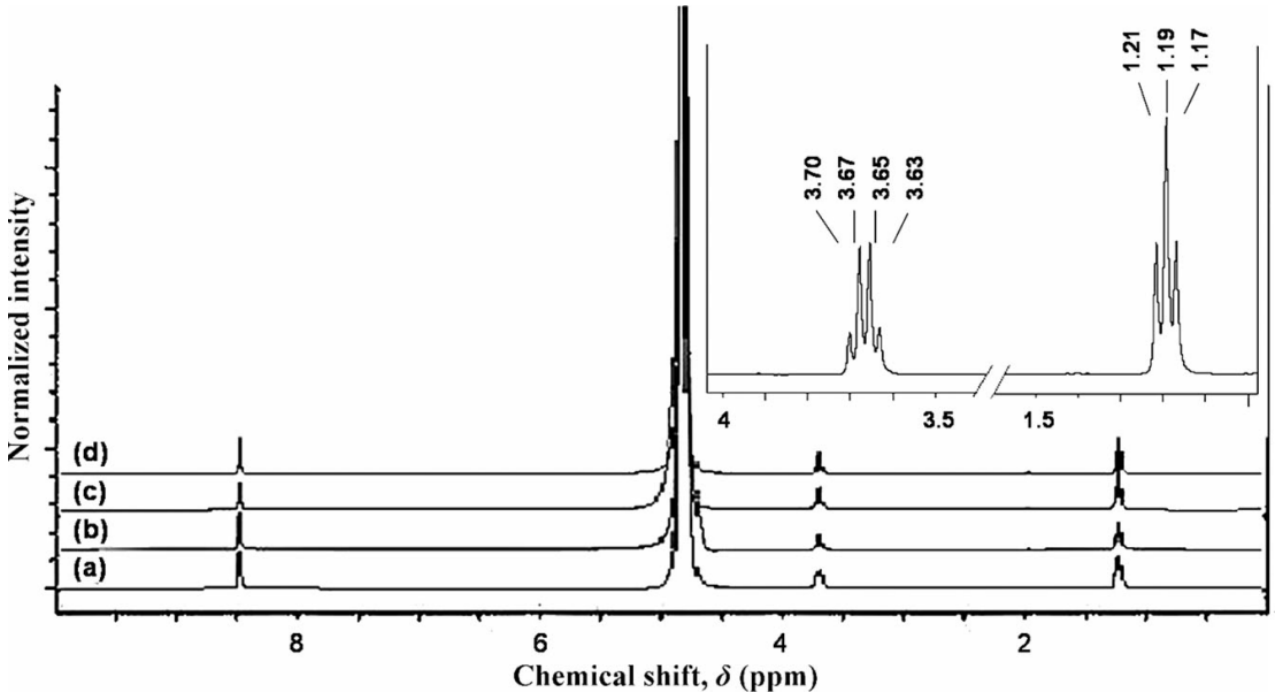

^{1}H NMR spectra of the starch fermentation product on the (a) 7th, (b) 14th, (c) 21st, and (d) 28th day

Inset shows the ethanol peaks—

a 3H (t) at 1.2 ppm and a 2H (q) at 3.7 ppm

Singlet peak at 8.4 ppm is the internal standard, HCOONa, and the peak at 4.8 ppm is the solvent

No other reaction by-products (glycerol or acetic acid) were observed in the analytes indicating the purity

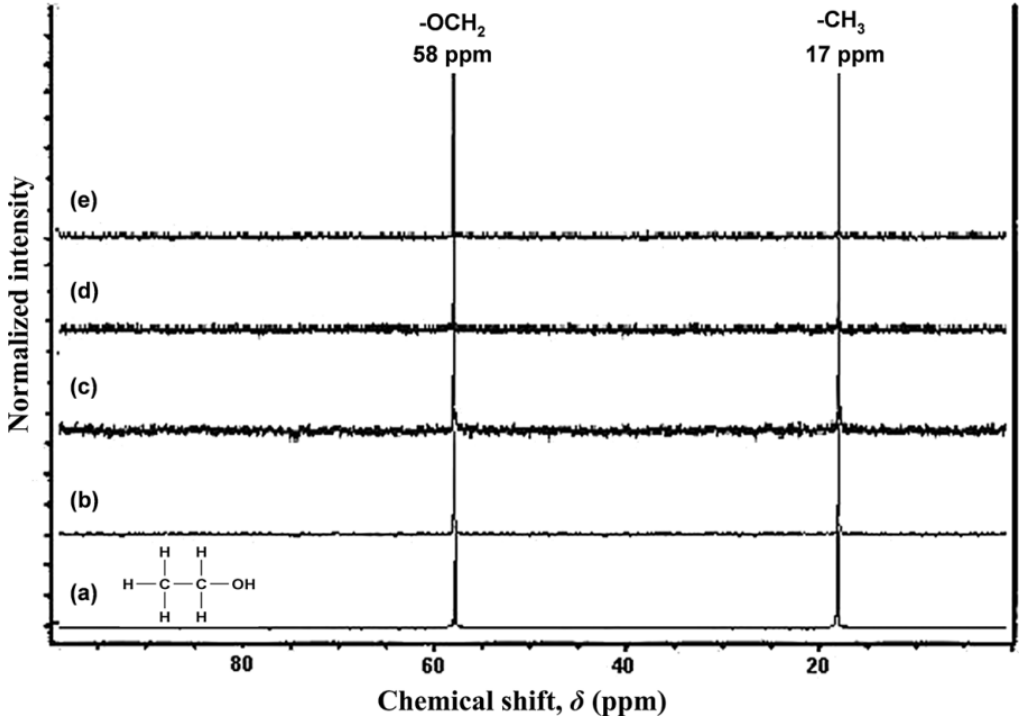

^{13}C NMR spectra of (a) authentic ethanol and the starch fermentation product on the (b) 7th, (c) 14th, (d) 21st, and (e) 28th day from the solar reactor

- ✓ Intense signals seen in all four samples at 17 and 58 ppm are characteristic of ethanol
- ✓ Reaction product is devoid of the reactant (starch), reaction intermediate (glucose), and the usual secondary metabolites of fermentation (glycerol and acetic acid)

Mass balance studies for the conversion of starch to ethanol

- 84% of the theoretical ethanol yield was collected over 63 days (from the outlet)
- **Initial amount of starch:** 5 wt% = 80 g starch in 1.6 L solution
- **Expected yield of glucose:** 1 g starch converts to 1.1 g glucose

  80 g starch should convert to 88.8 g glucose
- **Expected yield of ethanol:** 1 g glucose yields 0.51 g ethanol

  88.8 g glucose should yield 45.28 g ethanol
- **Actual yield of ethanol after 63 days:** 38 g ethanol = (38/45.28) x 100 = 84% yield
- The concentration of ethanol varied in the range of 1.8-2.6 wt. % over the course of study

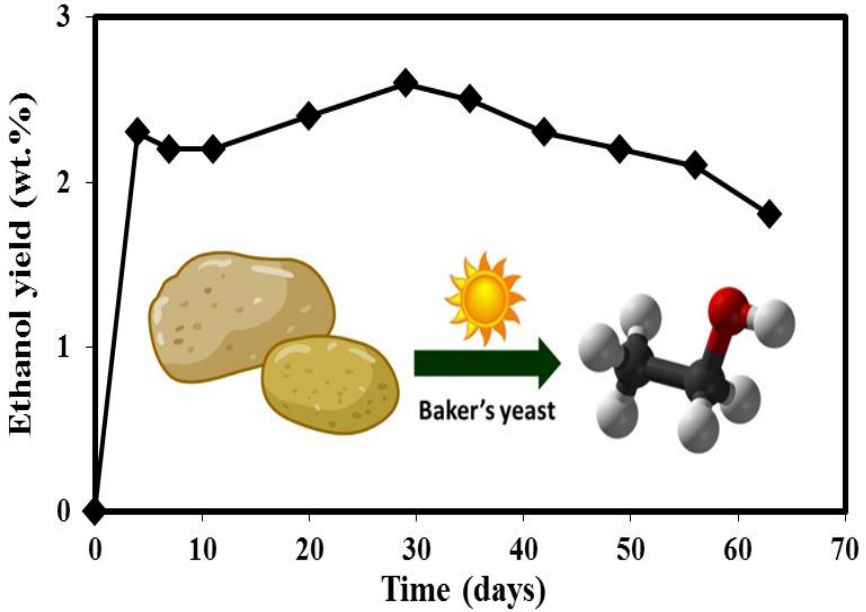

Starch-based bioethanol for direct ethanol fuel cells

- SSF was scaled up to 15 wt. % starch to be evaluated as fuel in DEFCs
- Voltammograms of as-produced bioethanol (1.3 M, 6 wt %) and commercial ethanol were similar, with comparable peak currents (high purity level)

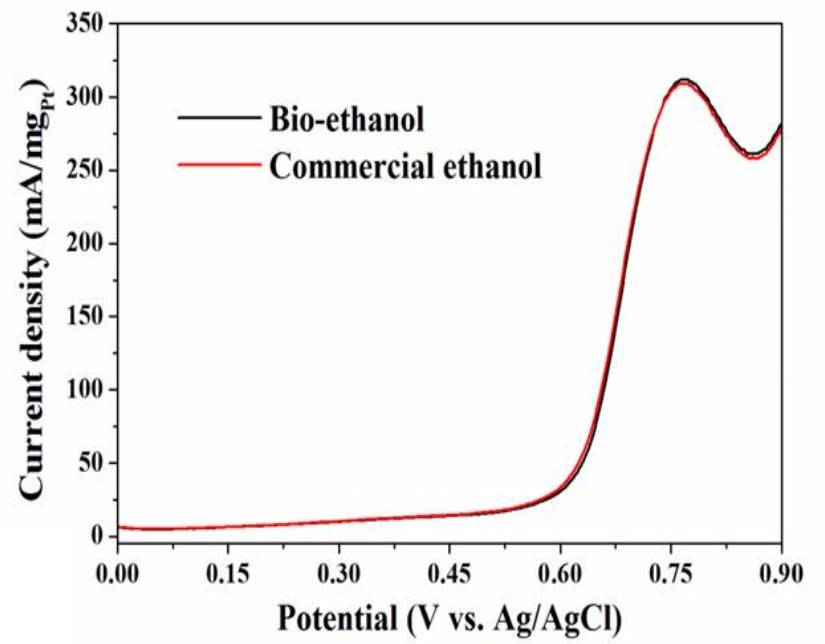

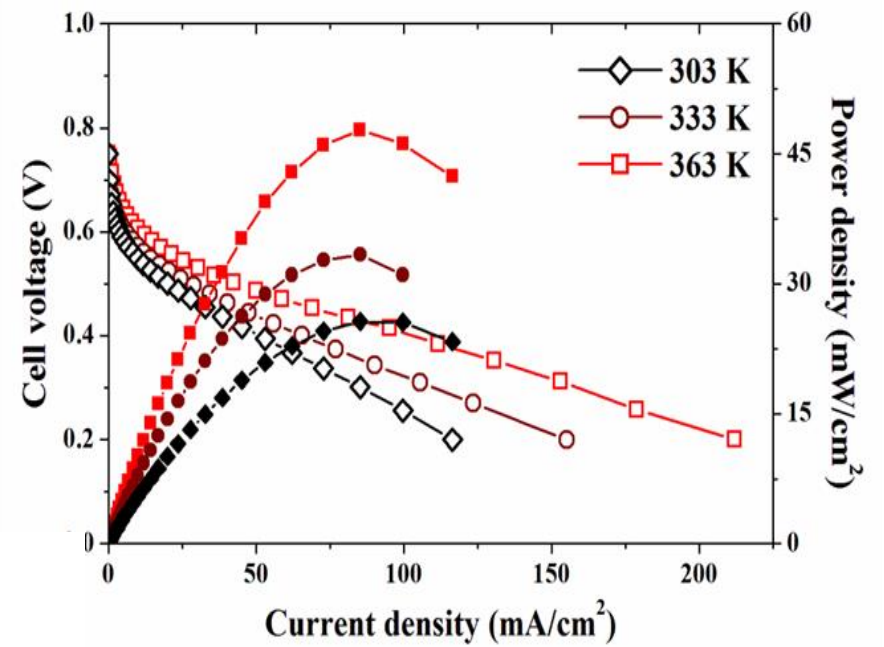

- The cell performance increased with temperature due to the enhanced kinetics of ethanol oxidation at the anode and oxygen reduction at the cathode
- In acid medium (0.5 M H_2SO_4) using Pt/C as anode electrooxidation catalyst, under modest operating conditions of 303 K, the open circuit voltage of the cell was found to be 0.75 V with a limiting current density value of 116 mAcm^{-2} and a corresponding power density value of 25.6 mWcm^{-2} was measured.

Electricity from biomass is feasible!

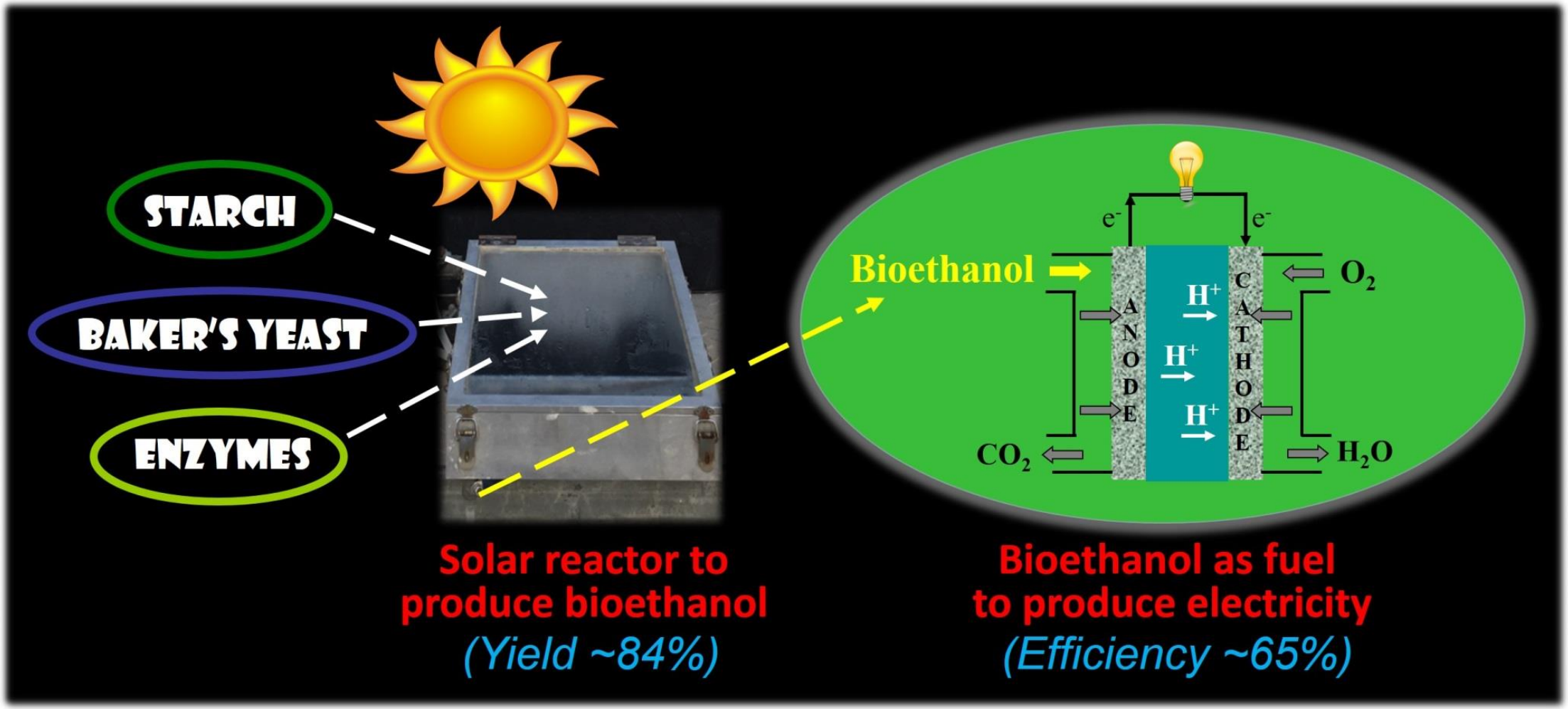

A leap towards decentralized power supply

Continuous-flow bioethanol production in the solar reactor

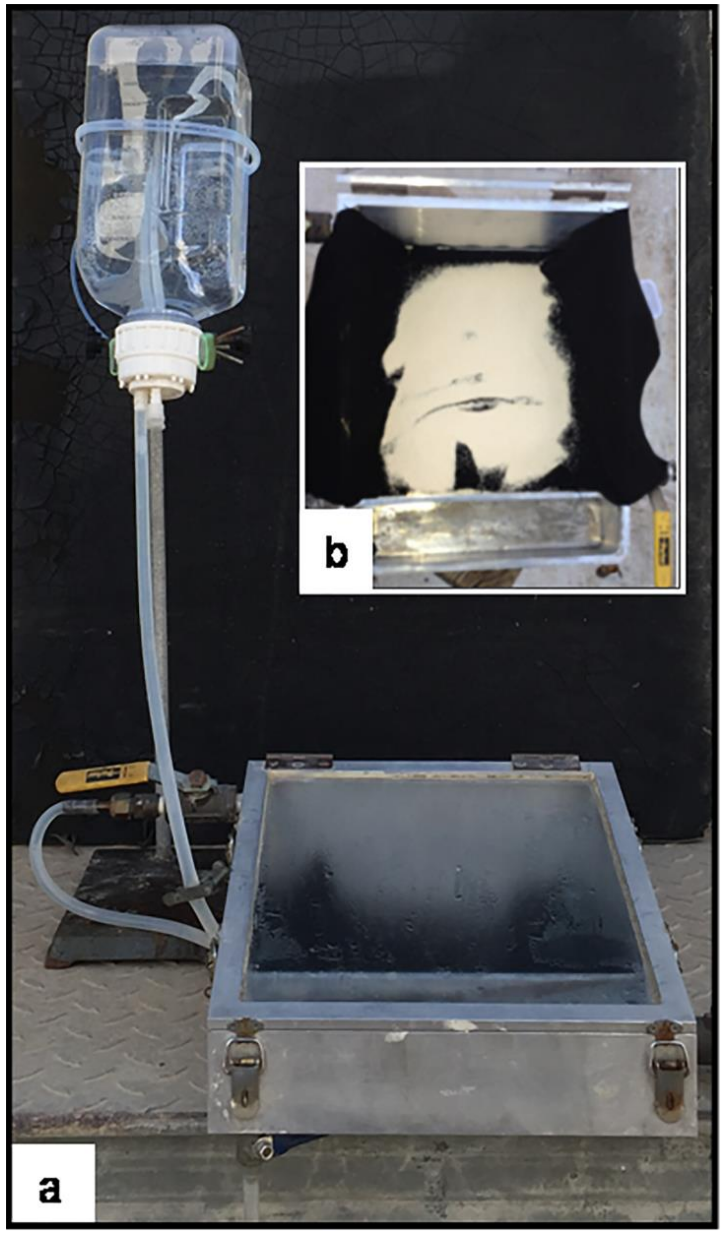

- The batch process was further developed to a continuous-flow bioethanol production
- The reactor was fed with 2 L of 10, 20, 30 or 40 wt.% aqueous glucose solutions (2.8 mL/h flow rate)
- For each glucose feed, the process was monitored for a month in the reactor at 20-25 °C
- The yeast was not supplemented with any additional nutrients (only glucose feed)
- The yeast bed was always in solid-state condition

Time on stream studies of ethanol yield from glucose

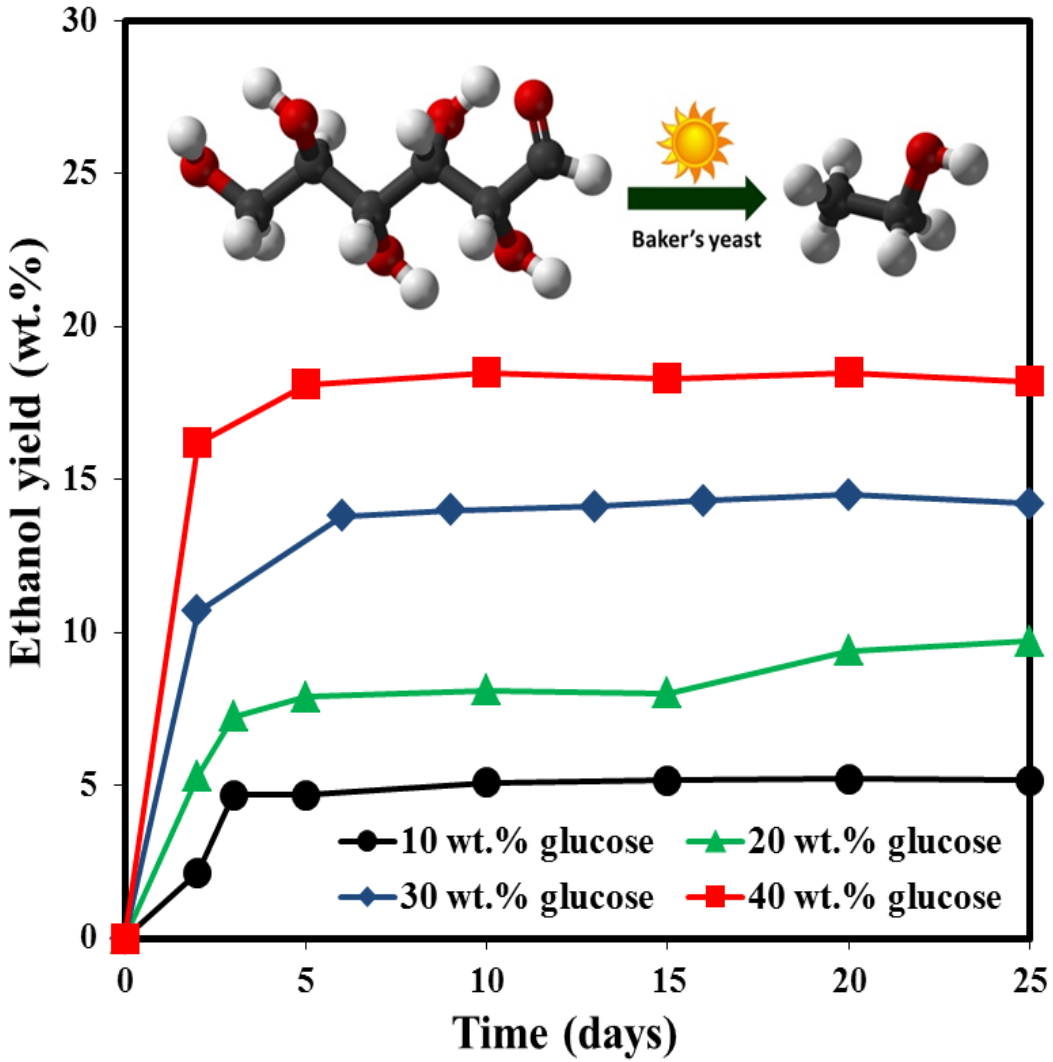

- High ethanol yields (91, 86, 89, and 88% of the theoretical yield) indicate the atom efficiency of the process
- No effluent in the reactor (very convenient to feed solutions between the experiments)
- There was almost no loss in the activity of the yeast even after two months of continuous operation of the process

Gedanken et al., RSC Adv., 2016, 6, 24205

Electricity from biomass is feasible!

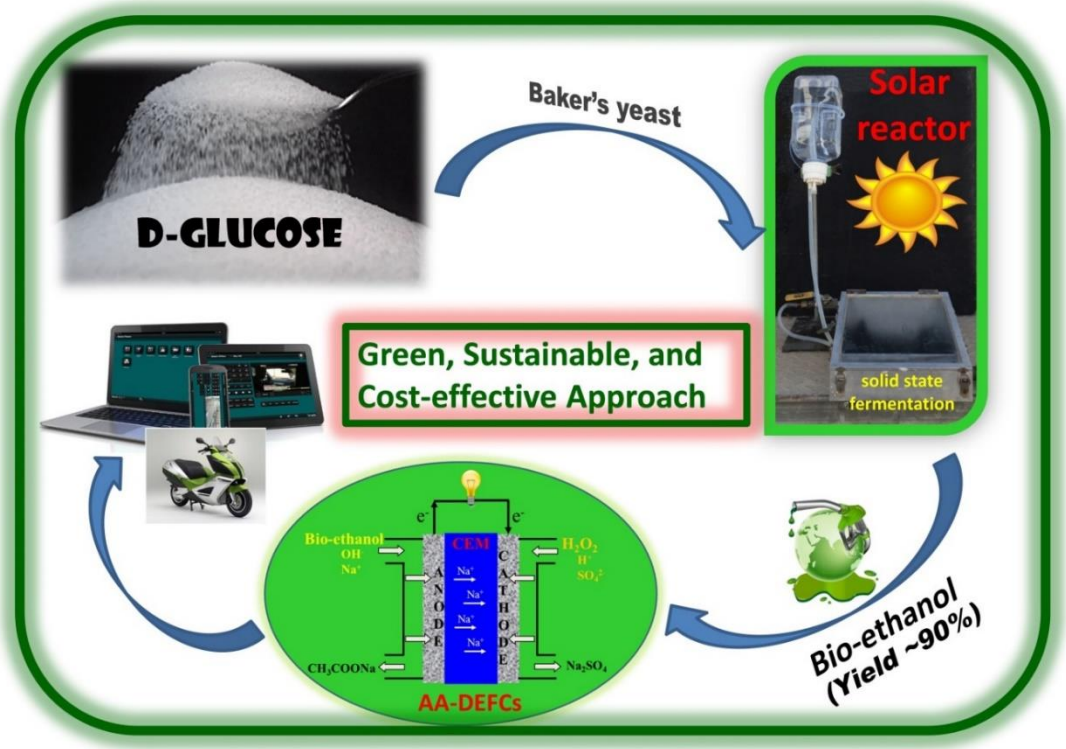

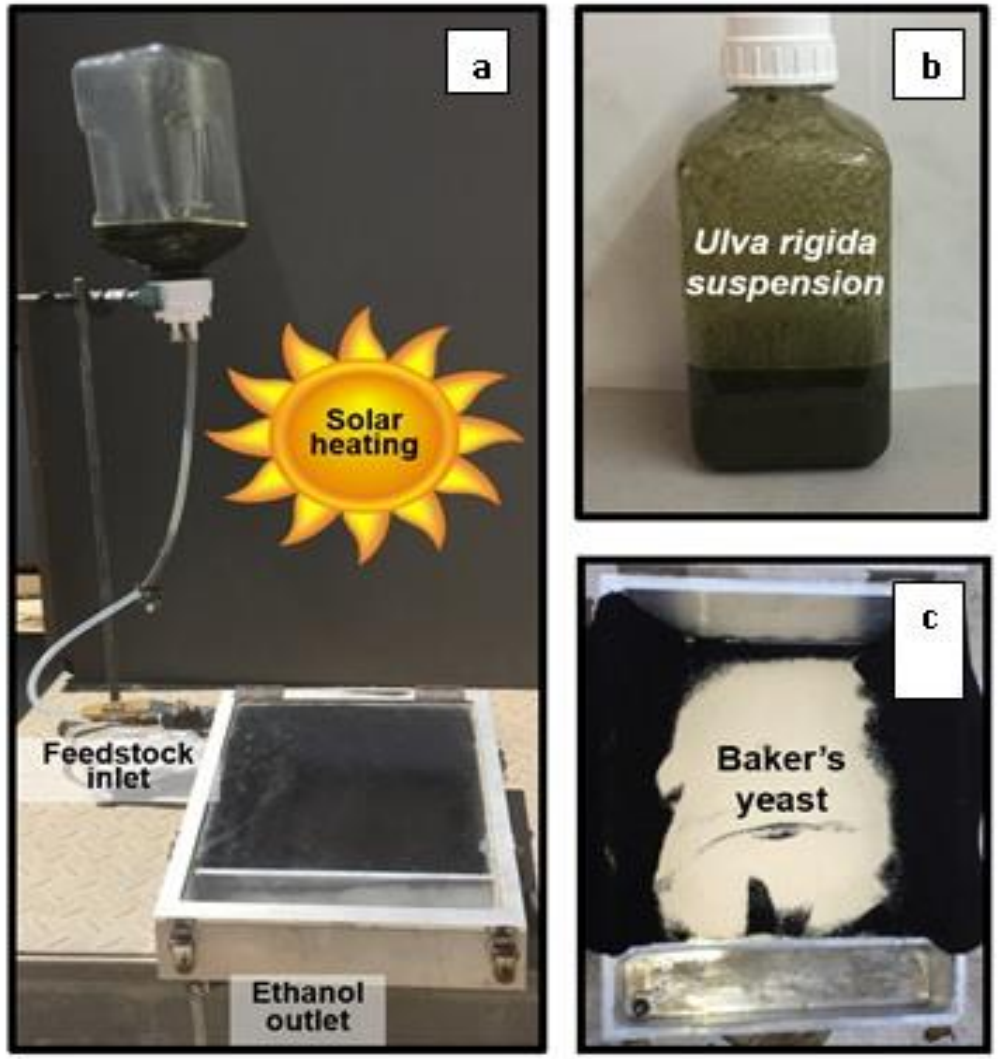

- ✓ Significant improvement in cell performance was achieved by the use of alkaline-acid DEFCs.
- ✓ Operation temperature: 303 K
- ✓ Anode for the bioethanol electrooxidation : PdNi/C
- ✓ Cathode for H_2O_2 electroreduction: PdAu/C
- ✓ Fuel: 2 M bioethanol as fuel (derived from 20 wt.% glucose)
- ✓ Current density and power density values of 700 $mAcm^{-2}$ and 330 $mWcm^{-2}$ were achieved at a modest operating cell voltage of 1.65 V.

Gedanken et al., J Mat Chem A., 2017, 5, 15486

Advantages over existing technology

Solar-energy-driven fermentation has **numerous advantages**:

- ✓ No external source of heating
- ✓ High ethanol yields without electricity consumption
- ✓ Using the same microorganism for a long time without loss in the activity
- ✓ No additional energy input for ethanol separation
- ✓ Micro organisms not supplemented by nutrients
- ✓ No requirement of use of buffer
- ✓ No polluting effluent produced in the process
- ✓ Insitu reduction of glycerol to 1, 3 propane diol

❖ Utilization of solar energy for driving SSF process and *in situ* separation of ethanol from the fermentation broth make the current process economically feasible, environment-friendly, industrially, appealing and adoptable

❖ The produced bioethanol was also demonstrated as a potential fuel for DEFCs

Biochemicals from Biorefinery

Economic drivers for a biorefinery - Top 12 value added chemicals

1, 4 – diacids (succinic, fumaric and malic)
aspartic acid,
glutamic acid,
2, 5-furan dicarboxylic acid,
3-hydroxy propionic acid,
glucaric acid,
itaconic acid,
levulinic acid,
3-hydroxy butyrolactone,
glycerol,
sorbitol and
xylitol/arabinitol.

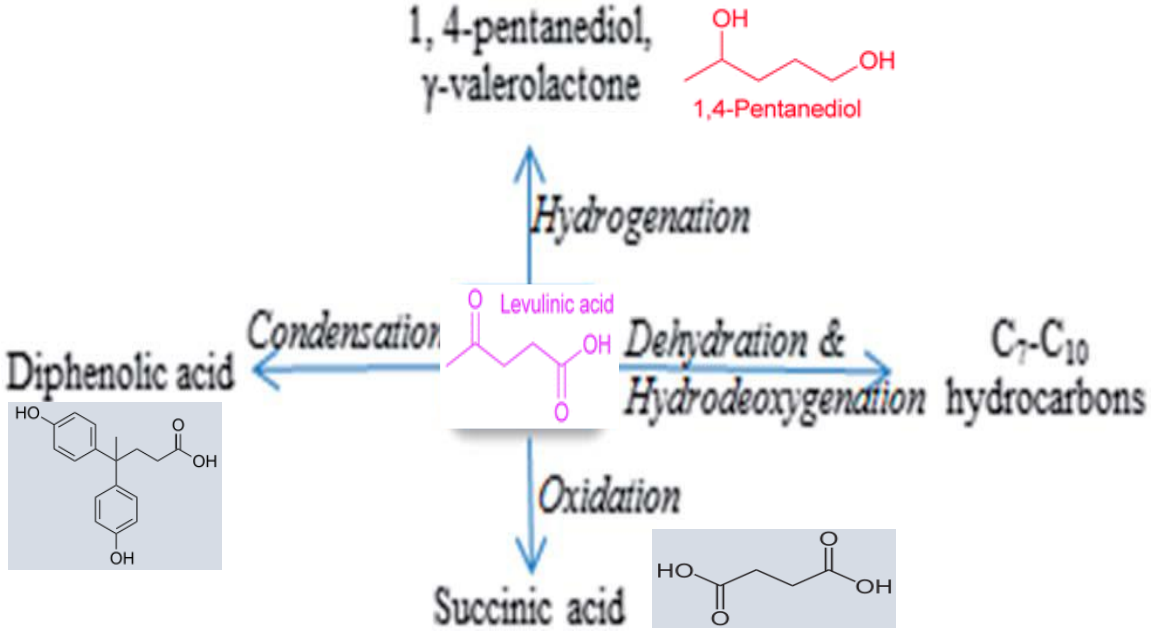

Levulinic acid to value added chemicals

Special structural feature - Multiple functional groups

Levulinic acid production from biomass is strategically significant

www.energy.gov/eere/bioenergy/downloads/top-value-added-chemicals

Solid acid catalysts for biomass conversion to biochemicals (glucose & levulinic acid)

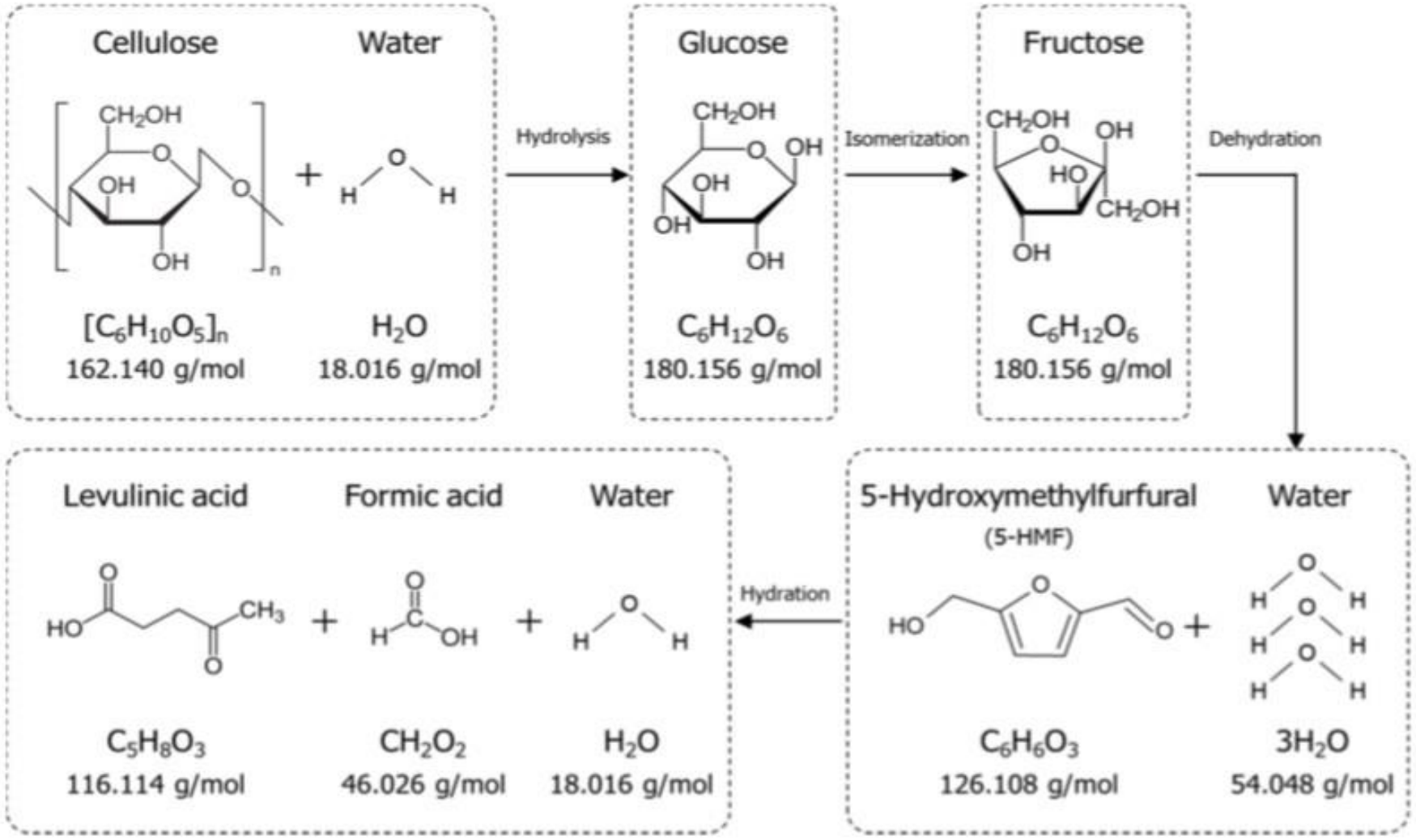

Net chemical reaction and mass balance in the conversion of cellulose to levulinic acid

Biomass type - LA yield

1M HCl,2h

Biomass	Temperature (K)			
	393 K		423 K	
	Conv. (wt.%)	Yield (wt.%)	Conv. (wt.%)	Yield (wt.%)
CA	66	10.8	82.4	32.6
PR	47.5	5	56	19.0
SCB	55.8	17.5	67.5	36.5
Cotton	7.1	4.7	78.7	44

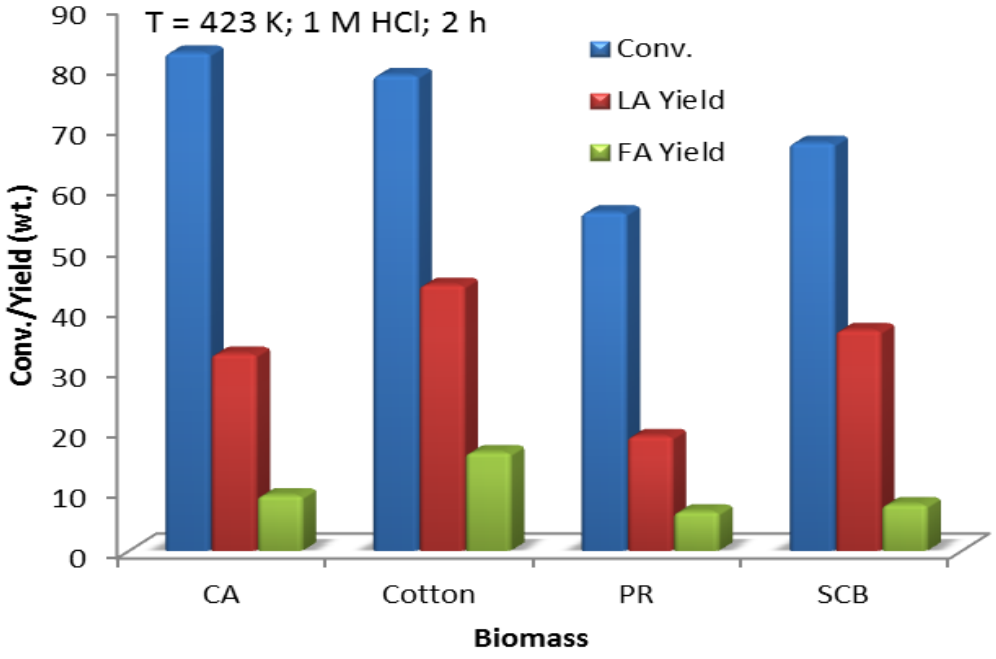

1.Effect of reaction temperature on rate of chemical reactions

2. Structural rigidity and reduced hydrogen bonding interactions

Gedanken et al., RSC Advances, 2014, 4, 44706

Intermolecular and intramolecular hydrogen bonding in cellulose structure

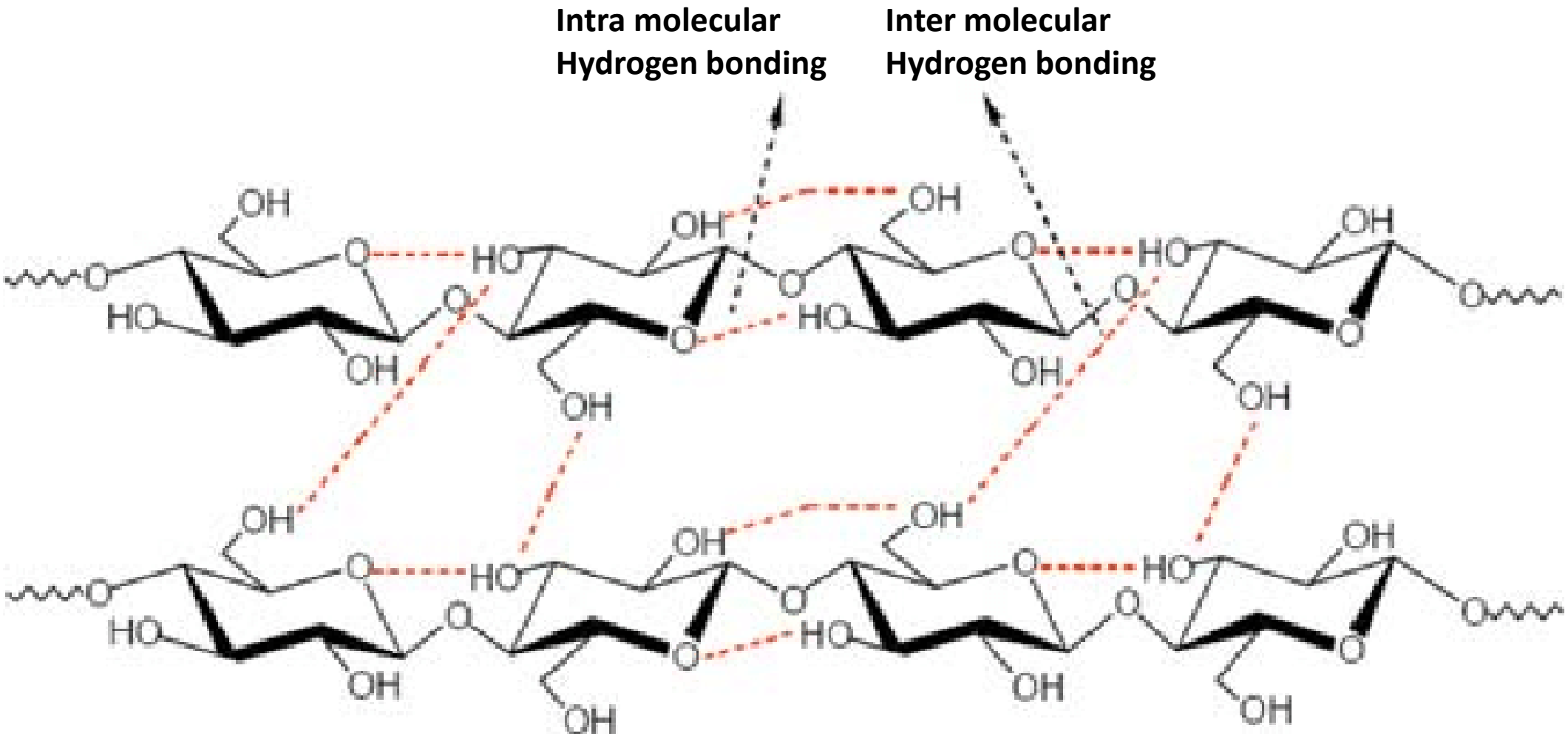

Reaction site, β-(1→4)-glycosidic bond, in cellulose hydrolysis

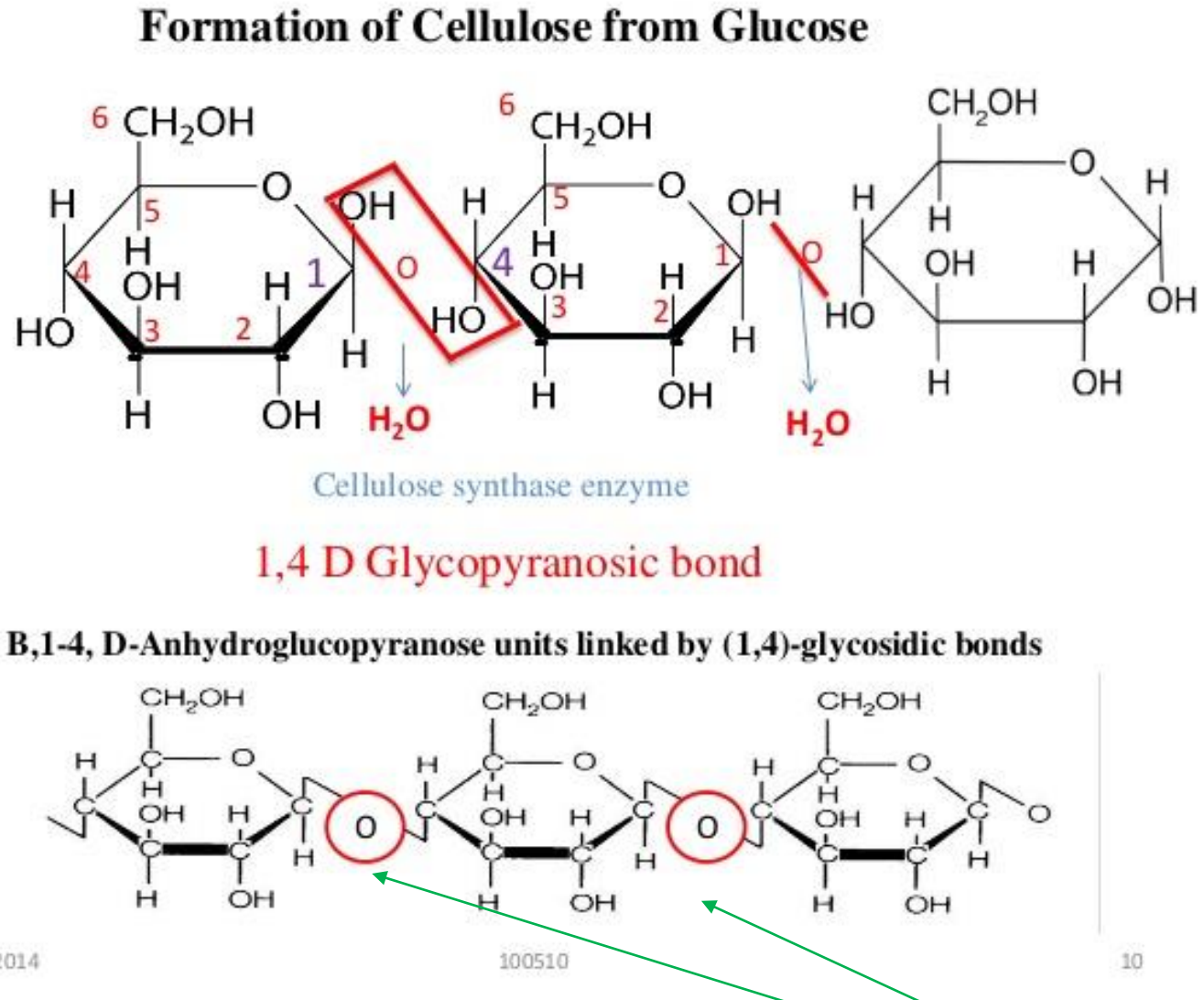

Reaction site of cellulose hydrolysis

^{1}H NMR spectra of hydrolysate from biomass (423 K, 1 M HCl, 2 h)

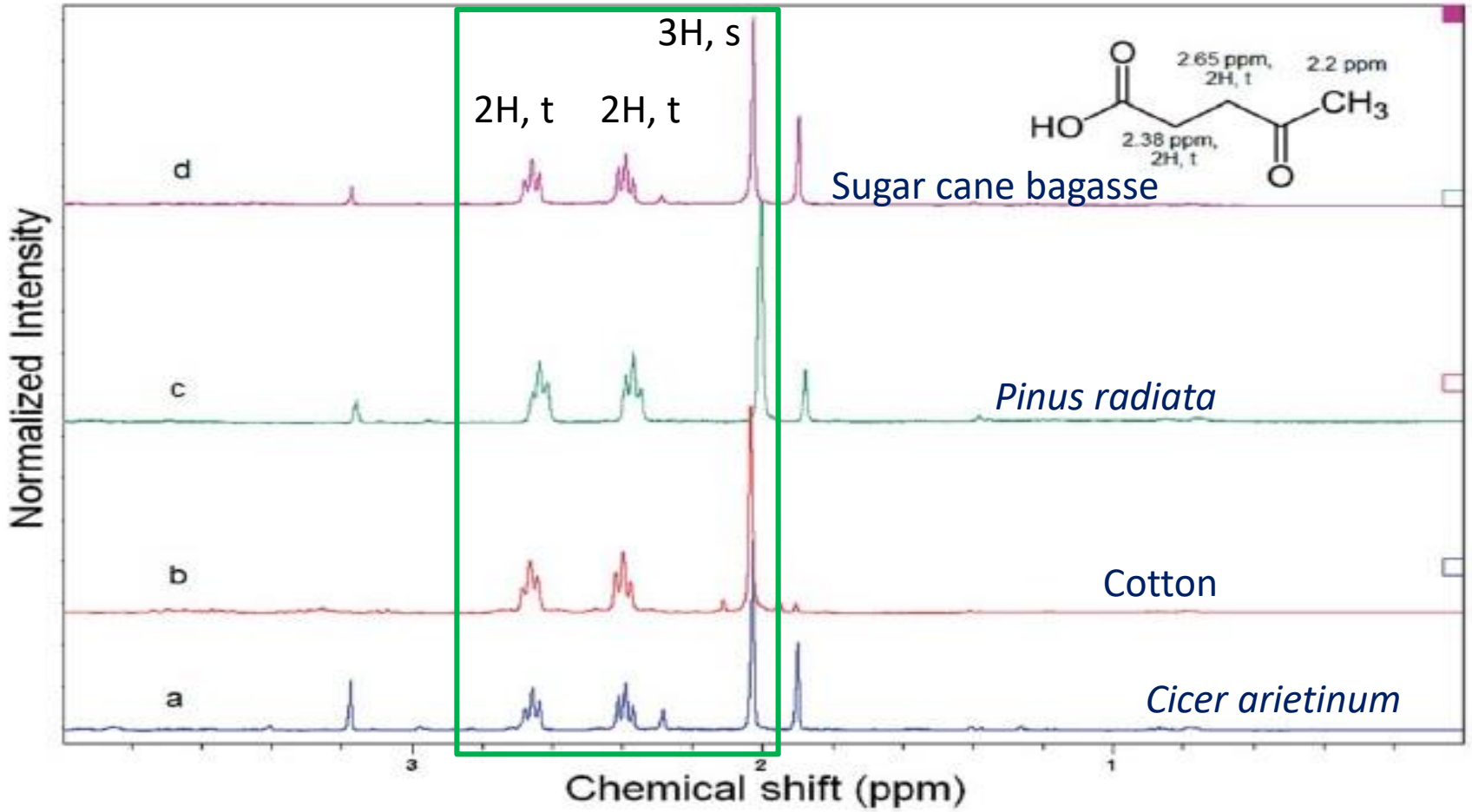

- ✓ A singlet signal at 2.2 ppm (3 H, s), two triplets at 2.38 (2H, t), and 2.65 (2H, t) ppm confirm the formation of LA acid
- ✓ Additional signal at 1.9 ppm was attributed to acetic acid, a reaction byproduct formed from the decomposition of the hemicellulose component of CA, PR, and SCB.
- ✓ As expected the signal of acetic acid is absent in the product obtained from cotton as cotton does not contain hemicellulose.

^{13}C NMR spectra of hydrolysate from biomass, 423 K, 1 M HCl, 2 h

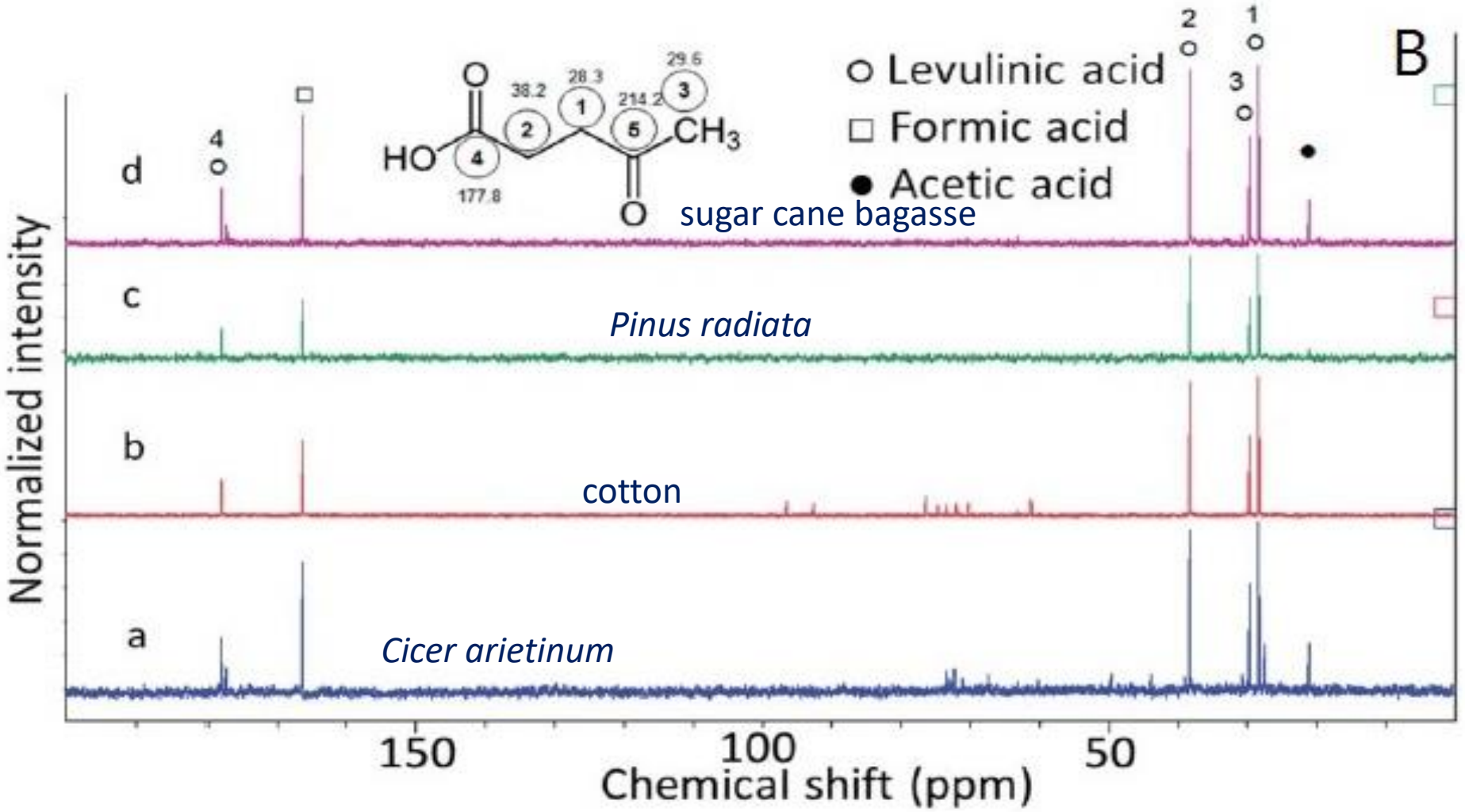

- ✓ Signals observed at 28.3 and 38.2 ppm correspond to two methylene groups, one adjacent to the carbonyl and the other adjacent to the carboxyl groups
- ✓ Signals at 29.6 and 177.8 arise due to the methyl and carboxyl functional groups of LA acid. Signals corresponding to the carbonyl carbon of LA acid appeared at 214.2 ppm which was not included in the presented region of the spectrum

Isolation of pure Levulinic acid from the biomass hydrolysate

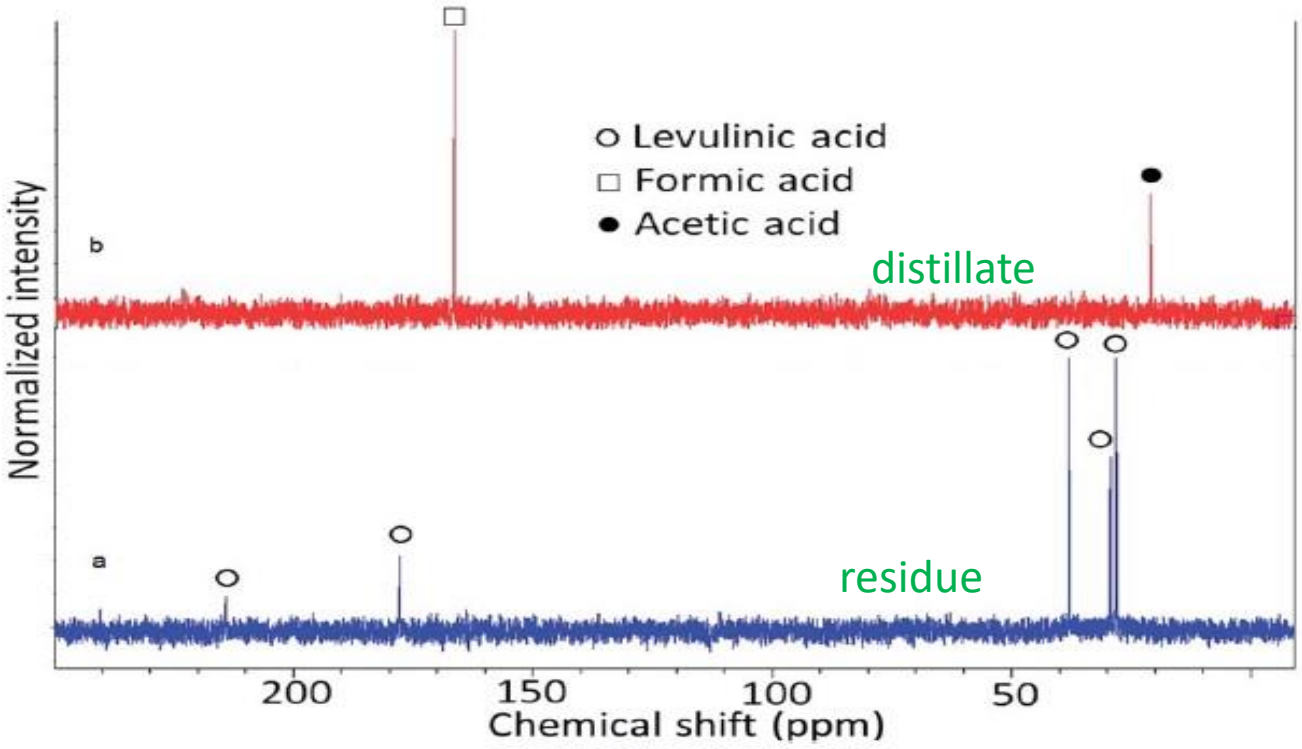

Owing to the high boiling point of LA acid (245 °C), the acid was easily isolated in pure form from the product mixture by roto evaporation at 70 °C for 1 h.

While the residue contained pure LA (**Fig. a**), the distillate contained the low boiling by-products (acetic and formic acid) (**Fig. b**).

^{13}C NMR spectra of (a) residue and (b) distillate separated from the hydrolyzate obtained from sugar cane bagasse using roto evaporation

Effect of particle size of corn stover on LA yield

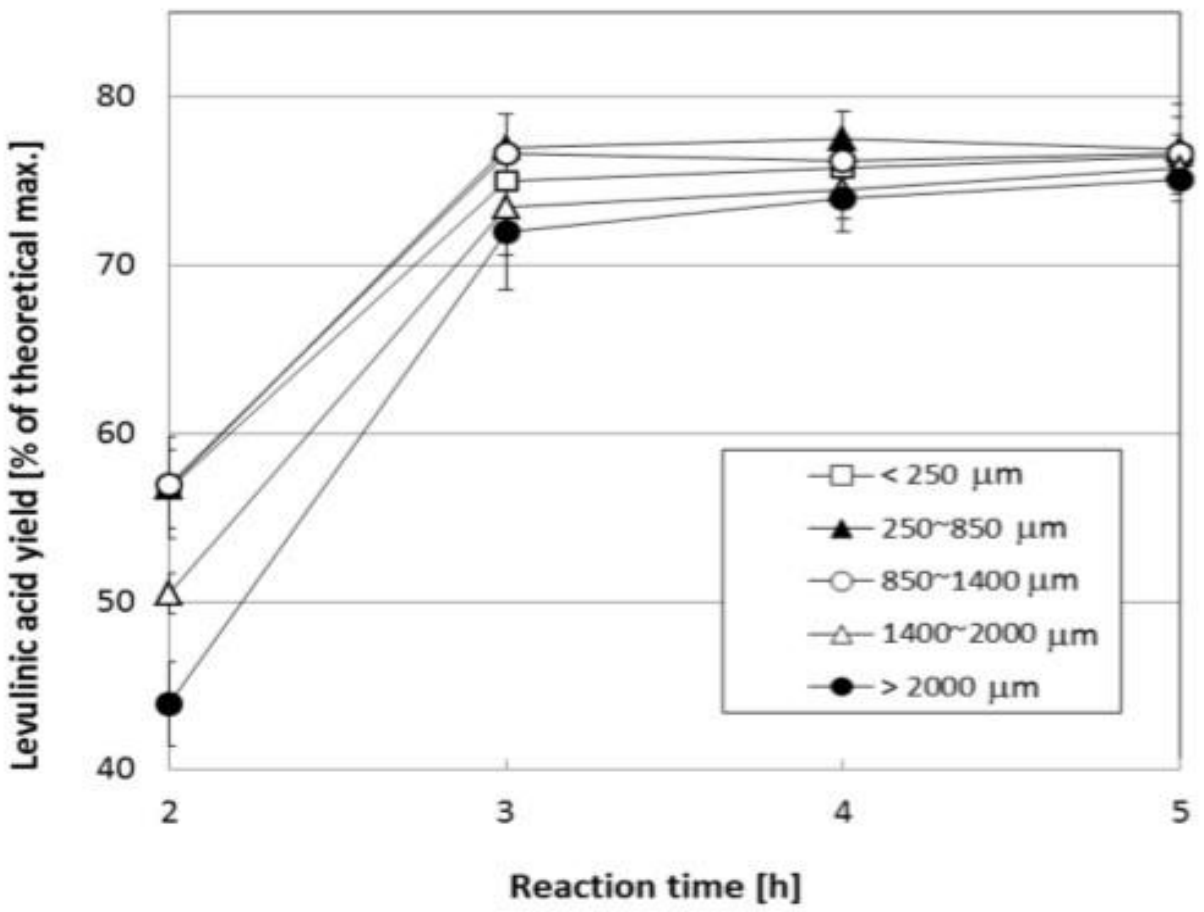

Effect of biomass (corn stover) particle size on the yield of levulinic acid upon reaction time 1 M HCl, 150 °C, 50 g/L solid loading).

After 2 h of reaction time, CS with large particle size (> 2000 µm) showed the low yield of LA (43.9 wt.%) where as biomass with smaller particle size (≤ 250 µm) resulted in higher LA yield (56.7 wt.%)

This is in accordance with the accessible surface area and reaction sites on the biomass for the acid catalyst (H^+)

However, with an increase in the reaction time (3-5 h), no significant effect of particle size on the yield of LA is observed

After 5 h of the reaction, irrespective of the biomass particle size high yields of LA (75.1 - 77 wt.%) were observed

This could be due to the attainment of a state of equilibrium in the penetration of the acid catalyst throughout the bulk of the biomass particles of varying sizes during 3-5 h of the reaction resulting in nearly constant yields of LA.

Pulidindi and Kim, Energies, 11, 2018, 621

Particle size of biomass effects LA yield only during initial stages of reaction

Effect of biomass type on Levulinic acid yield

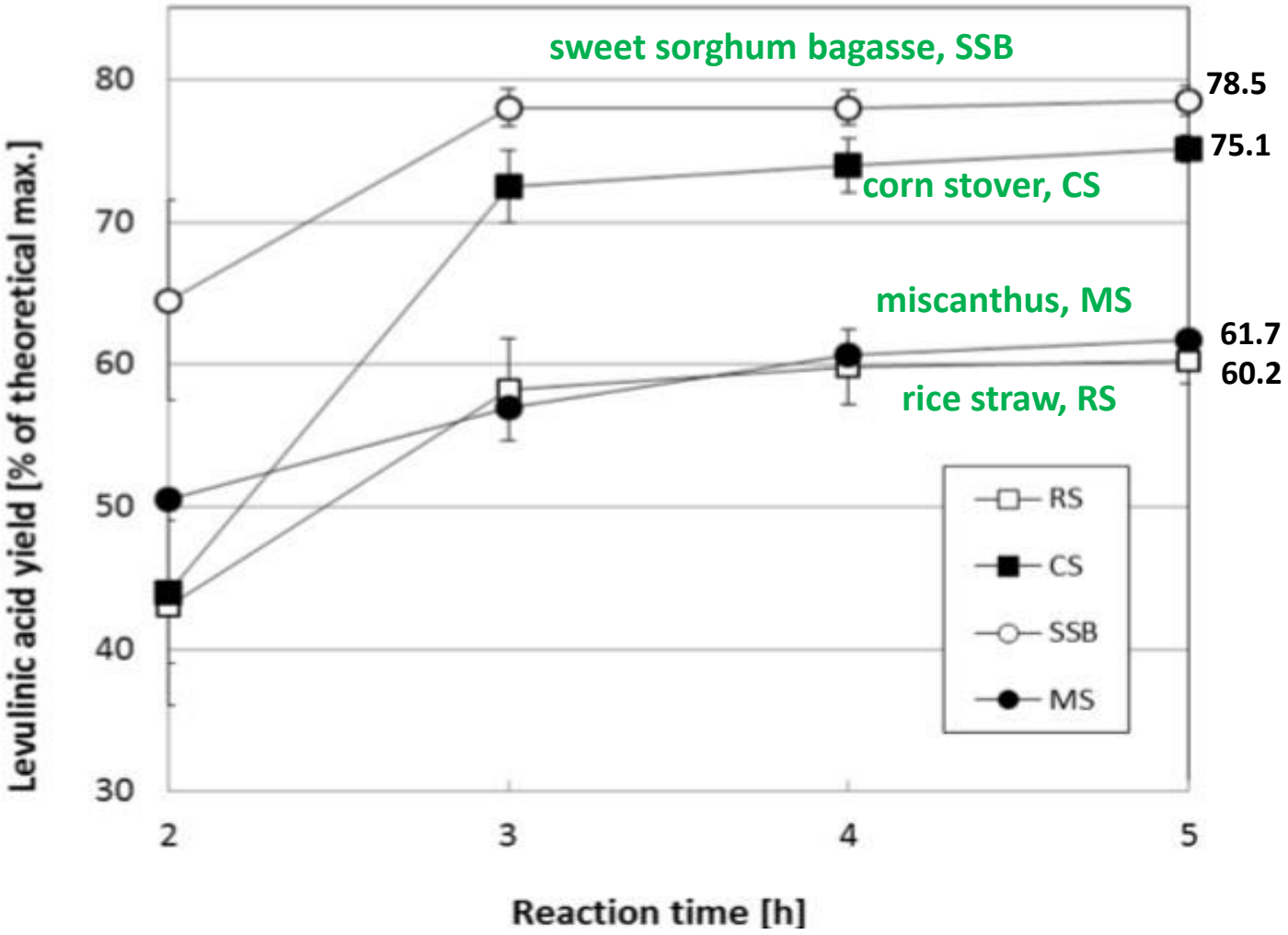

Sweet Sorghum Bagasse showed highest yield of LA

With an increase in reaction time from 2-5 h, the yield of from SSB increased from 64.5 to 78.5 wt.%.

Second highest LA yield (75.1 wt.%) was obtained from Corn Stover in 5 h

LA yield from Miscanthus and Rice Straw were only 61.7 and 60.2 wt.%, respectively

Presence of least amount of lignin (13.3 wt.%) in SSB could be attributed to the highest yield of LA

In a similar way, the presence of high amounts of lignin 17.1 and 19.6 wt.%, respectively, in RS and MS has contributed to the lower yield of LA

Reaction conditions: Particle size > 2000 µm; 1 M HCl, 150 °C, 50 g/L solid loading.

Chemical composition of biomass effects the yield of levuinic acid

Effect of green liquor pretreatment on biomass composition

Simulated green liquid: prepared by dissolving appropriate amounts of Na_2CO_3 and Na_2S in deionized water

SGL pretreatment conditions:

Total titratable alkali (Na_2CO_3 + Na_2S), 20 wt. % of total oven dry weight of biomass

Sulfidity (wt. % of Na_2S), 40 wt.% of TTA loading

SGL to biomass, 16:1 wt/wt %

Chemical composition of untreated and delignified biomass

Biomass	Composition							
	S.R.	Glucan	Xylan	Arabinan	AIL	ASL	Delignification	Ash
	(wt %)	(wt %)	(wt %)	(wt %)	(wt %)	(wt %)	(wt %)	(wt %)
RS	-	36.3 ± 0.1	14.0 ± 1.0	3.7 ± 0.0	15.0 ± 0.7	2.1 ± 0.4	-	8.2 ± 0.1
D-RS	57.2	63.5 36.3 ± 0.5	10.3 ± 0.1	2.3 ± 0.0	1.3 ± 0.1	0.9 ± 0.0	87.6 ± 2.0	2.6 ± 0.2
CS	-	33.0 ± 0.9	18.4 ± 0.7	5.3 ± 0.1	15.2 ± 0.3	2.2 ± 0.1	-	1.5 ± 0.1
D-CS	52.2	63.2 33.0 ± 3.7	10.0 ± 1.2	2.7 ± 0.1	0.8 ± 0.9	0.7 ± 0.1	91.2 ± 3.2	0.2 ± 0.0
SSB	-	41.3 ± 0.2	11.7 ± 0.0	3.1 ± 0.1	12.0 ± 0.3	1.3 ± 0.1	-	1.0 ± 0.1
D-SSB	60.4	68.4 41.1 ± 0.3	11.0 ± 0.2	2.1 ± 0.0	2.7 ± 0.7	0.9 ± 0.0	73.2 ± 2.1	0.2 ± 0.0
MS	-	44.3 ± 0.3	18.4 ± 0.1	3.5 ± 0.0	18.9 ± 0.3	1.1±0.1	-	2.1 ± 0.3
D-MS	71.8	61.7 43.3 ± 0.2	14.7 ± 0.1	2.7 ± 0.0	5.8 ± 0.3	0.7±0.0	64.8 ± 2.3	0.4 ± 0.2

Glucan contents of RS, CS, SSB and MS were increased to 63.5, 63.2, 68.4 and 61.7 wt.% respectively upon delignification

Green liquor pretreatment selectively removed lignin and ash content from biomass

Effect of delignification on LA yield

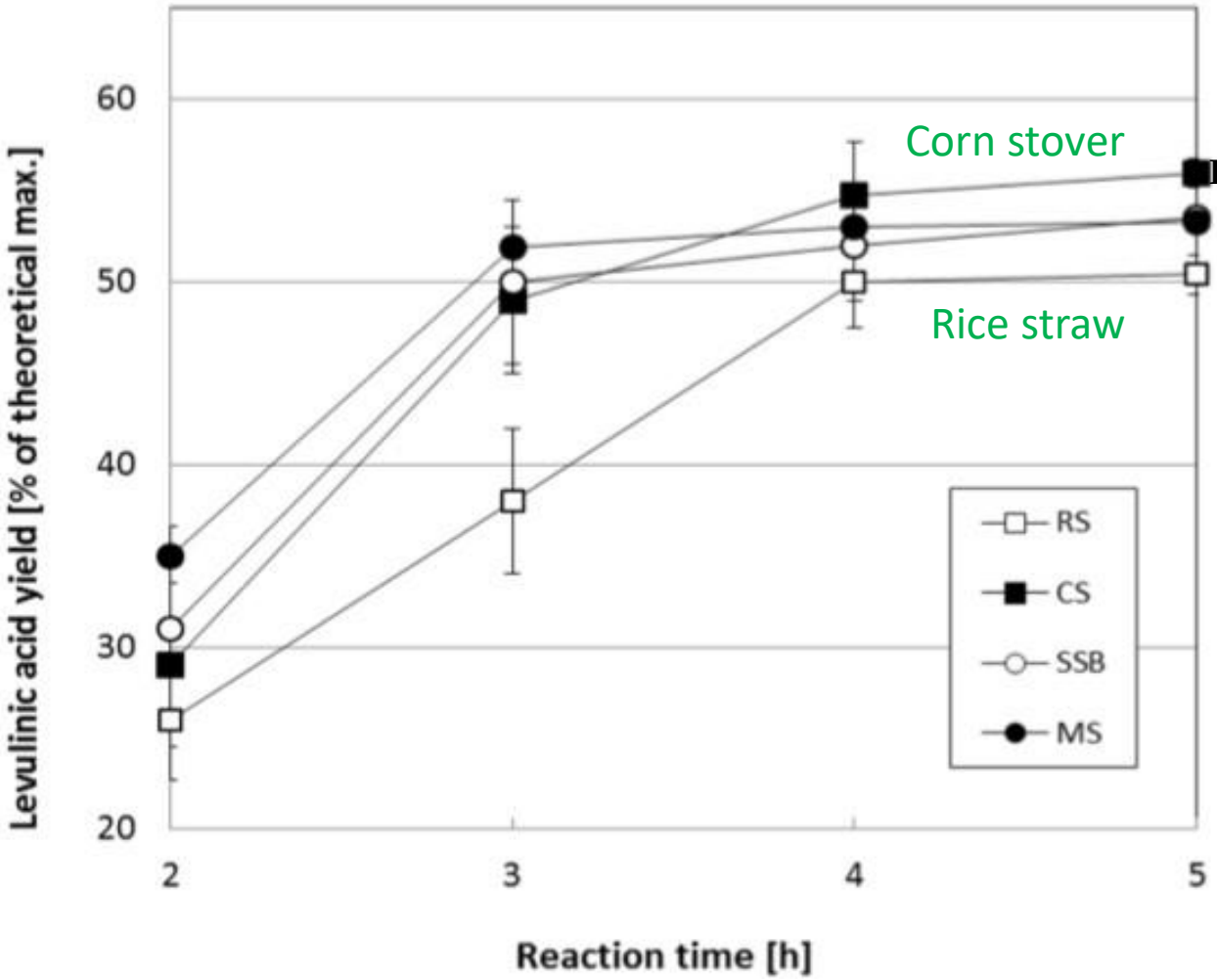

From RS, CS, SSB and MS, 87.6, 91.2, 73.2 and 64.8 wt.%, lignin was removed

LA 56.0; Lignin removed 91.2

LA 53.6, 53.3; Lignin removed 73.2 and 64.8

LA 50.4; Lignin removed 87.6

Regardless of the extent of delignification LA yields of all the delignified biomasses were about the same (50-56 wt.%).

Hemicellulose component of biomass which is branched and amorphous in nature could be easily hydrolyzed to C5 sugars (mainly to xylose) and undergoes dehydration reaction in acidic environment forming furfural.

Furfural further reacts with glucose and forms humins (insoluble polycyclic aromatic carbonaceous compounds) reducing the LA yield

With delignification the conc. of LA in the product was enhanced by a factor of 1.3 – 1.5

Reaction conditions: Particle size > 2000 µm; 1 M HCl, 150 °C, 50 g/L solid loading

Accelerated production of levulinic acid from glucose using microwave irradiation with synergistic catalytic performance

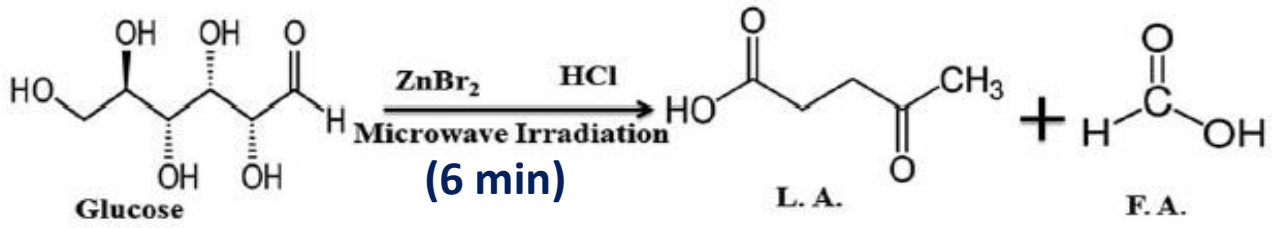

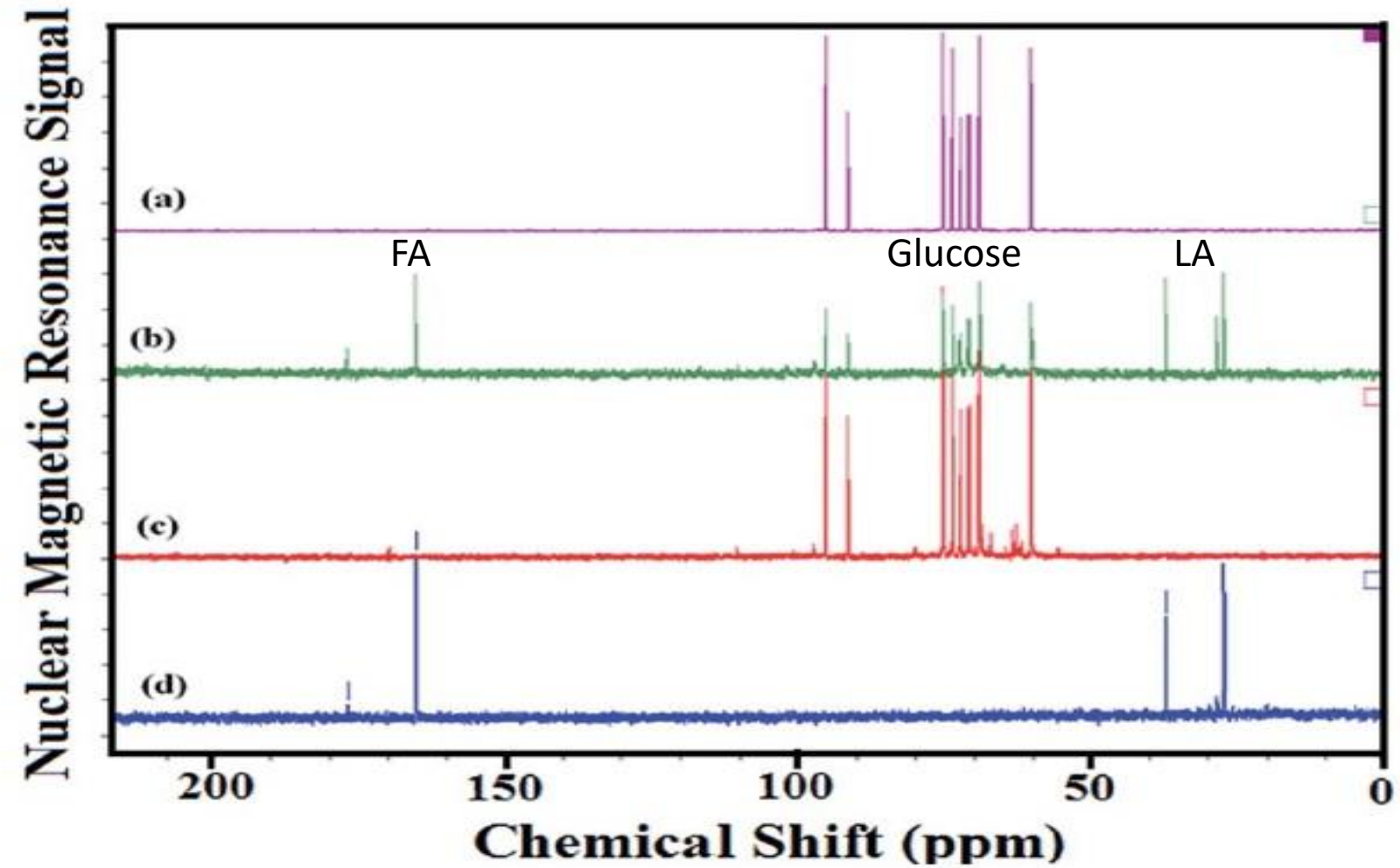

No catalyst; No reaction

Only HCl
Partial conversion

Only $ZnBr_2$
No reaction

Both HCl and $ZnBr_2$
Complete conversion

Effect of microwave irradiation time on LA yield (mixture of HCl and $ZnBr_2$ as catalysts)

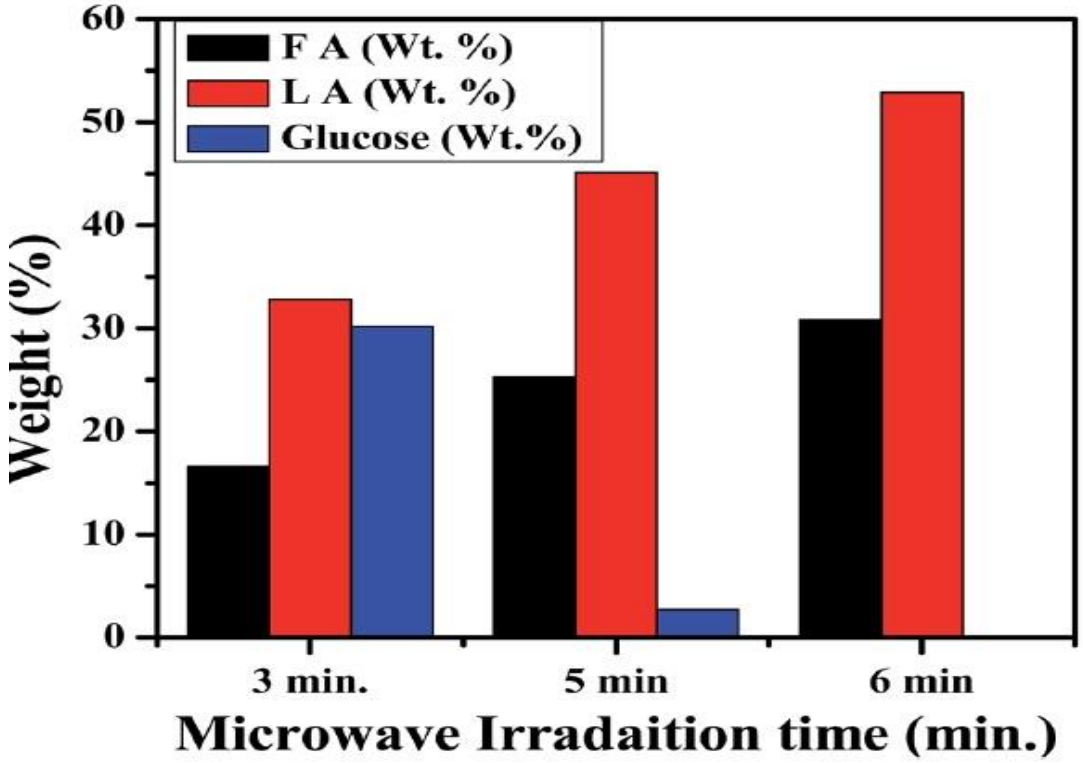

Quantification of levulinic acid, formic acid and glucose by HPLC in hydrolysate obtained after the reaction at different microwave irradiation time

A steady increase in the LA acid yield from 34 to 53 wt. % was observed as the microwave irradiation time of the reaction mixture was increased from 3 to 6 min

Towards the design of nanocatalysts for levulinic acid production!

Why Solid acids?

- Acid strength can be modulated
- High catalytic activity and selectivity
- Nature of acid sites is known
- Modification of acidity can be confirmed
- Do not corrode the reactors
- Repeated use is possible
- Separation is easy
- Safe to handle

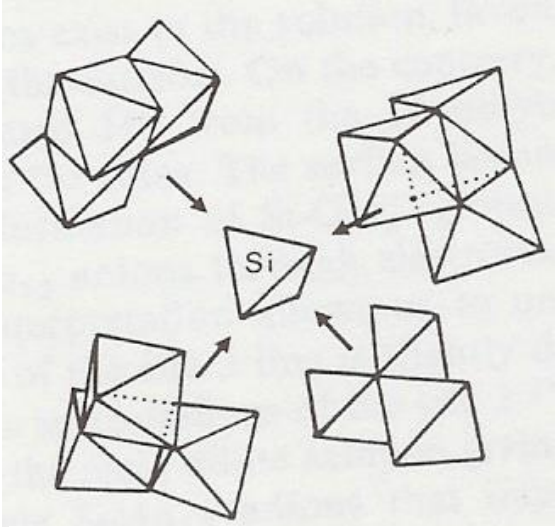

Heteropoly acids – Unique features

- Strong solid Bronsted acids
- Presence of large number of water molecules (~6 - 29)
- Multifunctionality
- Structural mobility
- Can function as homogeneous as well as heterogeneous catalysts
- Easy alteration of chemical composition
- Efficient oxidants
- Insoluble in non-polar solvents
- Environmentally benign

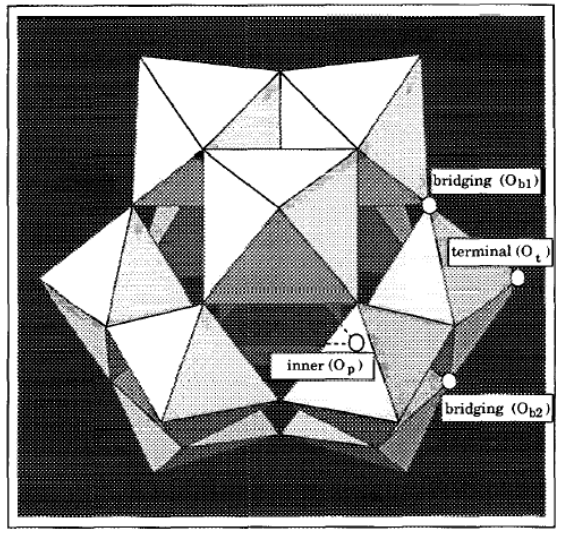

Formula	Compound
$H_3PW_{12}O_{40}.24H_2O$, HPW	Tungstophosphoric acid
$H_4SiW_{12}O_{40}.29H_2O$, HSiW	Tungstosilicic acid
$Cs_3PW_{12}O_{40}.8H_2O$, CsPW	Cesium salt of tungstophosphoric acid
$H_4PMo_{12}O_{40}.24H_2O$, HPMo	Molybdophosphoric acid

Biomass conversion to levuinic acid with solid acid catalysts

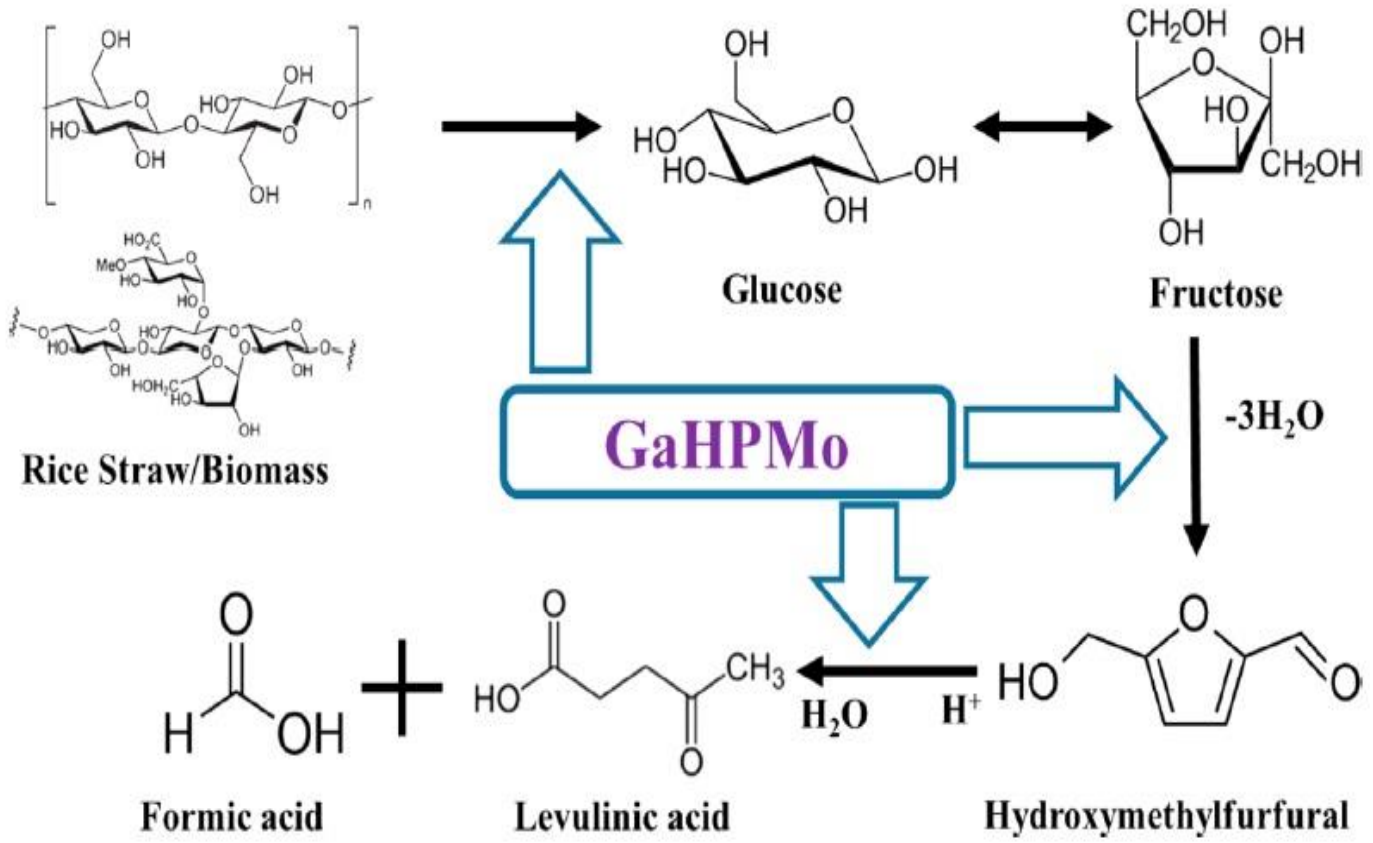

GaHPMo as solid acid catalyst for levulinic acid production

GaHPMo solid acid catalyst
UV-Vis and FT IR analysis

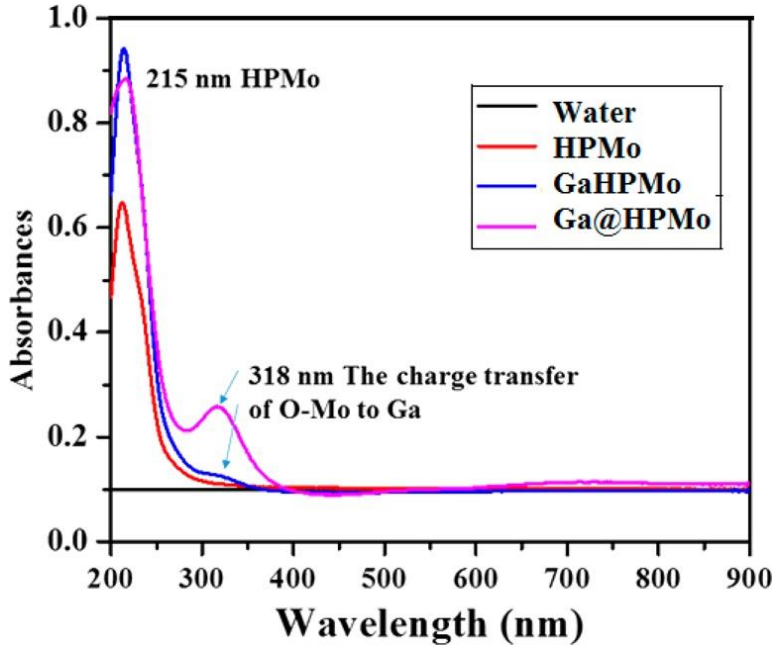

UV−vis spectra of HPMo, GaHPMo, and Ga@HPMo

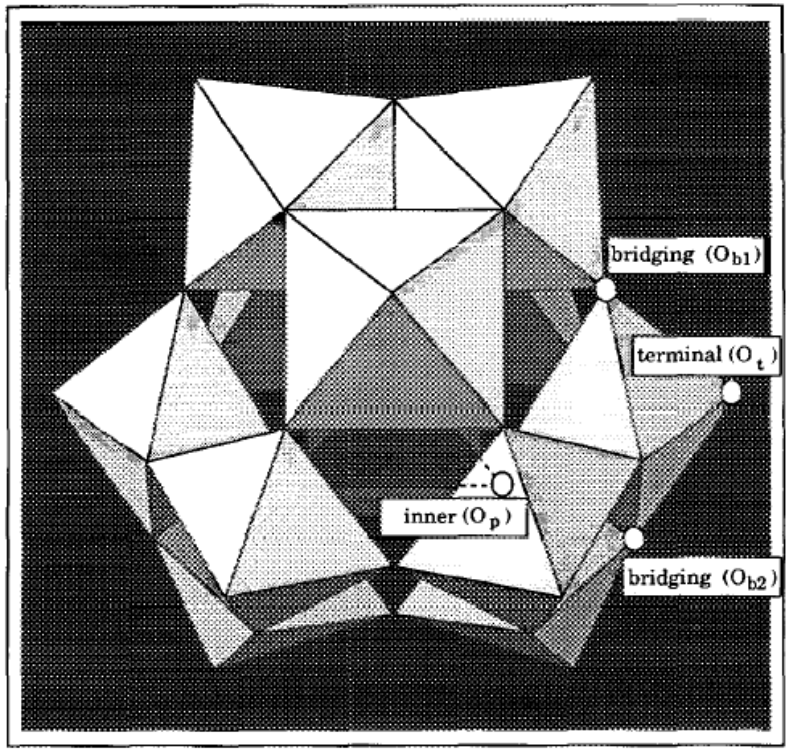

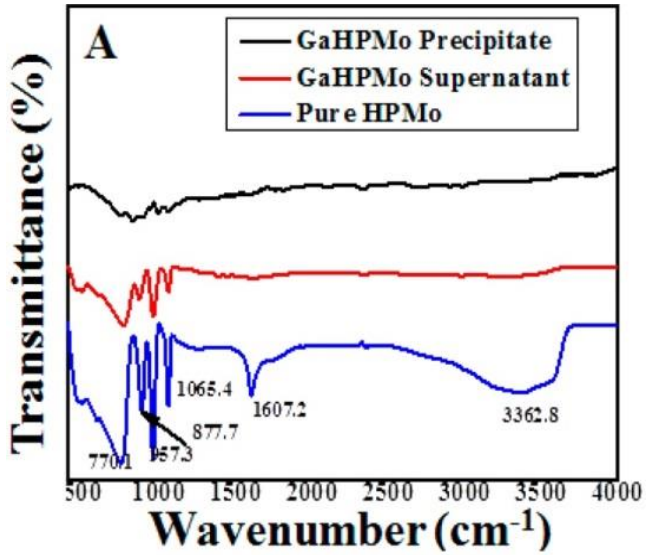

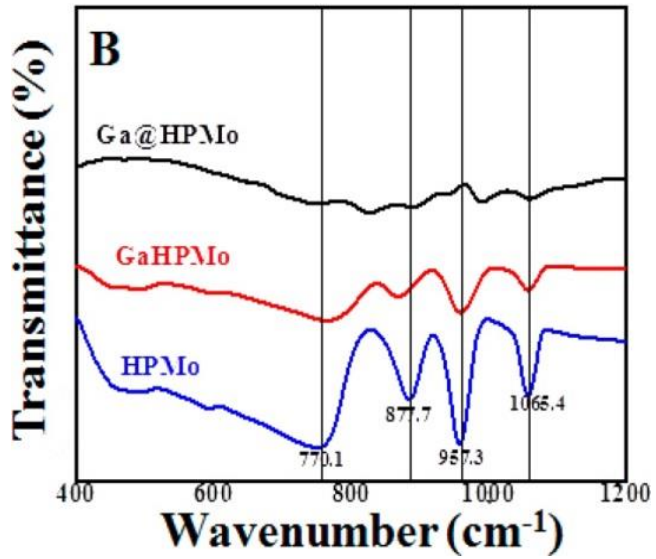

FTIR spectra

Bands at 1065, 957, 877 and 770 cm^{-1} were attributed to the stretching modes of P-O, Mo=O, Mo-O_e-Mo and Mo-O_c-Mo respectively

Gedanken et al., Energy & Fuels, 30(12), 10583-10591

GaHPMo solid acid catalyst – DLS, SEM and EDAX analysis

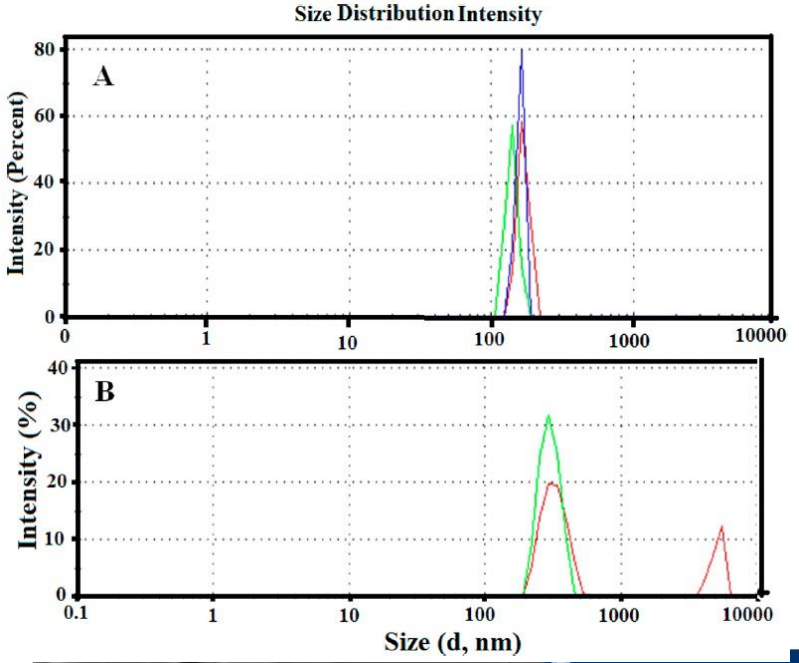

100-200 nm with a narrow size particle size distribution

50-400 nm particle size and broader particle size distribution

micrometer size particles of Ga@HPMo were also observed

Particle size distribution of (A) GaHPMo and (B) Ga@HPMo from DLS analysis

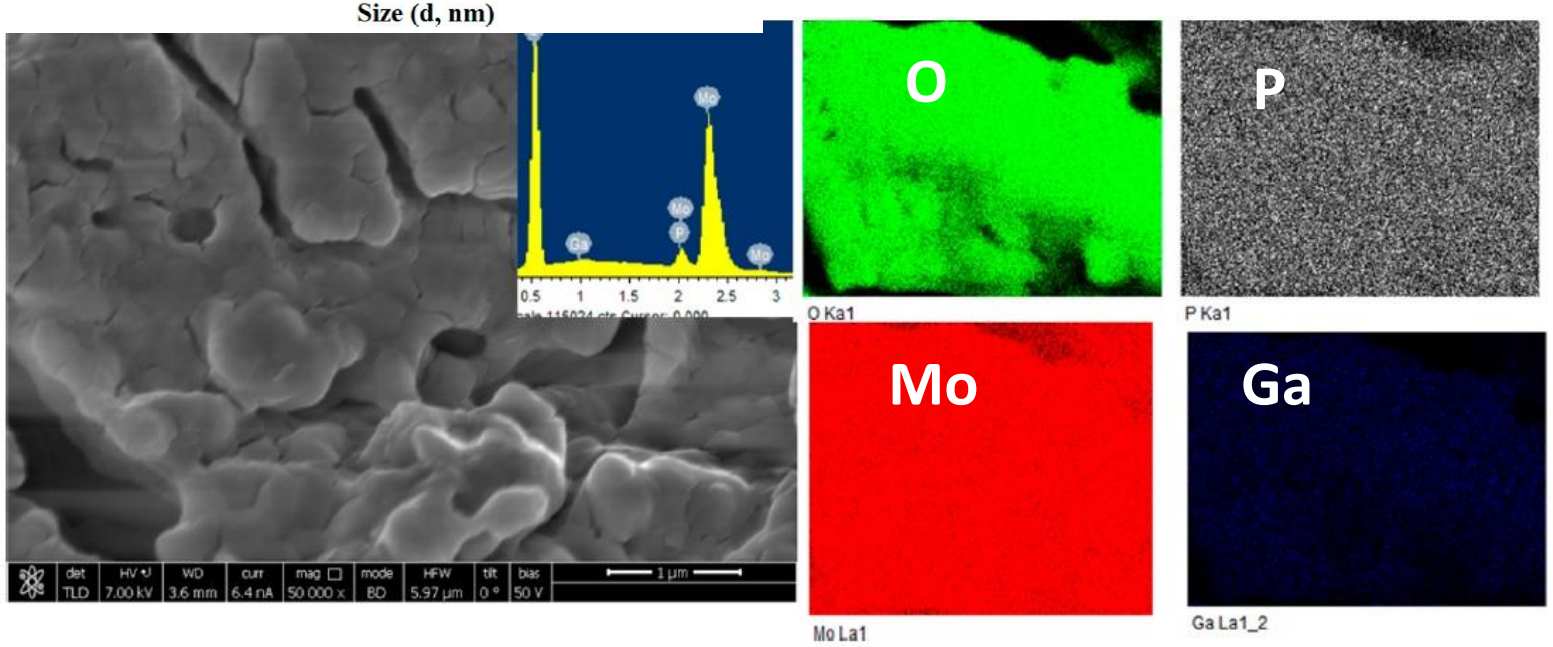

Uniform distribution of Ga metal particles near the location of oxygen indicate that the Ga^{3+} species are close to O^{2-} species of the $[PMo_{12}O_{40}]^{3-}$.

SEM images with elemental mapping of GaHPMo

GaHPMo solid acid catalyst – XPS analysis

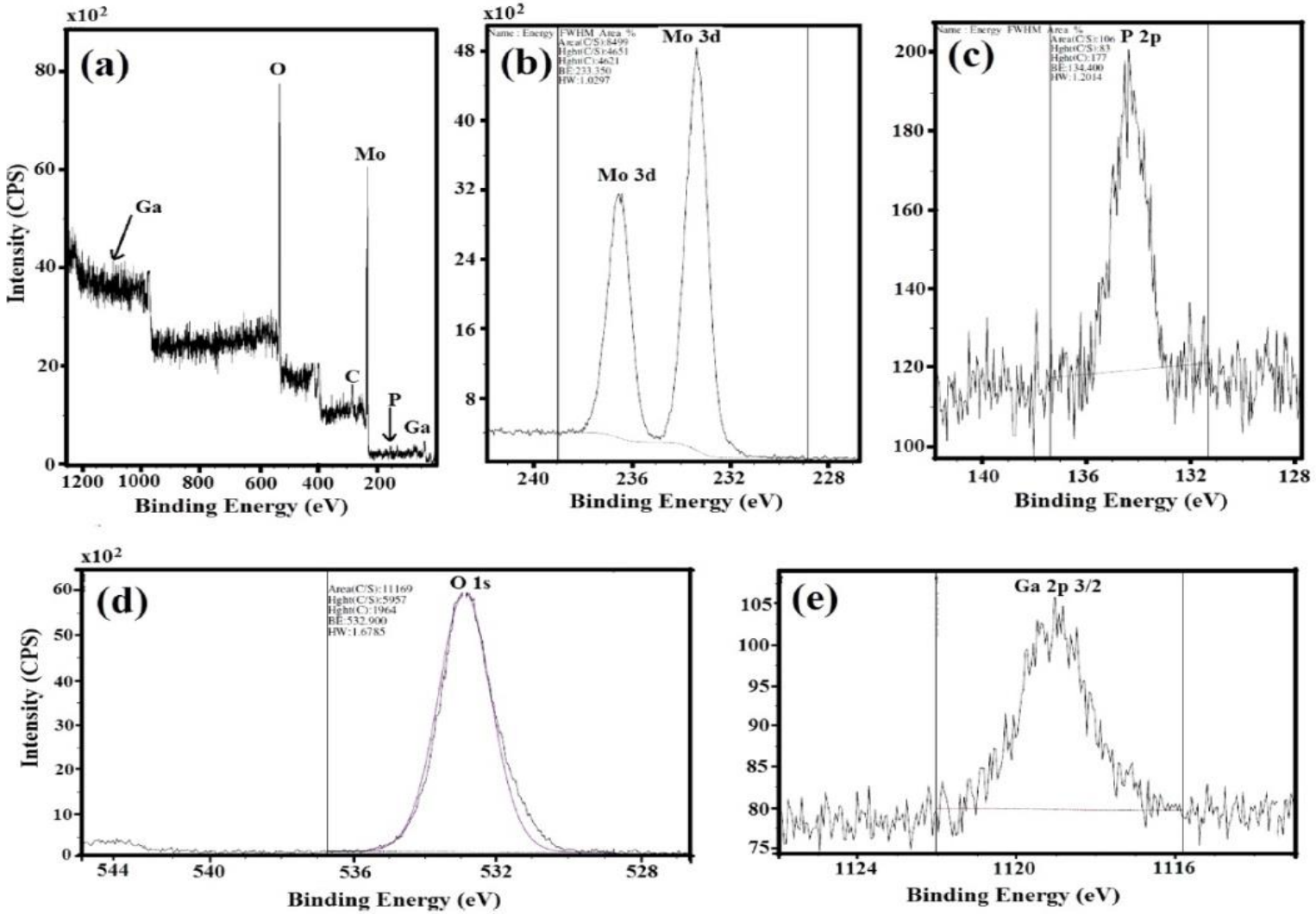

Ga (3d, 20.188 eV; 2p – 1118.612 eV) – Ga^{3+}
Mo (3d, 233.350 eV) – Mo^{6+}
P (2p, 134.400 eV), and O (1s, 532.900 eV)

XPS spectrum of (a) GaHPMo, (b) Mo 3d, (c) P 2p, (d) O 1s, and (e) Ga 2p and 3d regions.

GaHPMo catalyst for levulinic acid production

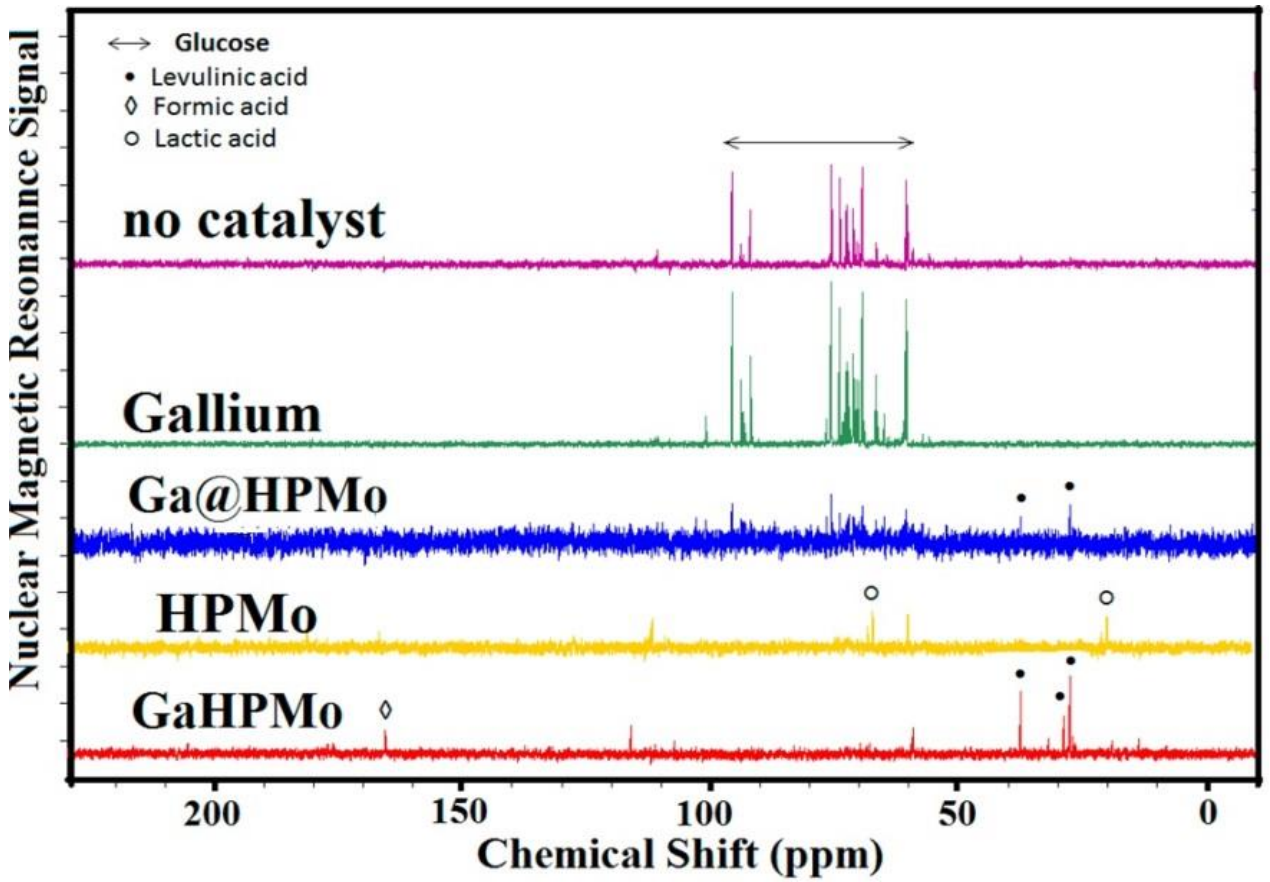

Levulinic acid yield - 56 wt.%

Best conditions:
T = 150 °C, t = 10 h,
GaHPMo/ glucose = 1:5, wt/wt

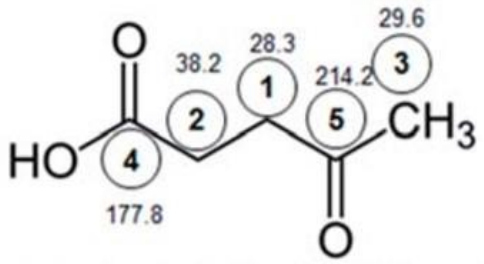

^{13}C NMR spectra of the reaction products obtained from the hydrothermal reaction (12 h at 150 °C) of glucose (0.5 g of glucose in 15 mL of H_2O) with different catalysts (0.1 g).

Gallium modified zeolite mordenite (Ga@mordenite) for the conversion of biomass to levulinic acid

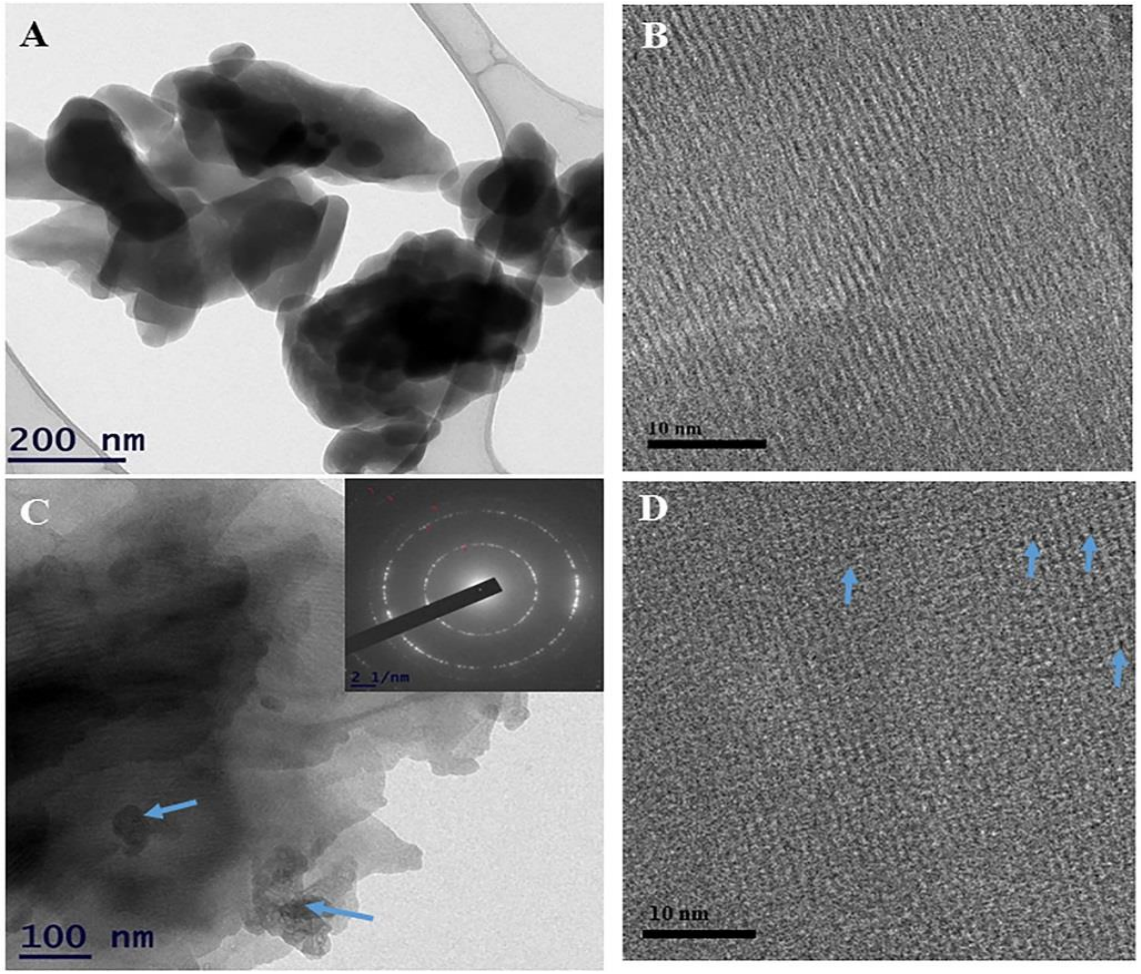

Straight cylindrical pores (fine channels) in the zeolite mordenite perpendicular to the viewing axis could be observed

Small particles of Ga metal (20 – 70 nm) were observed.

Selected area electron diffraction showed ring pattern typical of the polycrystalline nature of zeolite.

Small dot-like features seen in the HRTEM image of Ga@mordenite were attributed to the clusters composed of a few atoms of Ga.

The arrows marked in correspond to the metal particles supported on mordenite zeolite

(A) TEM (B) HRTEM images of mordenite alone (after activation) (C) TEM image of Ga@mordenite (inset: selected area electron diffraction) (D) HRTEM image of Ga@mordenite, (arrow mark indicate Ga particles on the surface of mordenite)

Gedanken et al., ChemistrySelect 2016, 1, 5952 – 5960

Characterization of Ga@mordenite)

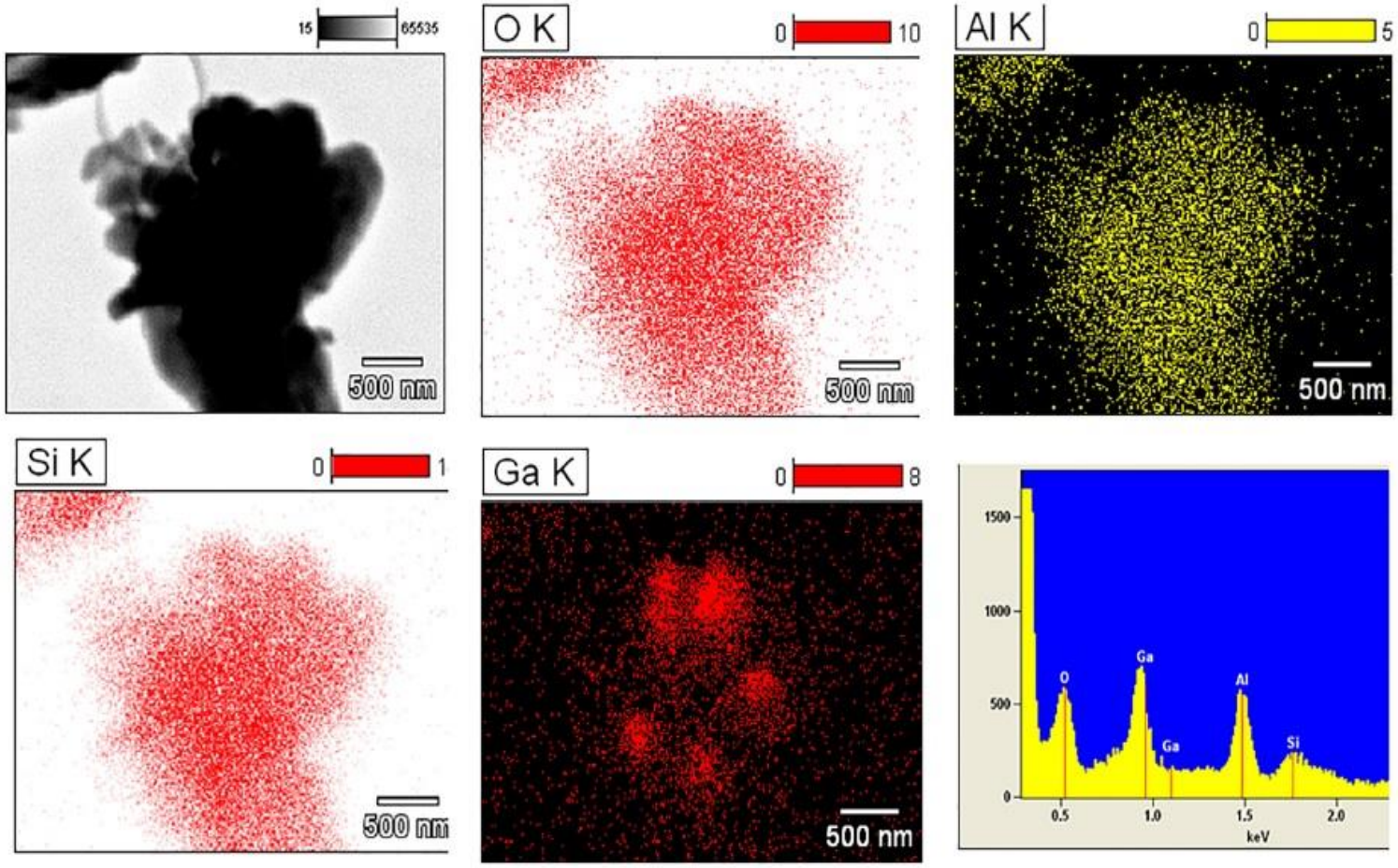

SEM image with the elemental mapping and EDS of Ga@mordenite

- Deposition of Ga on mordenite support was further analyzed by the SEM, EDS and elemental mapping
- Presence of elements like Ga, Al, Si and O was observed in the EDS spectrum
- Clusters of Ga were observed on mordenite surface from mapping of Ga on the alumino silicate (mordenite)

Characterization of Ga@mordenite

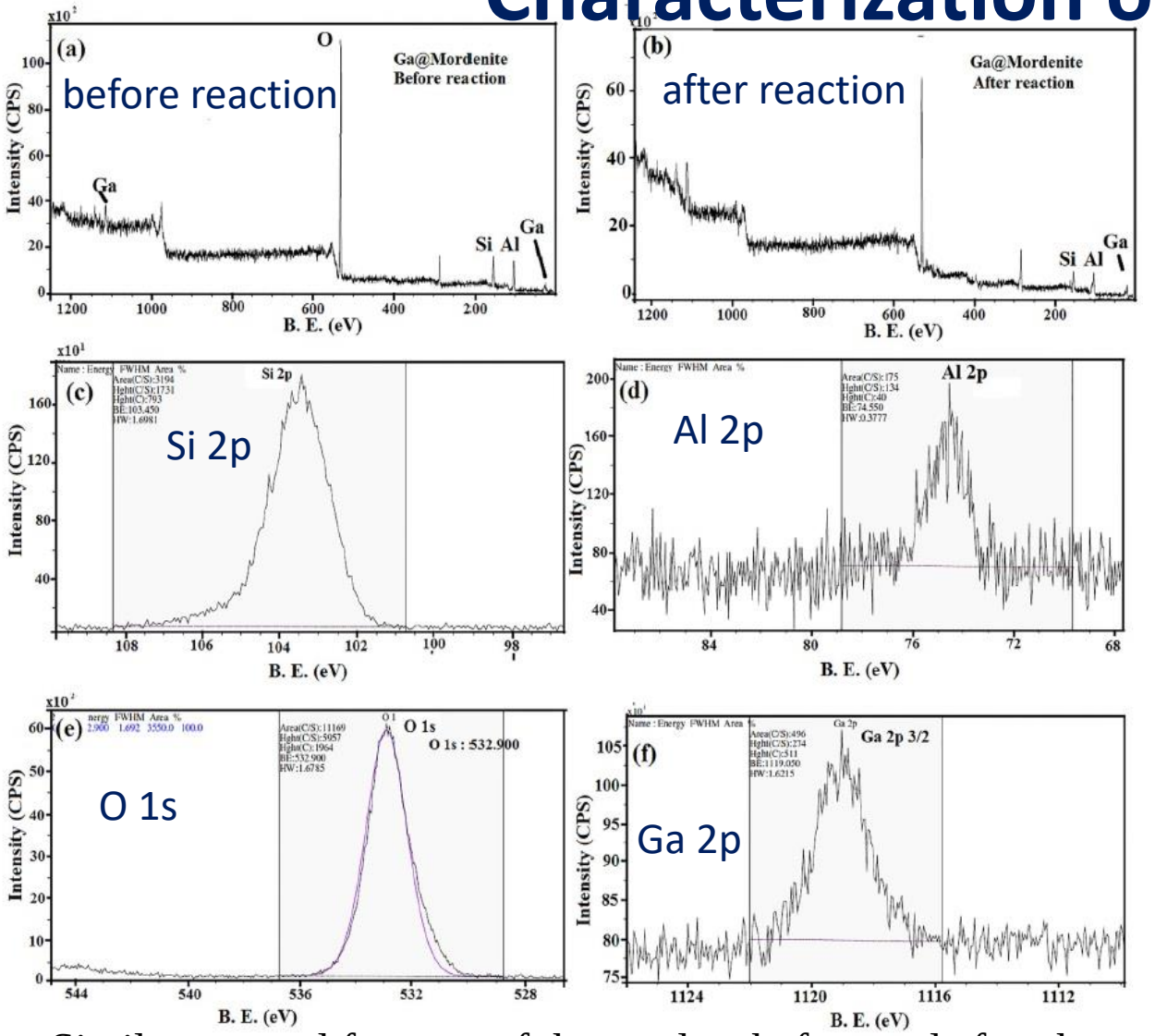

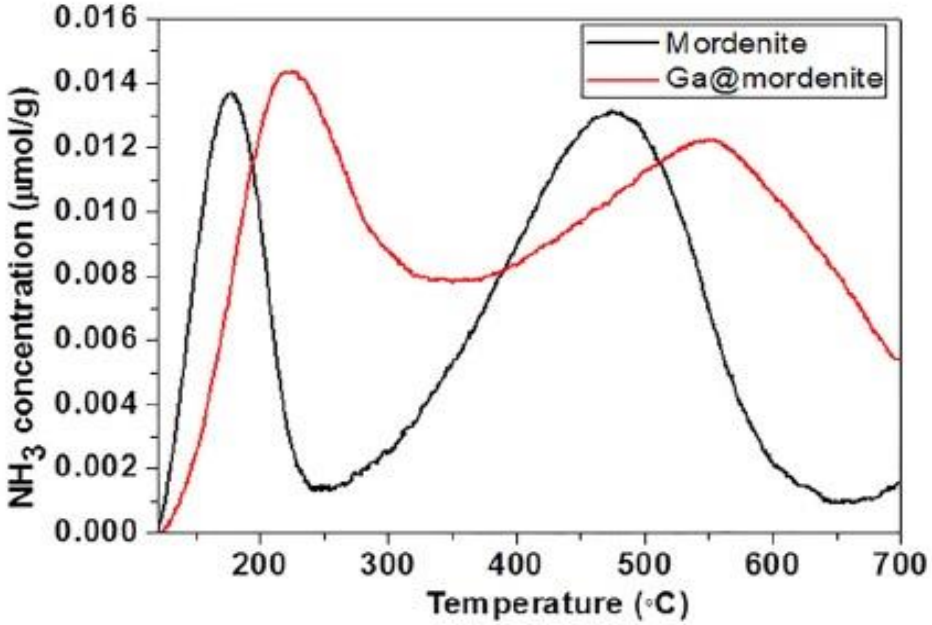

NH_3-TPD profiles of mordenite and Ga@mordenite

The peaks 178 and 476 °C in mordinite were shifted to 223 and 553 °C, respectively in Ga@mordenite. Not only the acid strength but also the acid amount (from 666.3 to 772.4 µmol/g) was increased upon modification of mordenite with Ga

Similar spectral features of the catalyst before and after the reaction indicate the stability as well as reusability of the catalyst. XPS spectra of the Si 2p (103.550 eV), Al 2p (74.850 eV), O 1s (532.900 eV) and Ga 2p (1118.612 eV) regions are shown Strong single peak at 1118.612 eV for Ga 2p and another less intense signal at 20.290 eV for Ga 3d confirm the presence of Ga^{3+} on the catalyst surface. The amount of Ga deposited on mordenite support was found to be 8.71 wt.% from ICP-OES analysis

Catalytic activity of Ga@mordenite for LA production

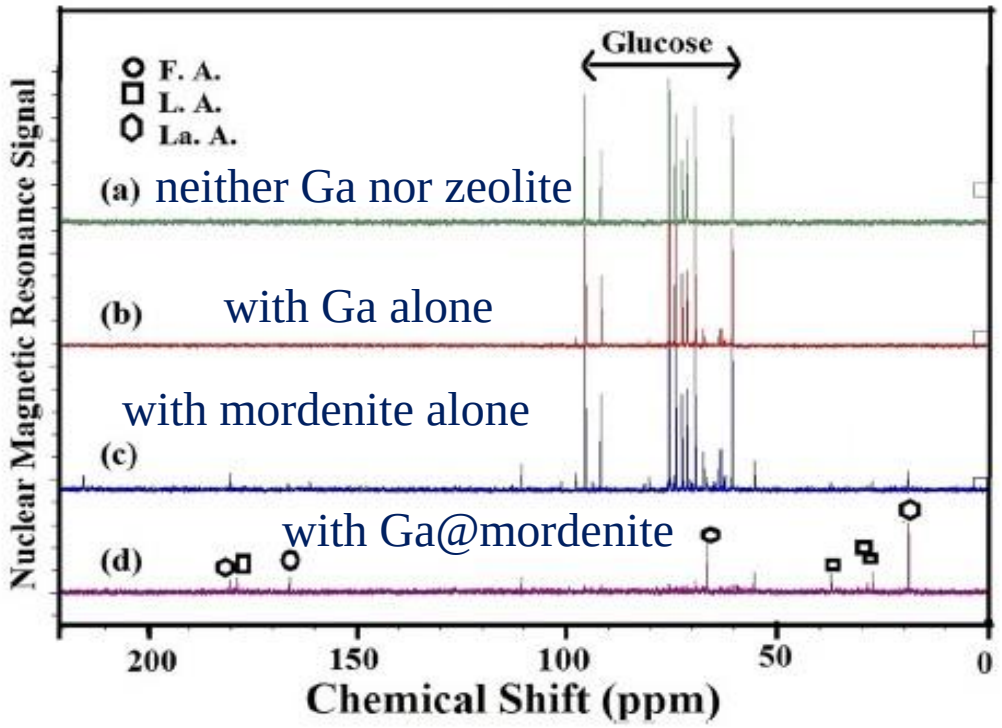

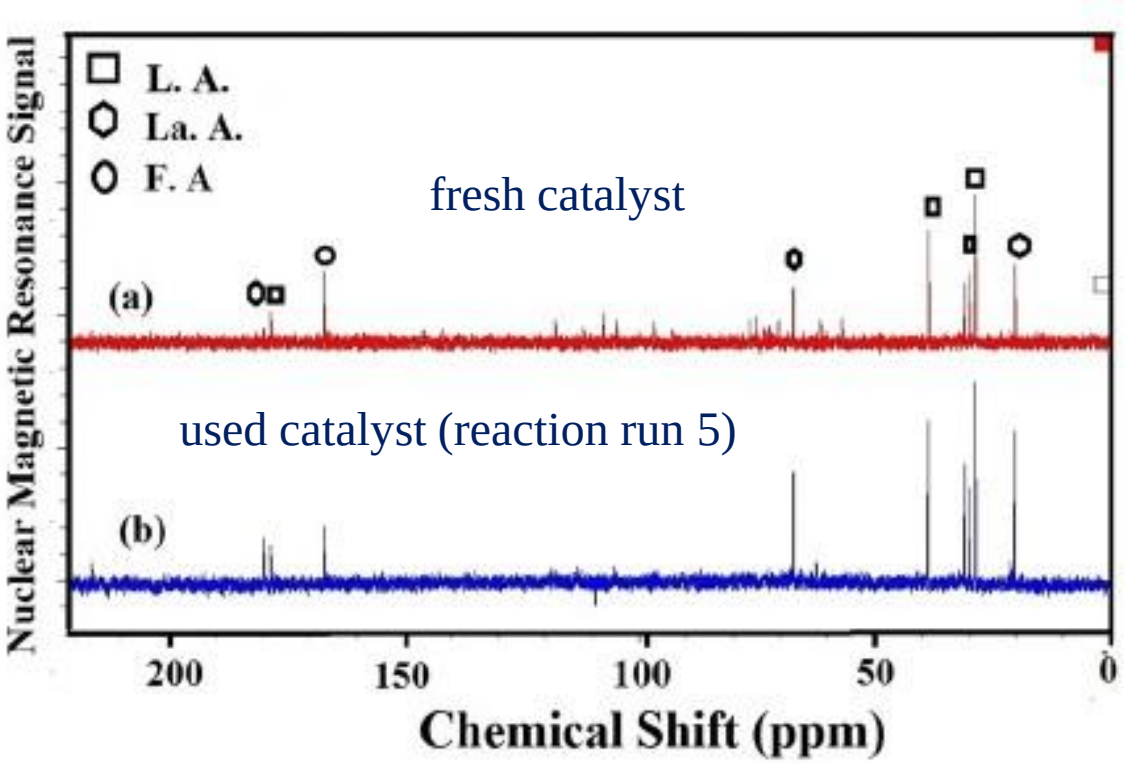

^{13}CNMR spectra of the product obtained from hydrothermal reaction (6 h, 120 °C) of glucose

Yield of LA from glucose – 59.9 wt.%

Selective production of glucose, a key economic driver of bio refinery

Glucose is a vital energy source.

This is not only true for biological metabolic activity for the sustenance of cells but also for the sustenance of the bio refinery operations.

Glucose fermentation to bioethanol operates at 51 % theoretical atom efficiency.

Likewise, glucose dehydration and rehydration to levulinic acid operates at 64.4 % theoretical atom efficiency.

Glucose is a renewable feedstock for carbon-neutral energy carrier, hydrogen.

The strategic significance of glucose prompts intense search for unconventional glucose feedstock as well as industrially adaptable methods for their conversion.

Starch hydrolysis using solid acid catalyst

Starch (potato) (0.2 g) + 20 wt.% HSiW/activated carbon (0.2 g) + 20 mL H_2O → Hydrothermal process → Glucose

Optimization of reaction temperature: 100, 120, 150 °C
Reaction time – 4 h

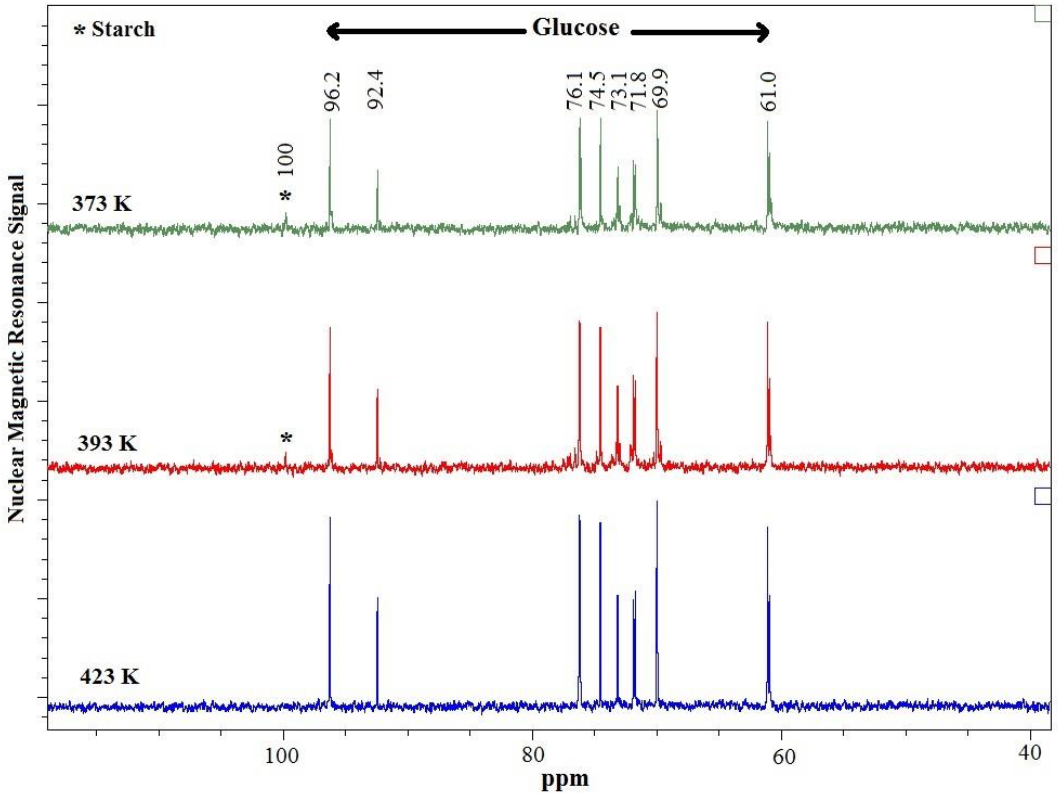

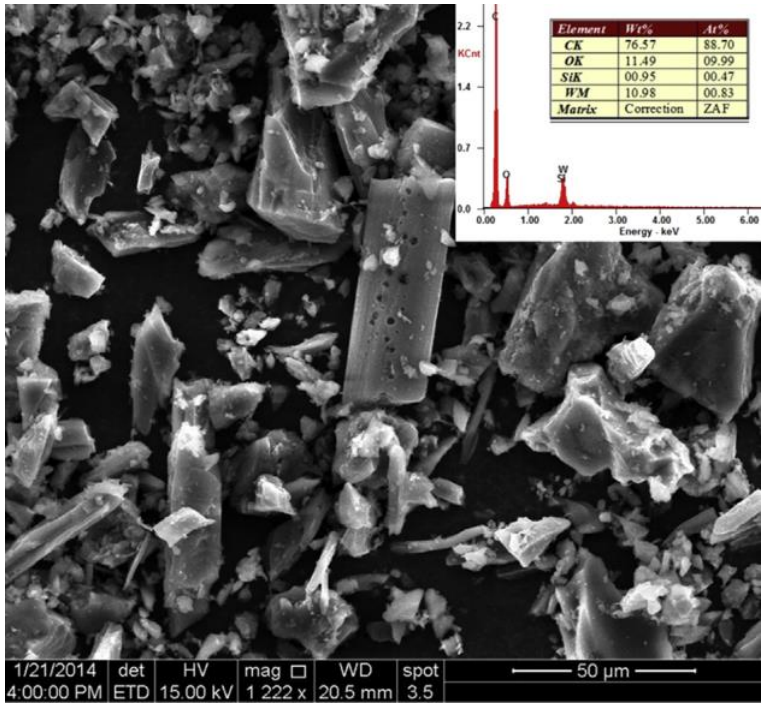

- ✓ 150 °C was found to be the optimum reaction temperature for the complete conversion of starch
- ✓ Starch is hydrolyzed selectively to glucose
- ✓ No side products like HMF, levulinic acid and formic acid were formed.

^{13}C NMR spectra of the hydrolyzate from starch as a function of temperature

Gedanken et al., Renewable Energy, 78, 2015, 141-145

Reusability of the HSiW/activated carbon catalyst

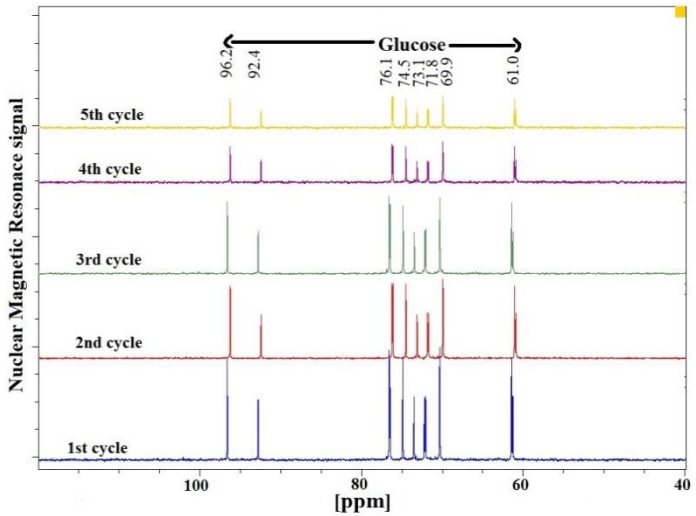

^{13}C NMR spectra of hydrolyzate from starch hydrolysis In different reaction runs

An active, selective and reusable solid acid catalyst is designed for glucose production from starch

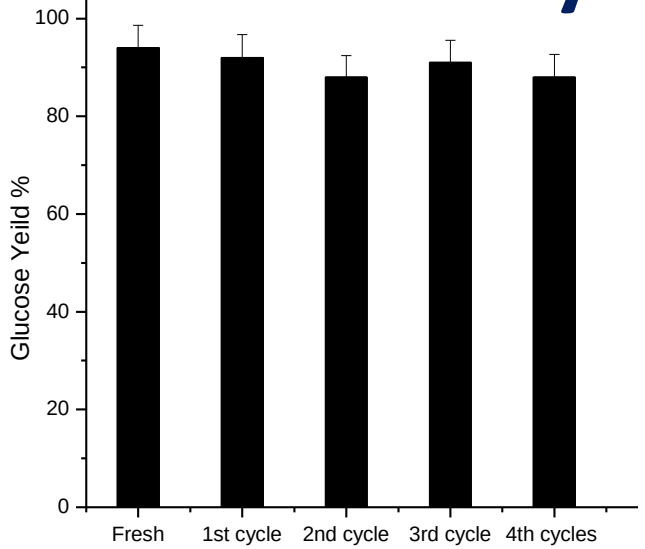

Plot of glucose yield Vs reaction cycles
(Starch - 0.5 g; HSiW/C - 0.5 g; H_2O - 20 mL; 423 K, 4 h)

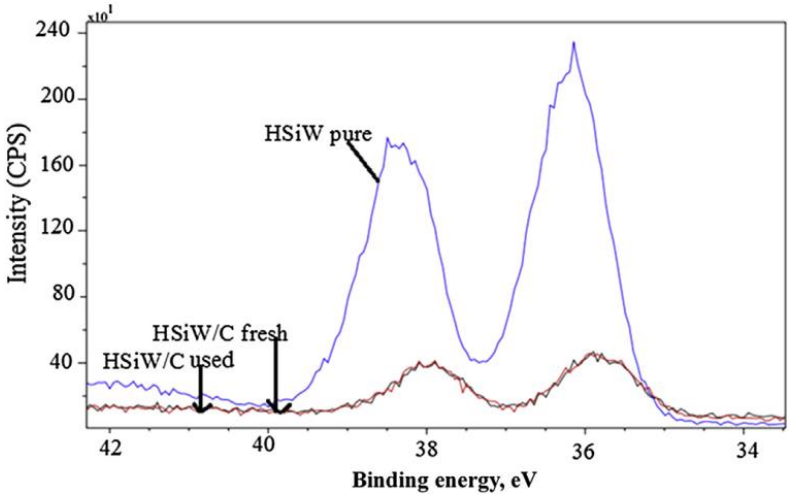

HSiW/activated carbon could be a possible substitute to amylase for starch hydrolysis

Glucose yield in each case was above 90 wt. %.

Theoretical yield of D-glucose expected from starch is equal to 111 wt. %

Peaks at 35.9 and 38.1 eV in the case of pure HSiW attributable to the W $4f_{7/2}$ and W $4f_{5/2}$ core levels respectively indicative of W(VI) species

HPA structure retained after the hydrolysis reaction

Can Glycogen be a Renewable Feedstock for Glucose?

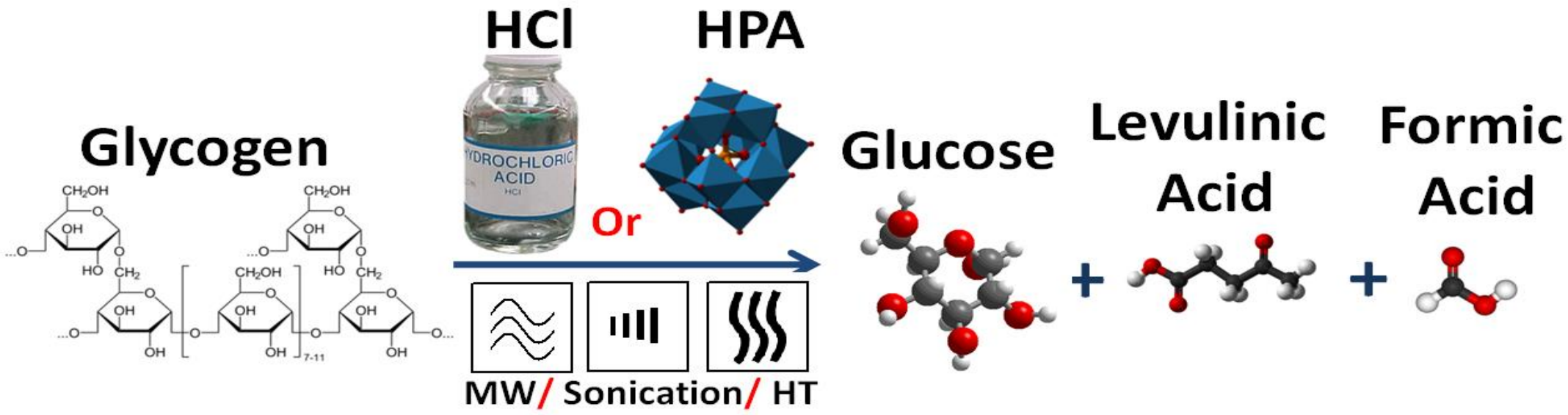

Hydrothermal, microwave and sonication based methods of hydrolysis employed
Heteropoly acids are green catalysts for glycogen hydrolysis
Glycogen from cyano bacteria is demonstrated as a potential feedstock for glucose

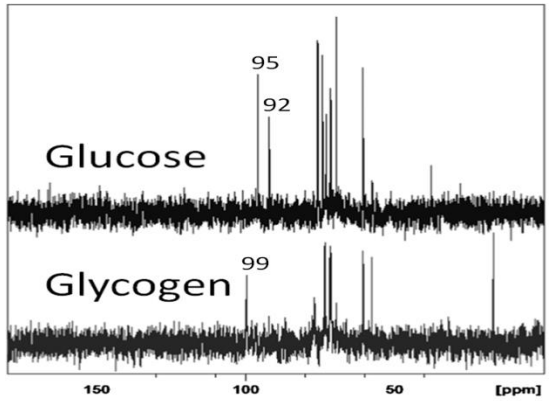

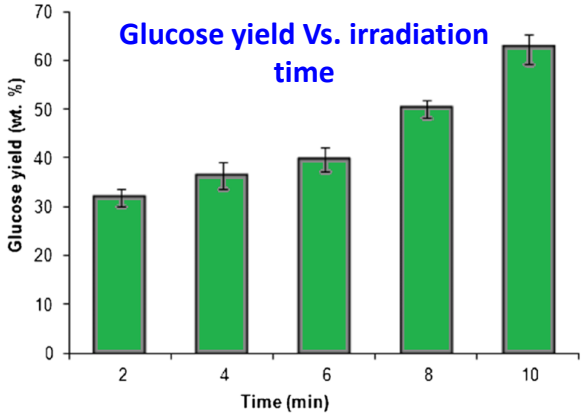

Hydrolysis conditions

- Catalyst: HCl; Irradiation time:10 min.
- Reactant/catalyst:
  0.2 g glycogen in 10 mL 1 M HCl.

Glycogen converted to glucose , levulinic and formic acids

Advantage:

complete conversion of glycogen in 10 minutes ;
yield increased from 32 to 62 wt%

Glycogen hydrolysis with microwave

Gedanken et al., RSC Advances, 2, 2012, 7262

HPW as an alternative to HCl catalyst

Hydrothermal reaction

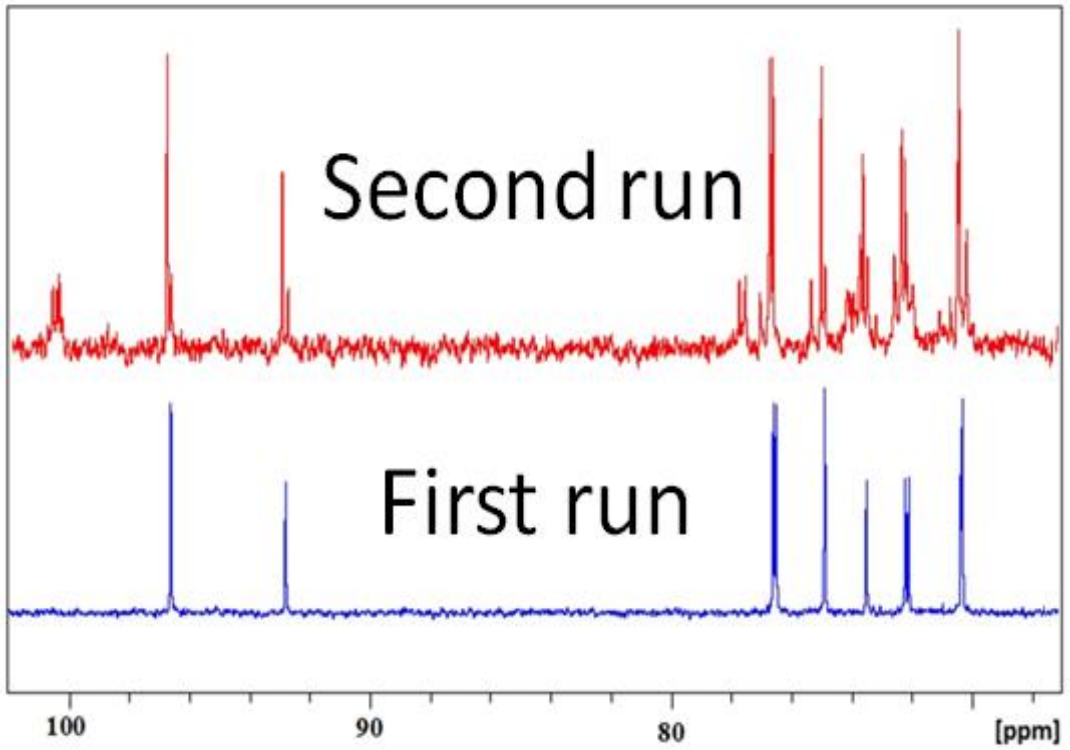

^{13}C NMR spectra of hydrolyzate with fresh and used HPW catalyst

- Reaction conditions:
1 g glycogen with 1 g HPW in 40 mL water
at 120 °C for 4 h

- Complete conversion of glycogen to exclusively glucose

No by-products like HMF, levulinic acid and formic acid were observed

- Catalyst regeneration by extraction of HPW with diethyl ether
Regenerated catalyst showed similar selectivity but lower activity for glycogen hydrolysis

Gedanken et al., Biomass Bioenergy, 76, 2015, 61

HPA's are reusable solid acid catalysts for glycogen hydrolysis

Reusability of catalyst

Catalyst stable after use (^{31}P NMR)

Peak typical of Keggin type poly anion is observed at -12 ppm before and after the hydrothermal hydrolysis reaction

In addition to HPW, HSiW was also evaluated

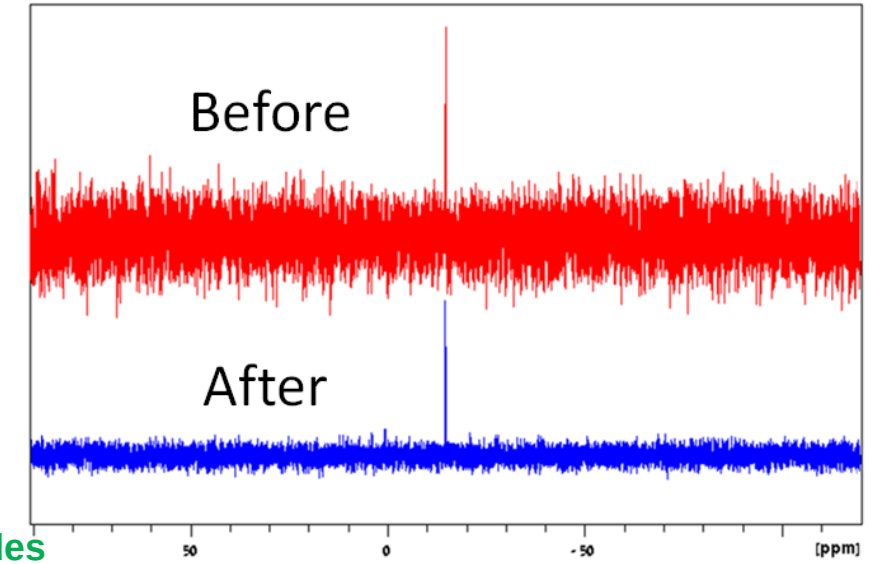

^{31}P NMR spectra of HPW

HPA's are selective and reusable catalysts for the production of glucose from polysaccharides

Glucose from cyanobacteria derived Glycogen using Heteropoly acids

Hydrolysis conditions:
0.5 g glycogen + 0.5 g HSiW + 10 mL H_2O
(from Cyanobacteria)

Microwave irradiation (2 min.) →

Glucose
+
Glycogen
(unreacted)

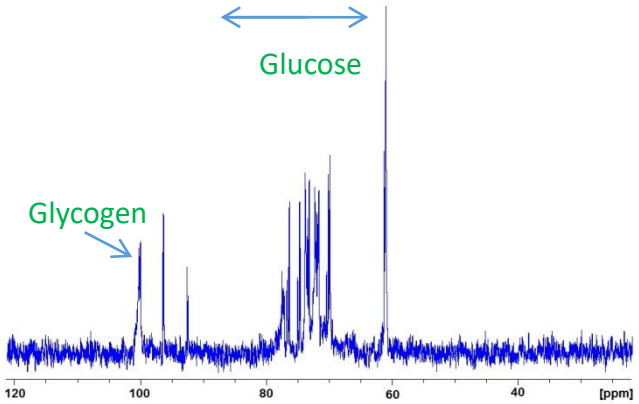

Hydrolyzate from glycogen hydrolysis after 2 min. irradiation

After 2 min. irradiation the hydrolyzate contained glucose and unreacted glycogen
Complete conversion of glycogen to glucose required 10 min. of microwave irradiation

HPA's are green and reusable catalysts for glycogen hydrolysis
Glycogen from cyanobacteria is a potential feedstock for glucose production

HSiW/graphene as solid acid catalyst for glycogen hydrolysis

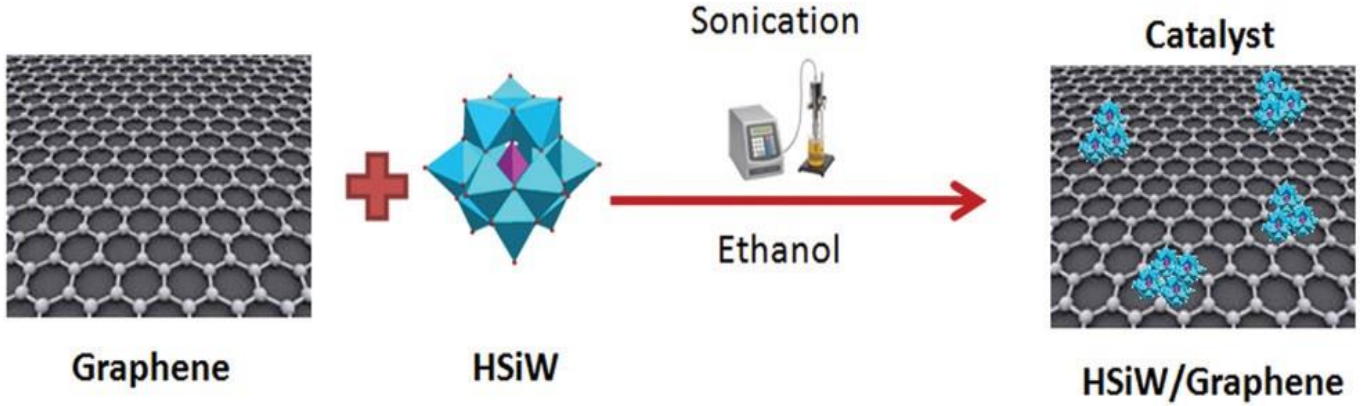

sonochemical synthesis of graphene supported silicotungstic acid catalyst

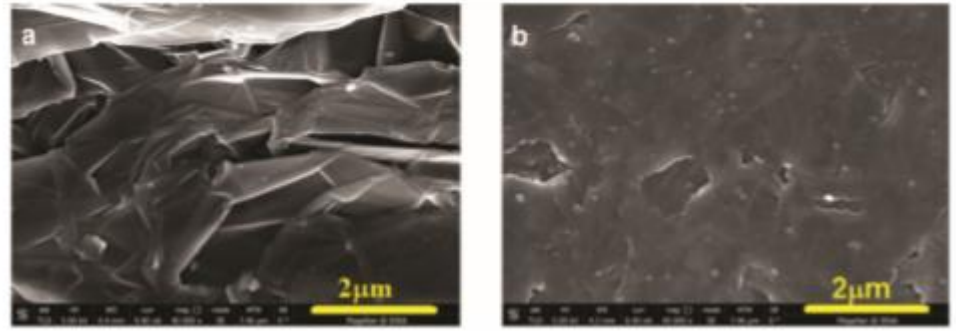

HR SEM imamges of (a) graphene and (b) HSiW/graphene

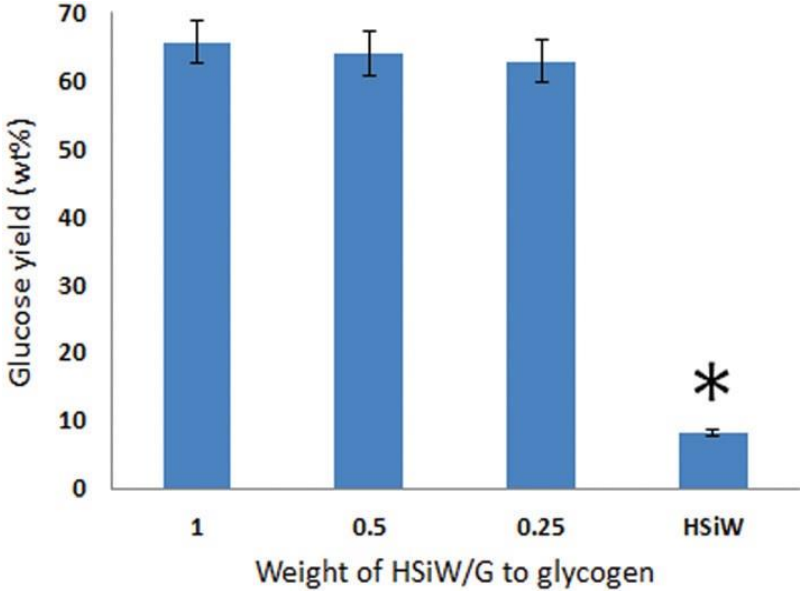

Effect of wt/wt ratio of catalyst to glycogen on glucose yield

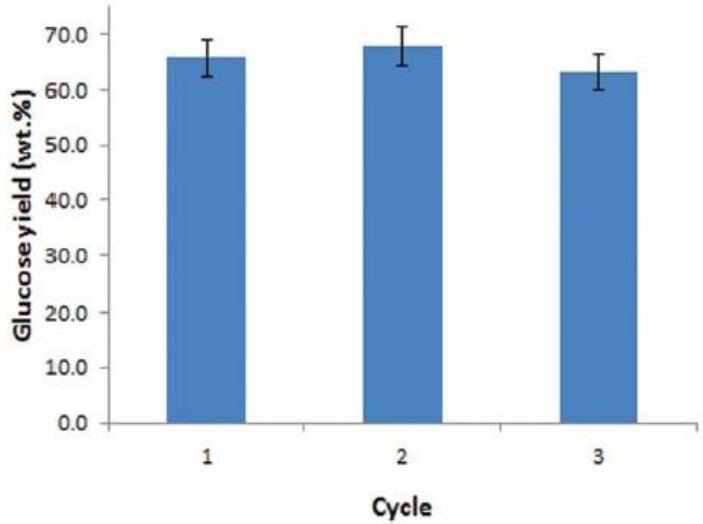

Reusability of the solid acid catalyst (HSiW/G) for glycogen hydrolysis

8 times high yield of glucose (66 wt%) that HSiW

Reused for at least 3 runs

Gedanken et al., Green Chemistry, 17, 2015, 2418-2425.

Selective conversion of rice straw to glucose

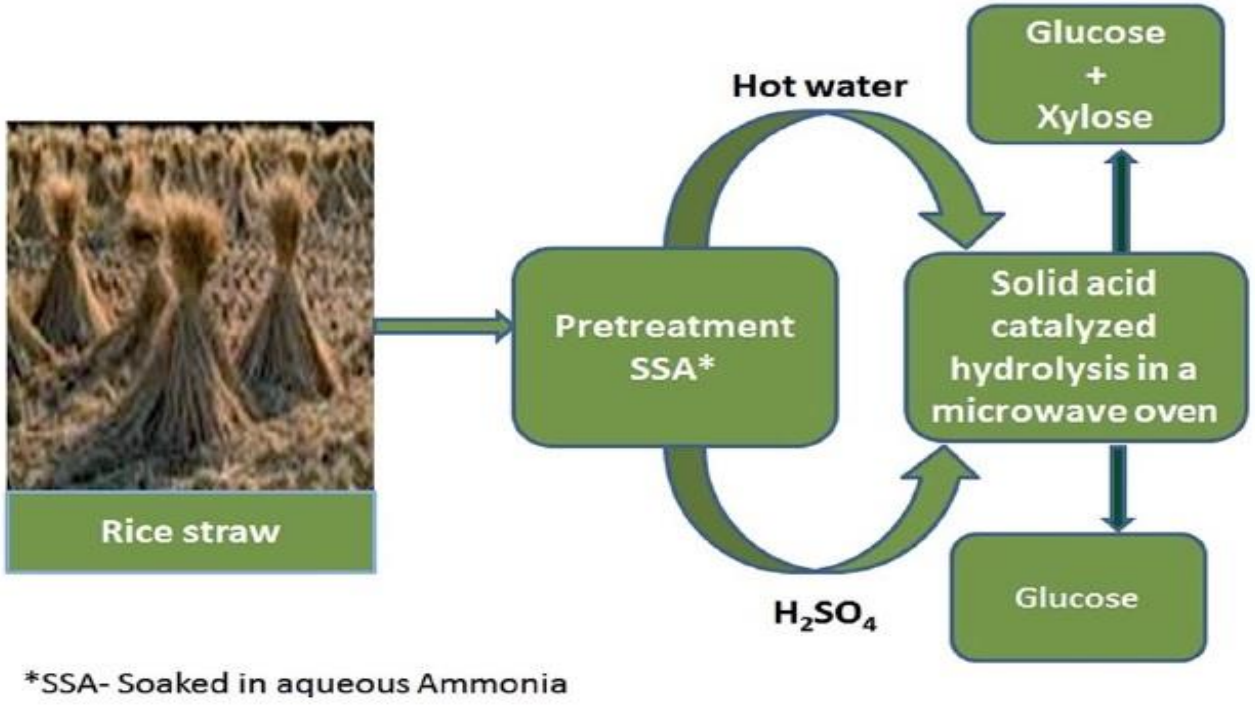

Various stages involved in the process of the conversion of rice to glucose were pictorially shown

First stage of pretreatment involves soaking of biomass in aq. NH_3 (15 wt. %, 12 h, 80 °C).

A stainless steel tubular reactor packed with dignified rice straw and held at 190 °C (2.3 MPa) was fed with dil. H_2SO_4 (0.2 wt. %) or hot water at a flow rate of 5.0 $mLmin^{-1}$.

Pretreatment with dil. H_2SO_4 was more effective than hot water pretreatment for the selective as well as higher removal of hemicellulose.

Mass balance of the untreated and pretreated rice straw (ASL-acid soluble lignin; AIL-acid insoluble lignin)

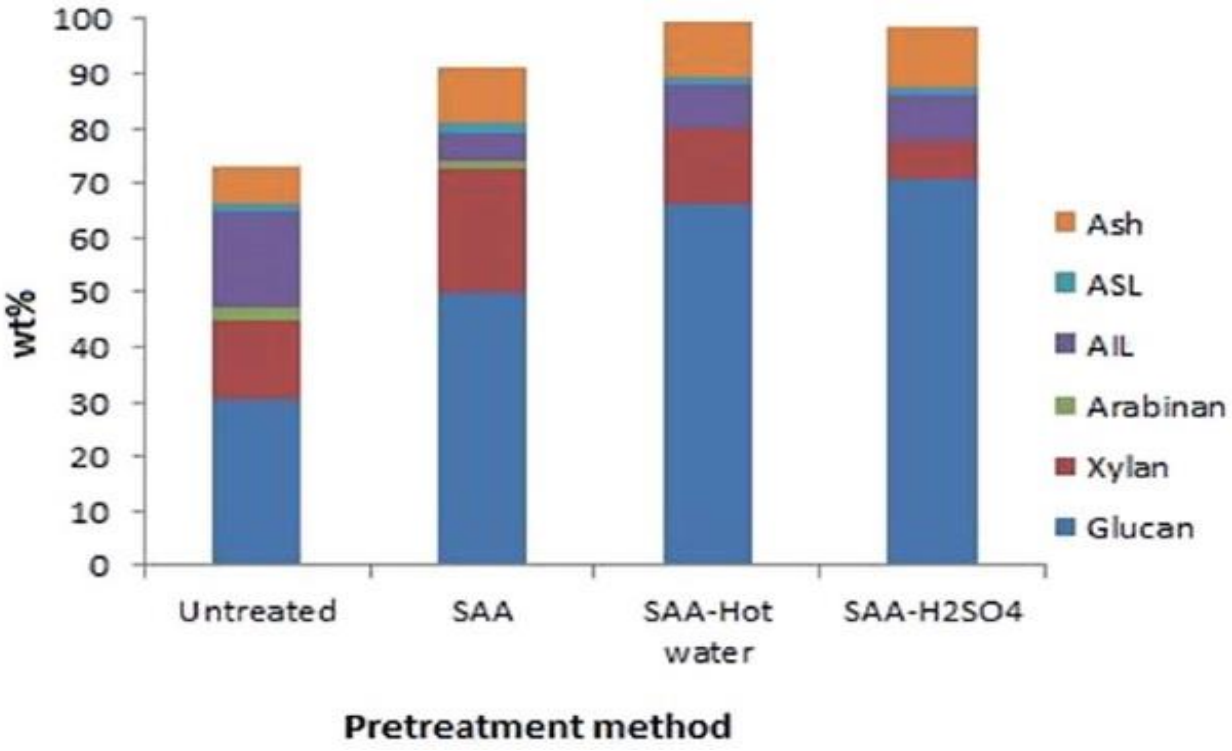

The cellulose content of the treated rice straw was improved from 30.6 to 70.6 wt.% as the pretreatment method is varied from treating with only aq. NH_3 to a two-stage pretreatment process involving soaking in aq. NH_3 followed by dil. H_2SO_4 treatment.

^{13}C NMR spectra of hydrolyzate from pretreated (SAA–H_2SO_4) rice straw hydrolyzed using a solid acid catalyst

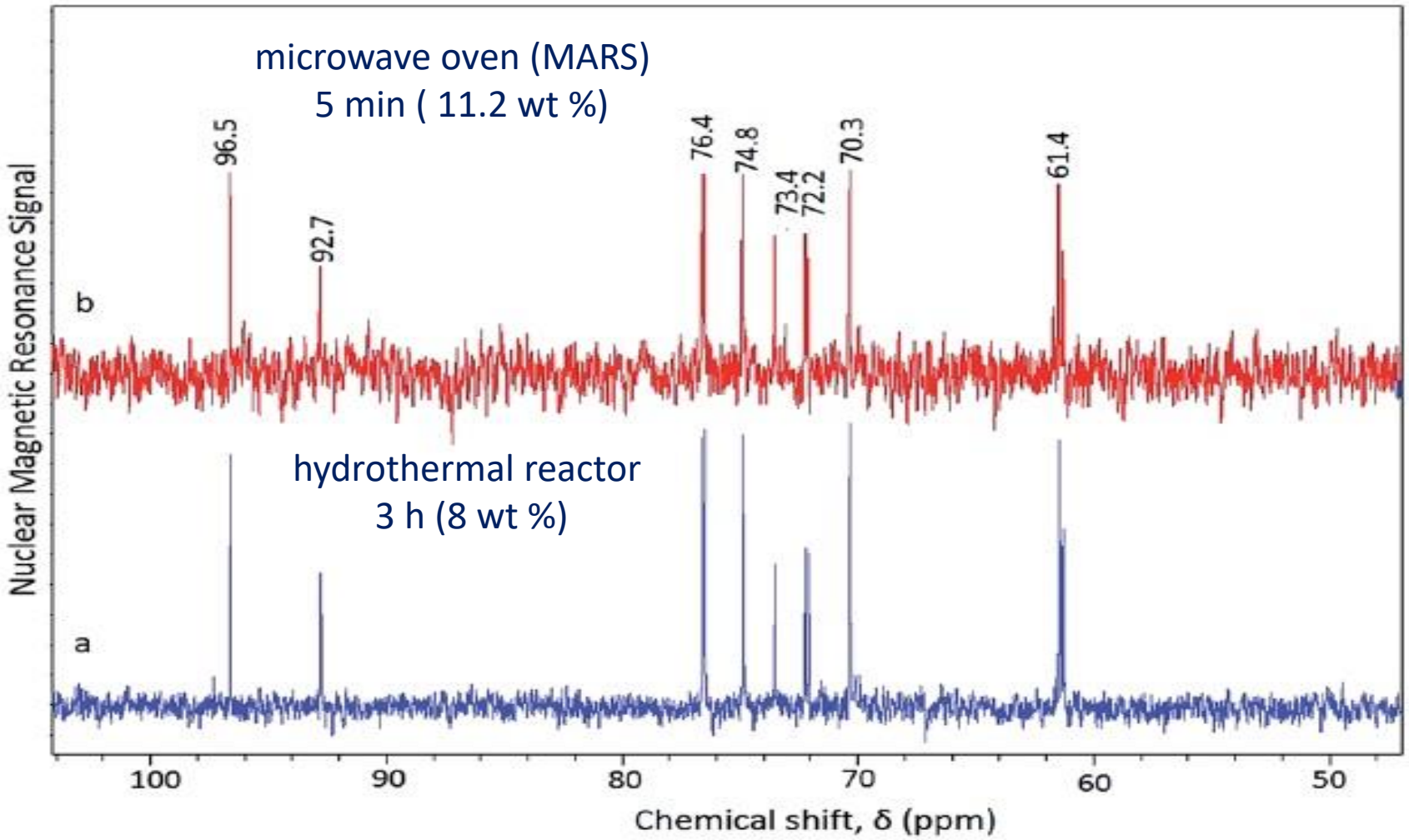

Signals at 61.4 (C6), 70.3 (C4), 72.2, 73.4 (C2), 74.8 (C3), 76.4 (C5), 92.7 (C1, α), 96.5 (C1, β) ppm indicate exclusive formation of glucose from the treated rice straw.

HPW/activated carbon for rice straw conversion to glucose

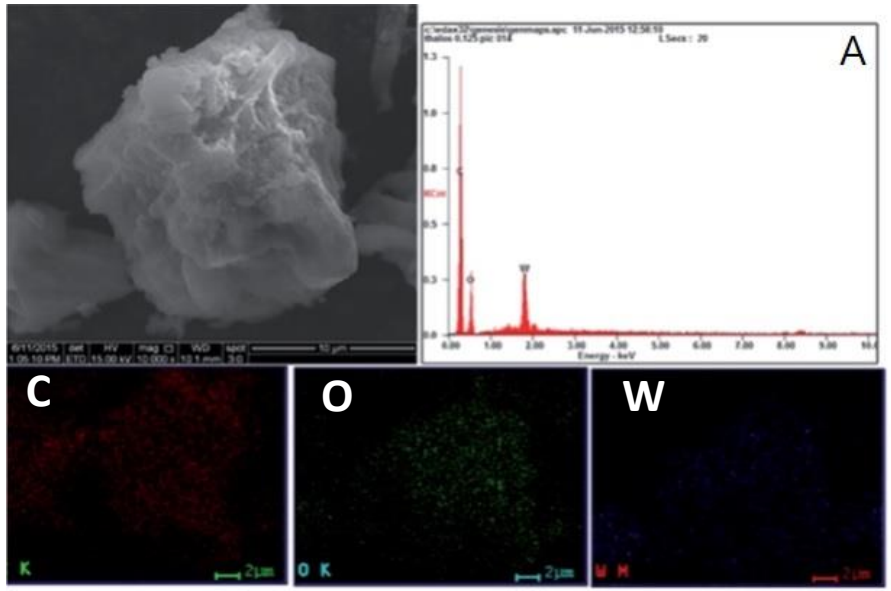

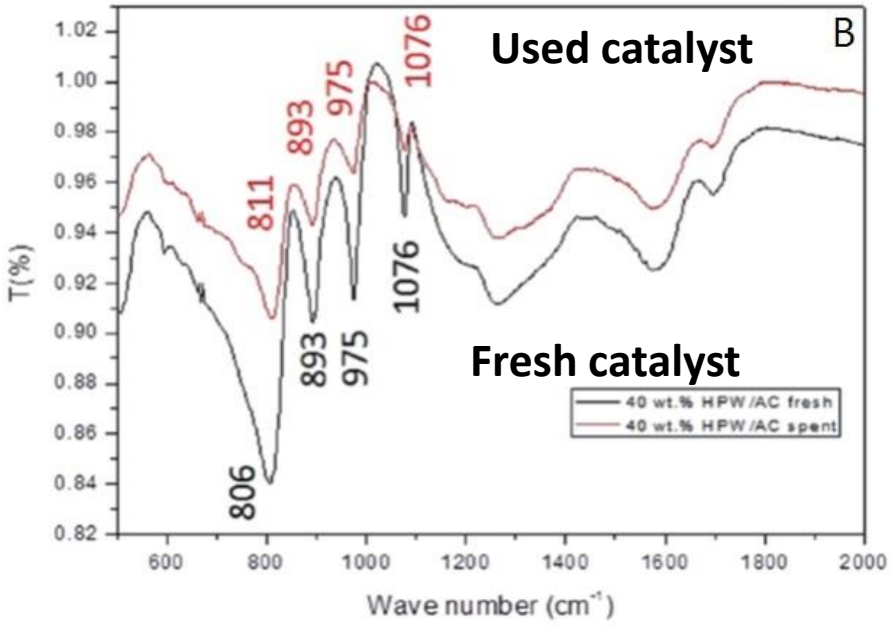

The presence of four consecutive bands in the region of 800-1100 cm^{-1} are typical of four different W-O bands existing in the heteropolyanion $[PW_{12}O_{40}]^{3-}$ and confirm the structural integrity of the solid acid catalyst after the hydrolysis reaction in a microwave oven.

Thus a promising strategy for the production of glucose from rice is demonstrated.

(A) E-SEM, EDAX and the elemental mapping (C, O, W) of ~ 40 wt % HPW/AC catalyst, and (B) FT-IR spectra of (a) fresh and (b) spent catalyst (~ 40 wt % HPW/ AC) used for the hydrolysis of rice straw under microwave irradiation.

Gedanken et al., RSC Adv, 6, 2016, 31-38

Solid base catalysis for biodiesel production

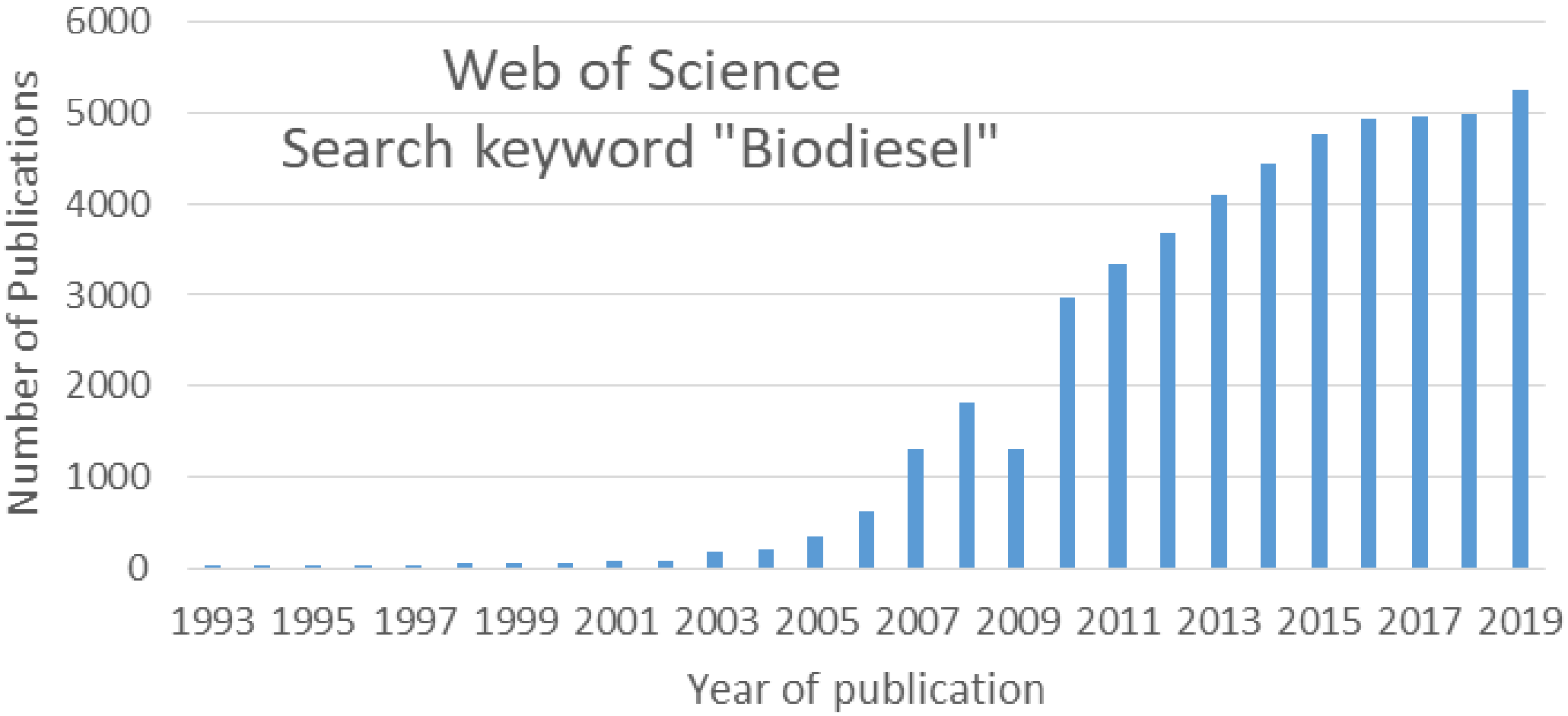

Ever since the disclosure of the first patent in 1993, on the use of biodiesel as an alternative to fossil based engine oil, by **Koracs from Hungary** [1], enormous progress in made in the development of processes for biodiesel production with a total of 52, 628 publications in the web of Science as on 31st May 2020.

Koracs, A., Plant based diesel oil comprises rapeseed oil alcohol and acetone. Koracs, A., HU62645-T, 28 May 1993, HU208994-B, 28 Feb 1994, Hungary

Continuous flow production of biodiesel from waste cooking oil (WCO) under microwave irradiation using SiO/SrO_2 as a fixed bed sold base catalyst

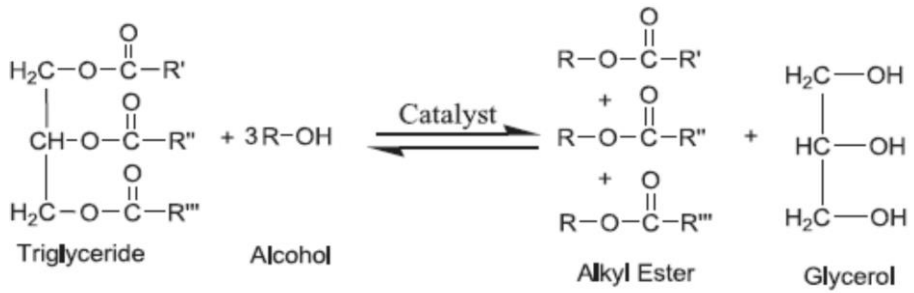

Schematic representation of transesterification process of triglycerides with methanol

Pictorial representation of the microwave assisted aqueous phase synthesis of SrO/SiO_2 catalyst

SrO nanoparticles supported on millimetric silica beads is designed as a heterogeneous solid base catalyst

Equimolar amounts of $Sr(NO_3)_2$ and Na_2CO_3 taken in water were vigorous stirred in a 250 mL round bottom flask.

10 mL of ethylene diamine (EDA) were then added. Subsequently SiO_2 beads (3-6 mm particle size) were added. The reaction mixture is irradiated in a domestic microwave oven for 30 s. The residual solid mass obtained after cooling was separated from the supernatant by centrifugation, washed with ethanol and subjected to vacuum drying overnight. The material thus obtained ($SrCO_3/SiO_2$) was calcined at 900 °C for 3 h in air resulting in SrO/SiO_2. The amount of SrO deposited on the SiO_2 beads is found to be 41.3 wt. %

Gedanken et al., Energy and Fuels, 30 (4), 3151–3160

SEM – EDS analysis of SrO/SiO_2 solid base catalyst

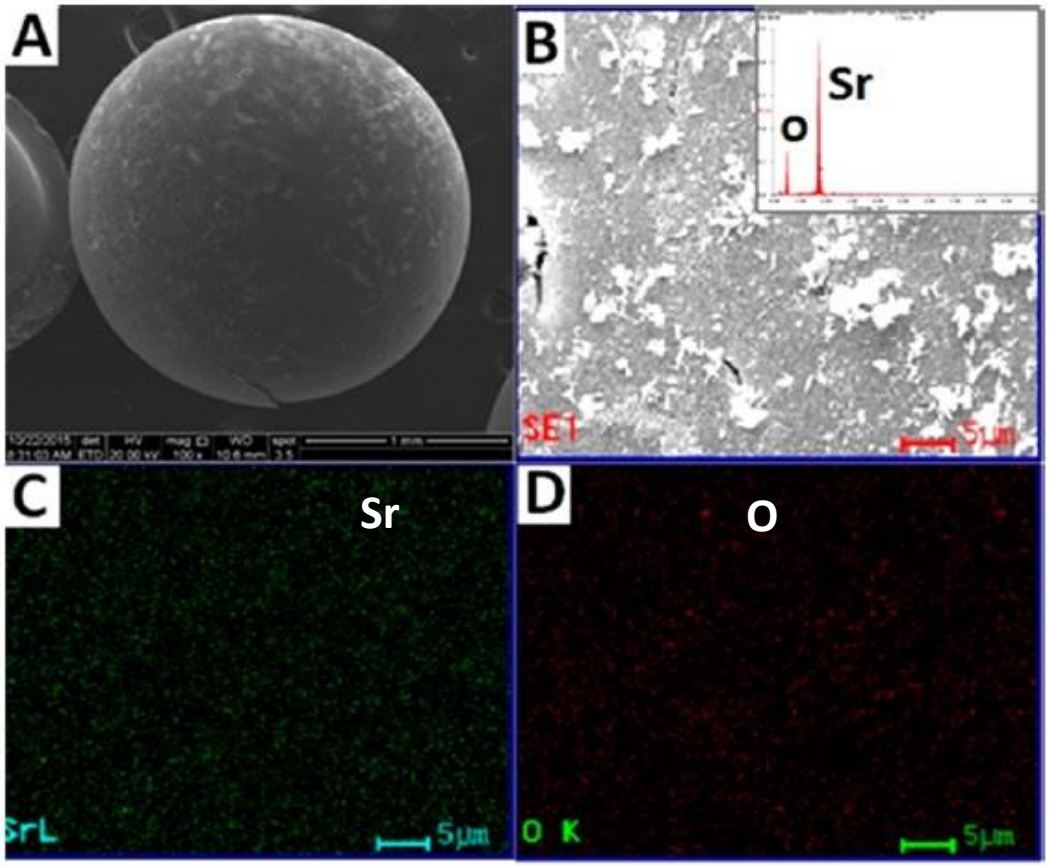

SEM images (A & B), EDS spectrum (inset B) and elemental mapping of Sr and O (C & D) of SrO/SiO_2 solid base catalyst

Spherical morphology of the SiO_2 beads (3-6 mm) was retained (though some beads were broken) even after microwave irradiation (30 s) and upon calcination at high temperature (900 °C for 3 h).

Uniform deposition of SrO on SiO_2 surface is observed from the presence of elements Sr and O (EDS spectrum) through out the SiO_2 surface in the elemental mapping.

All these features imply the potential of the catalyst synthesis methodology for the strong adhesion of SrO on SiO_2 surface.

Evaluation of the potential of the SrO/SiO_2 catalyst for the transesterification of WCO microwave irradiation in a batch process

Pretreatment of WCO:

- For avoiding the saponification of the FFA's and other hydrolysis reactions during the transesterification reaction, the FFAs and water are removed from the WCO prior to its use.
- The WCO was mixed with a solution of KOH to remove the FFA's via soap formation which was further separated from the oil content by centrifugation.
- The WCO was subsequently heated to 110 °C for evaporating the water content present.

Biodiesel synthesis process:

- Typical biodiesel prepartion in a batch process is carried out by taking WCO (15 g), methanol (4 mL) and SrO/SiO_2 (0.5 g) in a round bottom flask and irradiating the contents in a microwave oven for **10 s** at 70 % power.
- The reaction is carried out under stirring at 60 °C.
- After cooling the contents, the reaction mixture was centrifuged for the separation of the biodiesel and methanol (top layer) from the solid base catalyst and the reaction byproduct, glycerol.
- Excess methanol was further removed by a rotary evaporation process.
- The solid catalyst was separated by filtration and its reusability was further evaluated by adding cooking oil and methanol in the same amounts as used in the inital reaction run.
- The product biodiesel was analyzed by ^1H NMR spectroscopy using $CDCl_3$ as the solvent.

Reusability of SrO/SiO_2 catalyst

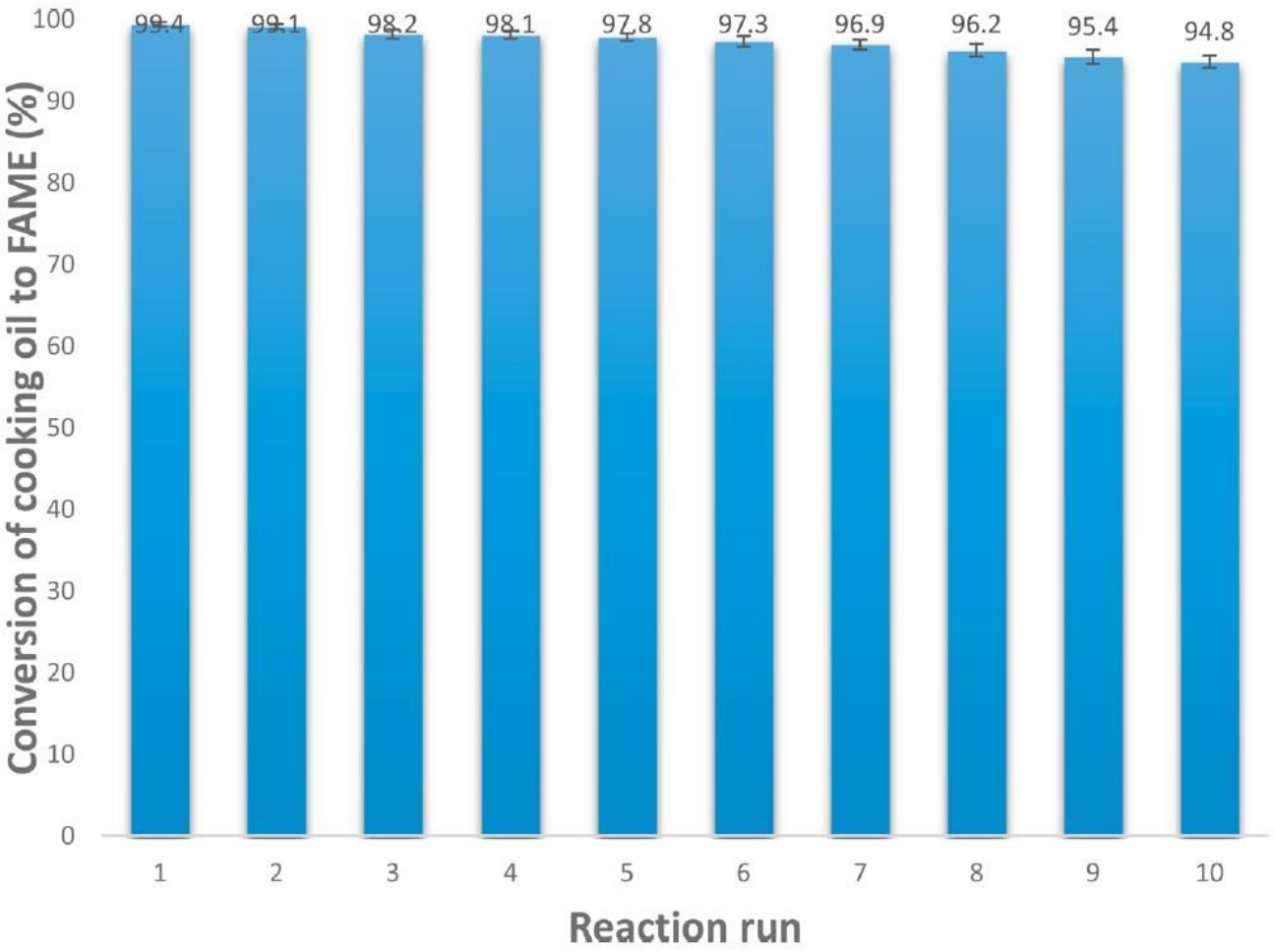

SrO/SiO_2 exhibited sustainable activity for a minimum of 10 consecutive cycles of the transesterification of WCO

Evenafter 10 repeated cycles, only slight reduction (from 99.4 to 95 wt.%) in activity

Moreover, the batch process was further transformed successfully into a continuous flow process on a commercial flowSYNTH microwave system.

Potential of SrO/SiO_2 as a reusable solid base catalyst for the conversion of waste cooking oil in a microwave driven batch process

Evaluation of the potential of the SrO/SiO_2 catalyst for the transesterification of WCO microwave irradition in a continuous flow process

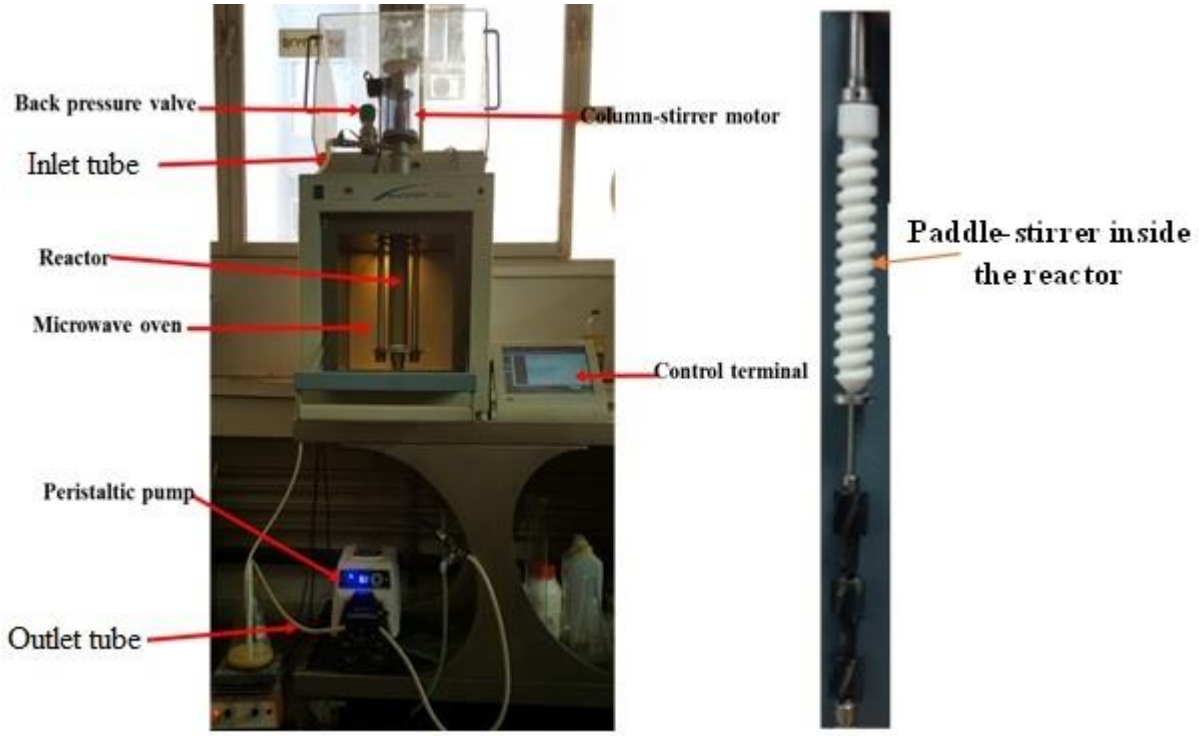

Experimental setup for the continuous-flow biodiesel production based on microwave irradiation.

Gedanken et al., Bioresource Technology, 224, 333-341

The flowSYNTH system is a continuous flow microwave reactor with 1000 W power, heating a vertically mounted (200 mL) flow-through reactor.

The reaction mixture was pumped by a high-pressure membrane pump from the top of the reactor.

Online sensors facilitate continuous monitoring of the reaction temperature.

Uniform temperature distribution through out the length of the reactor is facilitated by the magnetically driven paddle-stirrer.

The reaction mixture is stirred mechanically inside the microwave cavity by a stirring shaft equipped with three paddles.

The pump connected to the reactor enables the flow of the reaction mixture through the reactor.

The working volume of the reaction chamber mounted vertically in the microwave cavity is 190 mL.

The maximum working conditions of the microwave flow reactor are 200 mL, 30 bar and 1000 W.

The peristaltic pump connected to the microwave reactor enables the flow of reaction mixtures (0.06-3400 mL/min).

Continuous flow transesterification process on SrO/SiO2 fixed bed catalyst

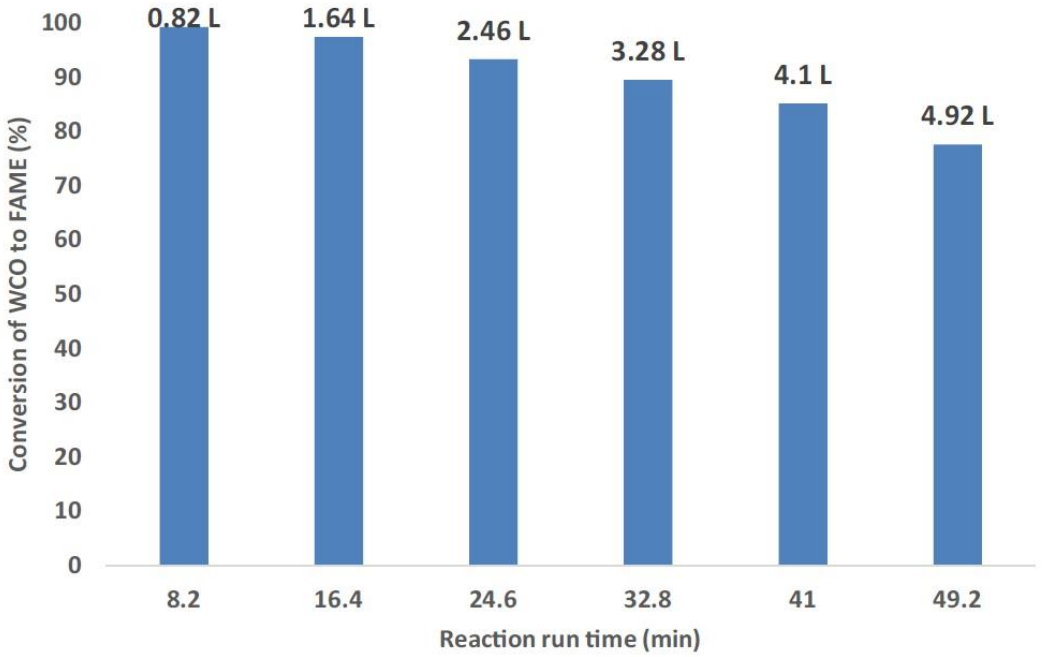

Best reaction conditions:
Stirring shaft rotation velocity of 20 %,
mole ratio of WCO to methanol of 1:12,
reaction temperature of 65 ˚C,
feed flow rate of 100 mL/min and
packed bed catalyst amount of 15 g (41.1 wt. % SrO/SiO_2).
Active amount of SrO component in the 15 g of supported catalyst is 6.195 g.

At this modest amount of catalyst loading, WCO conversion as high as 99.2 wt. % is achieved in the first 8 min of feed flow.

Life time of the fixed bed catalyst (41.3 wt.% SrO/SiO_2) for the conversion of waste cooking oil (WCO) to biodiesel

Catalyst could be used in the fixed bed for over a period of 24.6 min without appreciable loss in catalytic activity.
Even after converting ~ 2.46 L of feed into biodiesel, the catalytic activity was retained as observed from the high conversion value of 93.3 % at 24.6 min.
After 24.6 min of running time, a slow decrease in the conversion values from 89.5 to 77.6 wt. % is noticed corresponding to feed flow of 3.28 to 4.92 L, respectively.
The loss in activity beyond 24.6 min. was attributed to the partial dissolution of SrO from the surface of SiO_2 support.
The amount of SrO retained in the spent catalyst (SrO/SiO_2) used for 49.2 min in the continuous flow process is 24.7 wt. % indicating leaching of significant amount of SrO from the support.

Structure-activity relationship of SrO/SiO_2 catalyst of biodiesel production

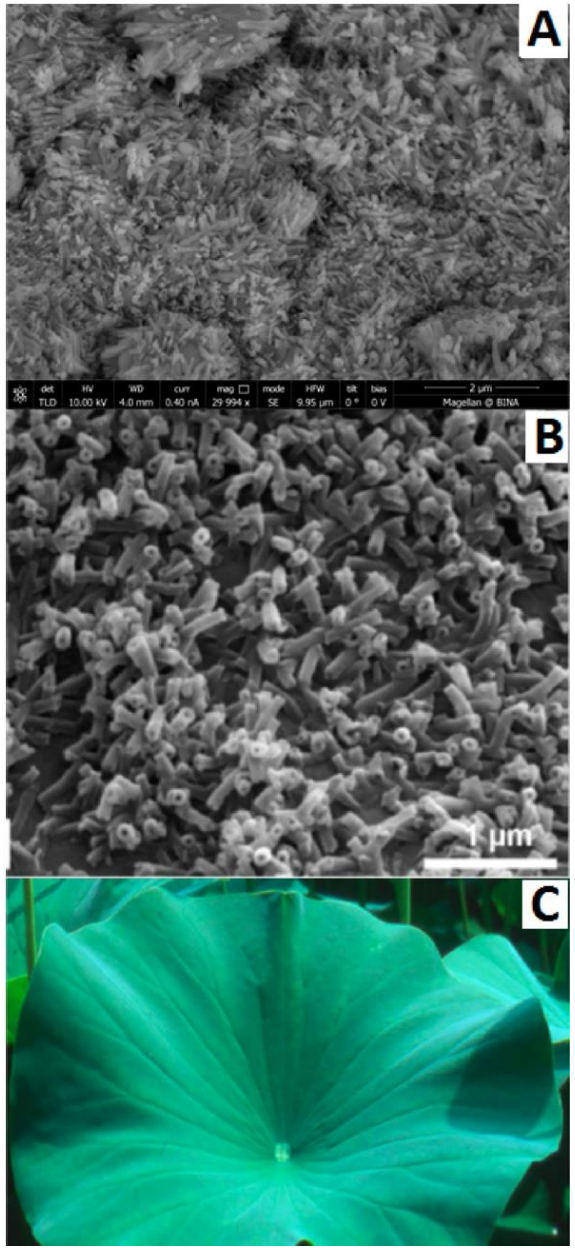

Major challenges in industrial continuous flow processes, like the mass flow constraints, pressure build-up, diffusion constraints and temperature gradient could be effectively surmounted using the SrO/SiO_2 catalyst.

A uniqe structure-activity relationship was noticed in the catalytic acitivity of SrO/SiO_2 for the conversion of WCO to biodiesel. The HR-SEM image of the ~41 wt.% SrO/SiO_2 catalyst prepared under optimal reaction conditions

Nanometric tubules of SrO were formed on the surface of the mm silica beads under the synthesis conditions (microwave irradiation followed by calcination at high temperature)

Average length and width of the nanotubles of SrO were 139 and 50 nm.

These structural features were comparable to the surface of the nano structure of lotus leaf imparting its hydrophobic property.

Nano tubules present on the SrO/SiO_2 could be attributed to the observed high and sustained activity of SrO/SiO_2 at a modest loading of ~ 41 wt. % of SrO.

Such nanotubules may have water repelling ability and promote transesterification of waste cooking oil effectively.

HR-SEM image of SrO/SiO_2 (A), SEM image of the upper leaf side with nanotubules of wax (B) and lotus leaf with extraordinary hydrophobicity (C).

Carbon fiber reinforced composites

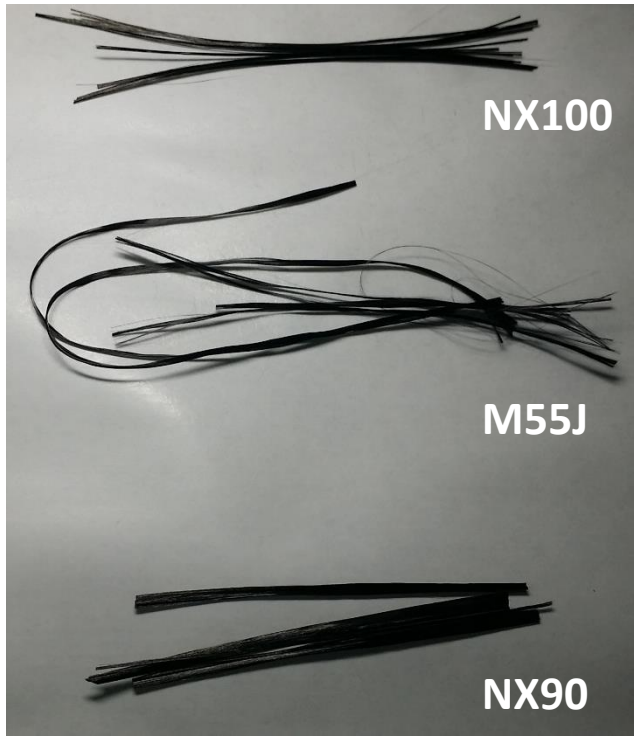

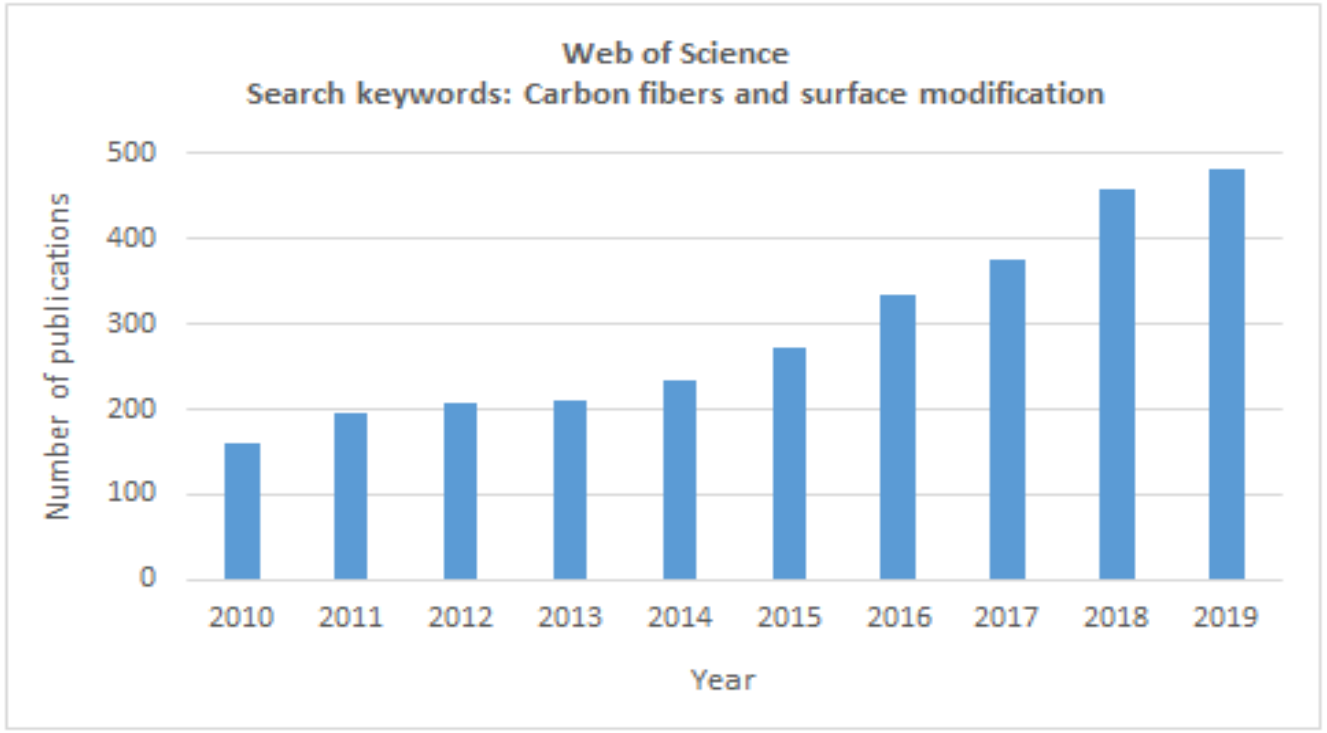

Surface modification of Carbon fibers

- **Sizing**
- **Physical methods**
- **Mechanical**
- **Chemical methods (**oxidation, amination, silanization)
- **Electrochemical**
- **Polymerization (coating; grafting)**
- **Functionalization with nanoparticles**

A web of Science search with the keywords, “carbon fibers” and “surface modification” for the years from 2010 to 2019 shows growing interest in field of “Carbon fiber surface modification”

Total results - 2937

Revolutionary applications of surface modified Carbon fibers (SMCF's) in health

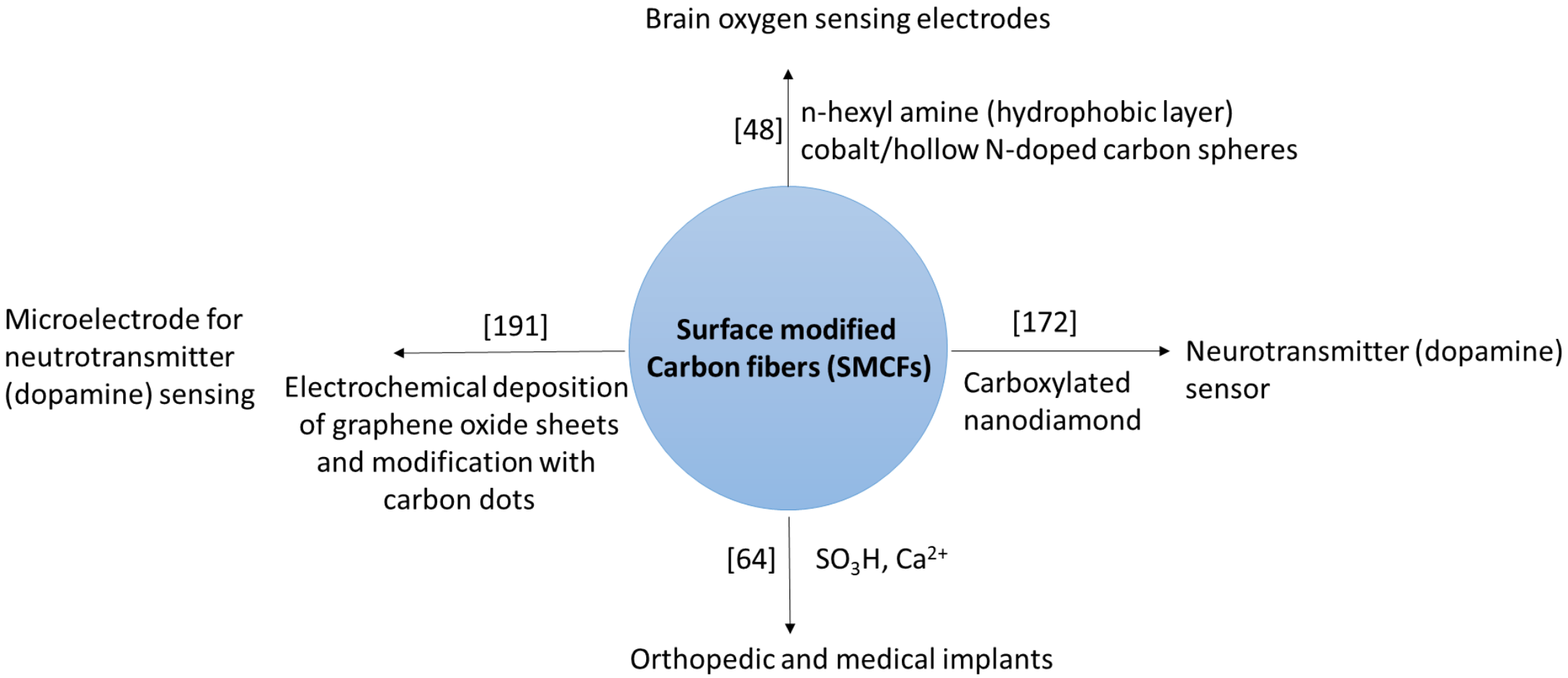

[48] Mao et al., Microelectrode for detecting oxygen in brain, comprises carbon fiber electrode, hydrophobic modified layer formed on outer surface of carbon fiber electrode and catalyst layer. 14 Feb 2020, China, CN110794012-A.

[64] Cheng et al., Effect of surface chemical modification on the bioactivity of carbon fibers reinforced epoxy. Surface and coatings technology, 377, 2019, 1-10.

[172] Puthongkham and Venton, Nanodiamond coating improves the sensitivity and antifouling properties of carbon fiber microelectrodes. ACS Sensors, 4 (9), 2019, 2403-2411.

[191] Fang et al., Co-deposition of carbon dots and reduced graphene oxide nano sheets on carbon –fiber micro electrode surface for selective detection of dopamine. Applied surface science, 412, 2017, 131-137.

Revolutionary applications of surface modified Carbon fibers (SMCF's) in energy

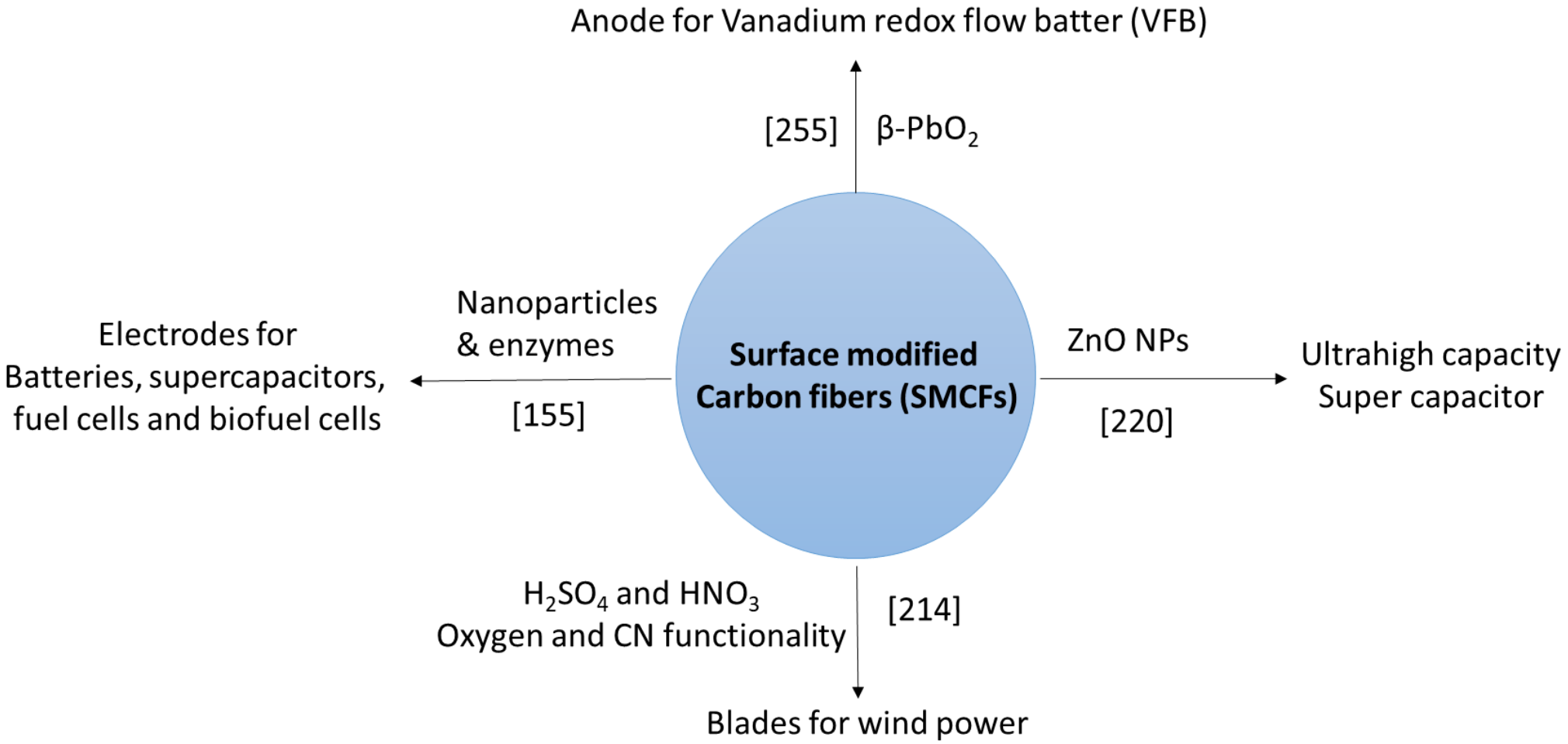

[155] Kakhki, R. M., A review to recent developments in identification of carbon fiber electrodes. Arabian Journal of Chemistry 12 (7), 2019, 1783-1794.

[214] Li, M., Improved power generation efficiency of a wind power generator and reducing noise, comprises choosing carbon fiber blade of wind power generator, subjecting the activation treatment, surface modification, and applying a performance coating. CN108864457-A, 23 Nov 2018.

[220] Joo, S. W., Dillip, G. R., Kim, C. S., Carbon fiber/metal oxide complex composite used in electrode for ultrahigh capacity capacitor, comprises carbon fiber, and at least one metal oxide bonded to the carbon fiber. KR2018082799-A, 19 July 2018; KR1960154-B1, 4 Jul 2019.

[255] Sun, H., Yao, C., Method for modifying carbon fiber that is utilized in anode material of vanadium redox flow battery, involves preprocessing carbon fiber fabric, depositing beta-lead oxide particles, and scanning fiber fabric for multiple times. CN104064781-A, 24 Sep 2014; CN104064781-B, 4 Jan 2017.

Revolutionary applications of surface modified Carbon fibers (SMCF's) in environment

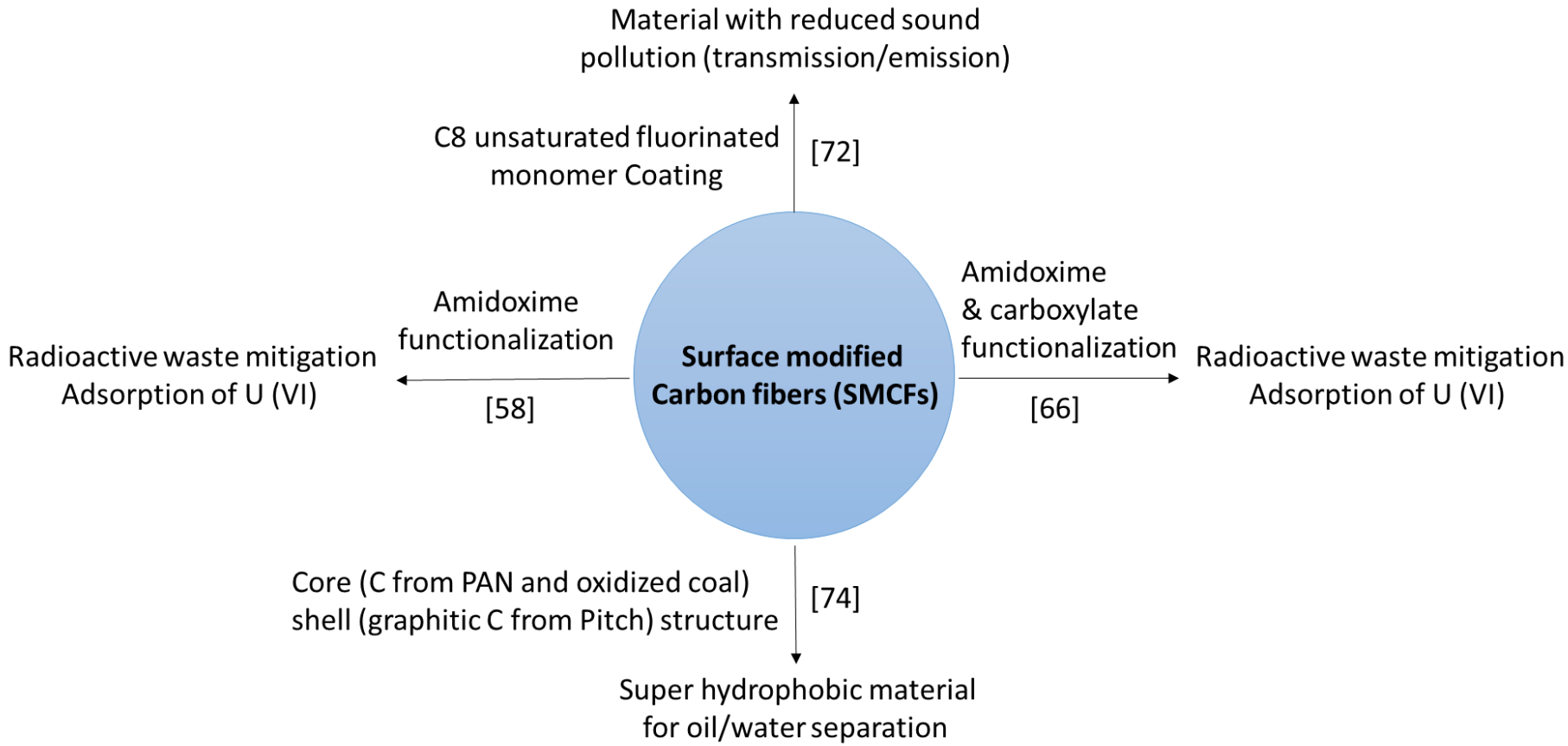

[58] Ashrafi, F., Firouzzare, M., Ahmad, S. J., Sohrabi, M. R., Khosravi, M., Preparation and modification of force spin polypropylene nanofibers adsorption of uranium (VI) from simulated seawater. Ecotoxicology and environmental safety, 186, 2019, Article No. UNSP 109746, 1-9.

[66] Wang, F., Wang, X. L., Jiang, Y. J., Niu, Z. W., Wu, W. S., Zhang, H. X., Study of adsorption performance and adsorption mechanism for U (VI) ion on modified polyacrylonitrile fibers. Journal of radio analytical and nuclear chemistry, 323, (1), 2020, 365-377.

[72] Regner, S., Drechsler, K., Sentpali, S., Modification of the fiber/matrix bonding by a plasma treatment to reduce the structure-borne sound transmission. Applied Acoustics, 153, 2019, 78-86.

[74] Feng, S. Z., Luo, W. X., Wang, L. X., Zhang, S., Guo, N. N., Xu, M. J., Zhao, Z. B., Jia, D. Z., Wang, X. C., Jia, L. X., Preparation and property of extremely stable superhydrophobic carbon fibers with core-shell structure. Carbon, 150, 2019, 284-291.

Revolutionary applications of surface modified Carbon fibers (SMCF's) in defense

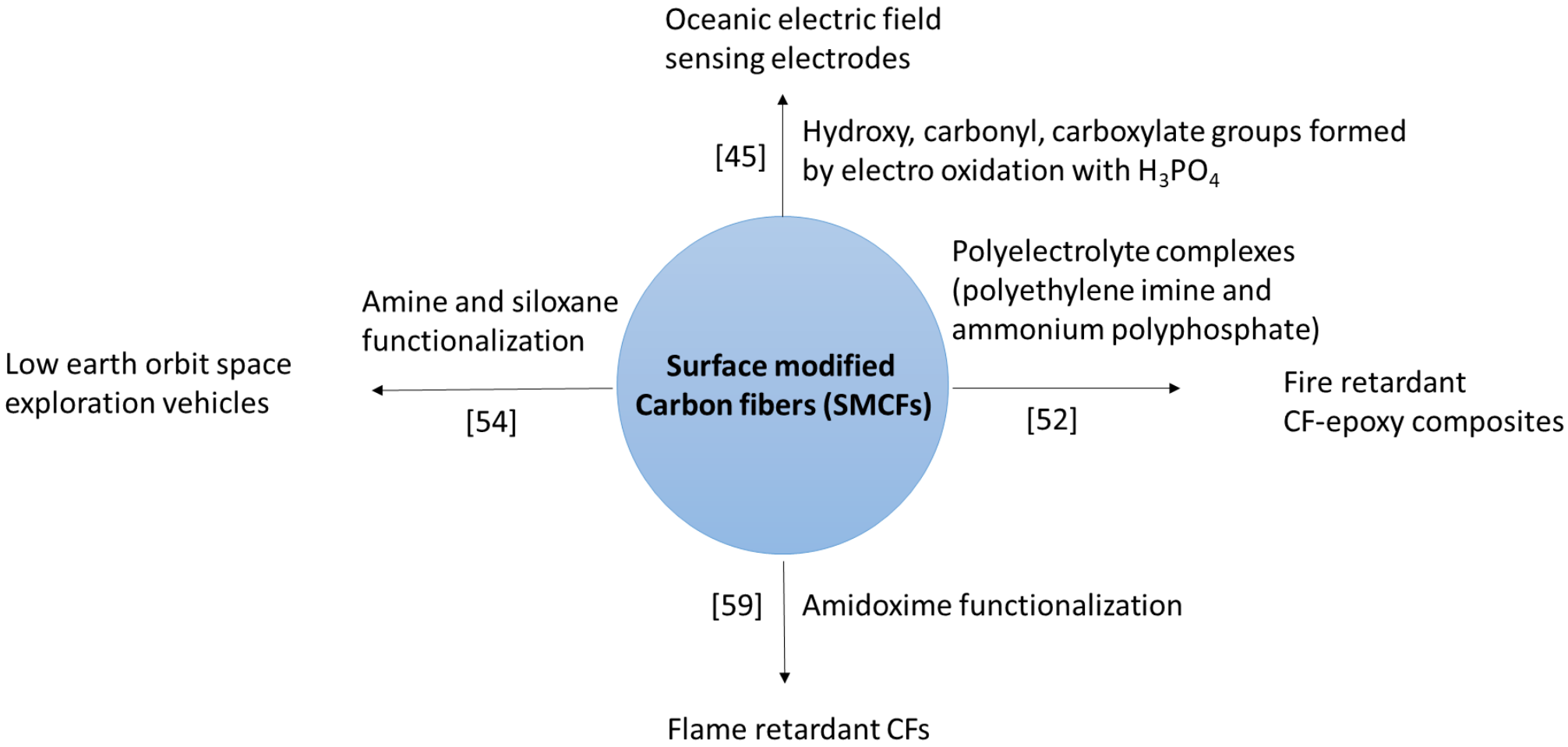

[45] Zai, X. R., Liu, A., Tian, Y. H., Chai, F. G., Fu, Y. B., Oxidation modification of polyacrylonitrile based carbon fiber and its electro-chemical performance as marine electrode for electric field test. Journal of Ocean University of China, 19 (2), 2020, 361-368.

[52] Shi, X. H., Chen, L., Zhao, Q., Long, J. W., Li, Y. M., Wang, Y. Z., Epoxy resin composites reinforced and fire-retarded by surficially-treated carbon fibers via a tunable and facile process. Composites Science and Technology, 187, 2020, 1-7.

[54] Zhao, D., He, J. M., Zheng, N., Huang, Y. D., Improved atomic oxygen erosion resistance of the carbon fiber-epoxy interface with polyhedral oligomeric silsesquioxane. High performance polymers, 2020, DOI: 10.1177/0954008319896828

[59] Sun, X. L., Song, J. Y., Zhang., Liu, J. Y., Ke, H. Z., Wei, Q. F., Cai, Y. B., Effects of chemical pretreatment on structure and property of polyacrylonitrile based pre-oxidized fibers. Journal of Engineered fibers and fabrics, 15, 2020, 1-8.

Revolutionary applications of surface modified Carbon fibers (SMCF's) in catalysis

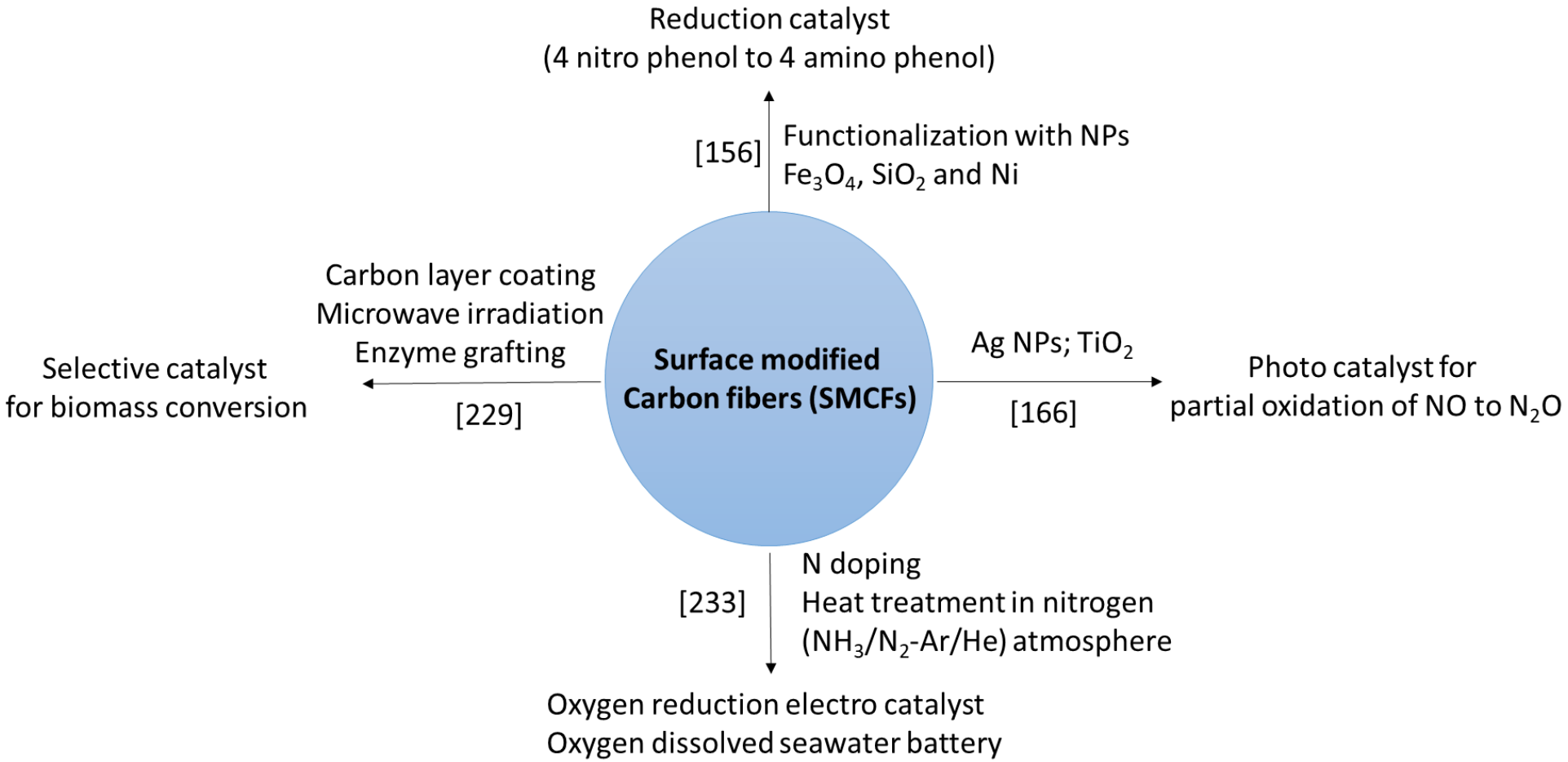

[156] Zhang, M. Ding, L., Zheng, J., Liu, L. B., Alsulami, H., Kutbi, M. A., Xu, J. L., Surface modification of carbon fibers with hydrophilic Fe_3O_4 nanoparticles for nickel based multifunctional composites. Applied Surface Science, 509, 2020, 1-11.

[166] Kusiak-Nejman, E., Czyzewski, A., Wanag, A., Dubicki, M., Sadlowski, M., Wrobel, R. J., Morawski, A. W., Photocatalytic oxidation of nitric oxide over AgNPs/TiO_2 loaded carbon fiber cloths. Journal of environmental management. 262, 2020, 1-10.

[229] Wang, L., Chang, Z., Wei, Q., Hu, Y., Chen, W., Wang, J., Modifying immobilized enzyme vector by using microwave assisted method comprises e.g. pretreatment of enzyme vector, using organic reagents for carbon fiber surface treatment and drying, stirring and washing. CN107058280-A, 18 Aug 2017.

[233] Ren, L., Sang, L., Ding, F., Liu, X., Zhao, Q., Li, Y., Preparation of cathode used for oxygen dissolved seawater battery, involves forming surface active layer by subjecting poly acrylonitrile carbon fiber material surface matrix core to surface modification treatment and heat-treating surface. CN106654163, 10 May 2017.

Revolutionary applications of surface modified Carbon fibers (SMCF's) in smart materials

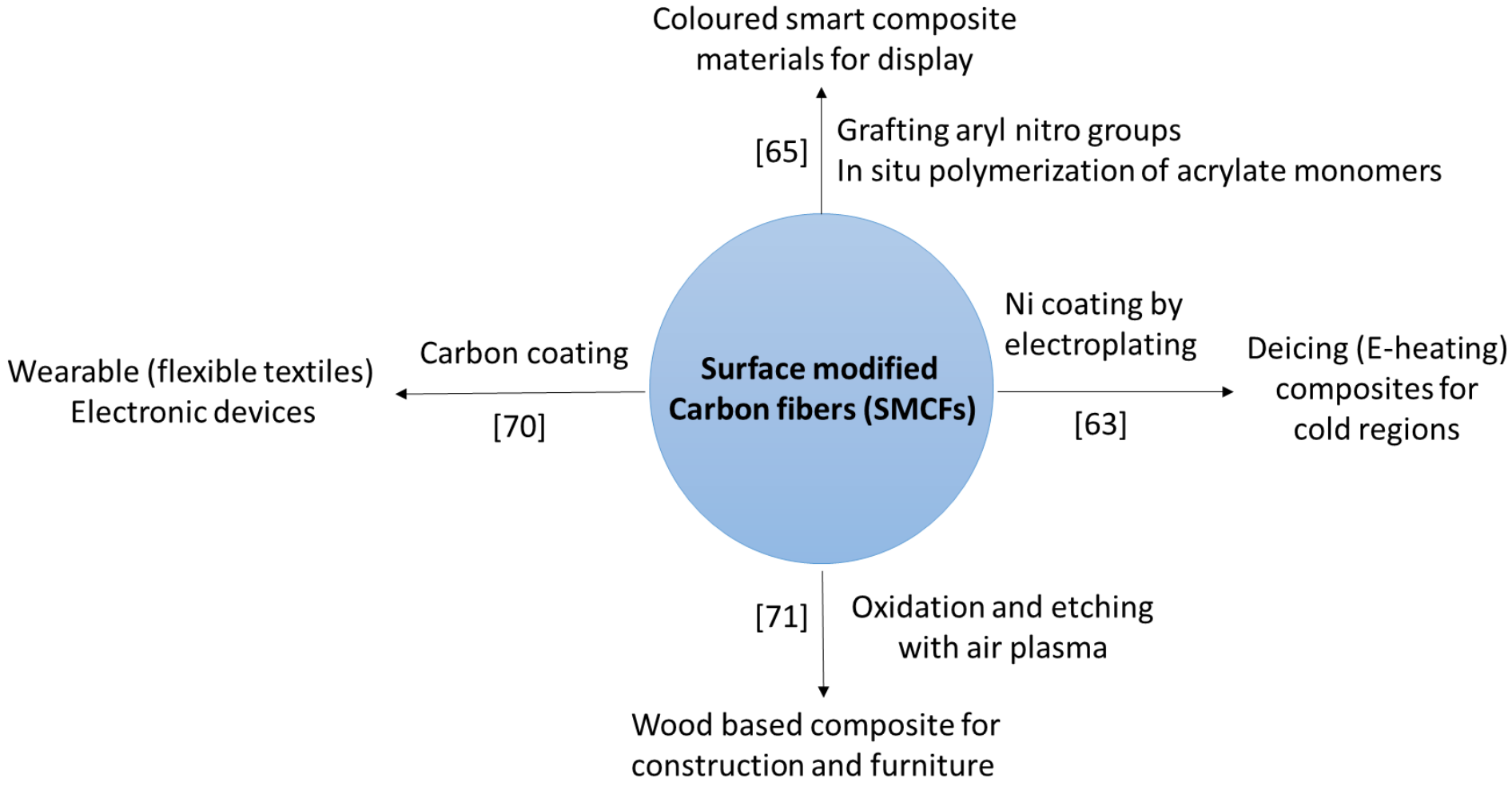

[63] Cao, Y. H., Farha, F. I., Ge, D. S., Liu, X. H., Liu, W., Li, G., Zhang, T., Xu, F. J., Highly effective E-heating performance of nickel coated carbon fiber and its composites for de-icing application. Composites, 229, 2019, 1-7.

[65] Eyckens, D. J., Arnold, C. L., Randall, J. D., Stojcevski, F., Hendlmeier, A., Stanfield, M. K., Pinson, J., Gengenbach, T. R., Alexander, R., Soulsby, L. C., Francis, P. S., Henderson, L. C., Fiber with butterfly wings: Creating colored carbon fibers increased strength, adhesion, and reversible malleability. ACS Applied Materials and Interfaces, 11 (44), 2019, 41617-41625.

[70] Fang, C., Hu, P., Dong, S., Song, J. T., Zhang, X. H., An efficient hydrothermal transformation approach for construction of controllable carbon coating on carbon fiber from renewable carbohydrate. Applied Surface Science, 491, 2019, 478-487.

[71] Zhan, W., Cao, Y. Z., Yang, P, Chen, M. Z., Zhou, X. Y., Manufacturing and interfacial bonding behavior of plasma-treated carbon fiber reinforced veneer based composites. Composite structures, 226, 2019.

Wettability of Carbon fibers (NX-90) with epoxy resin (AG80)

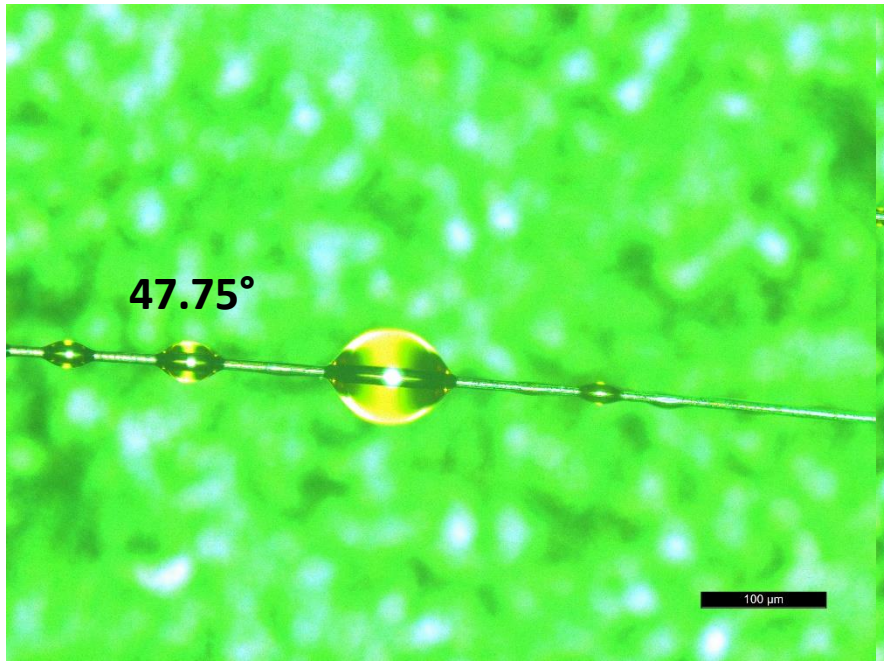

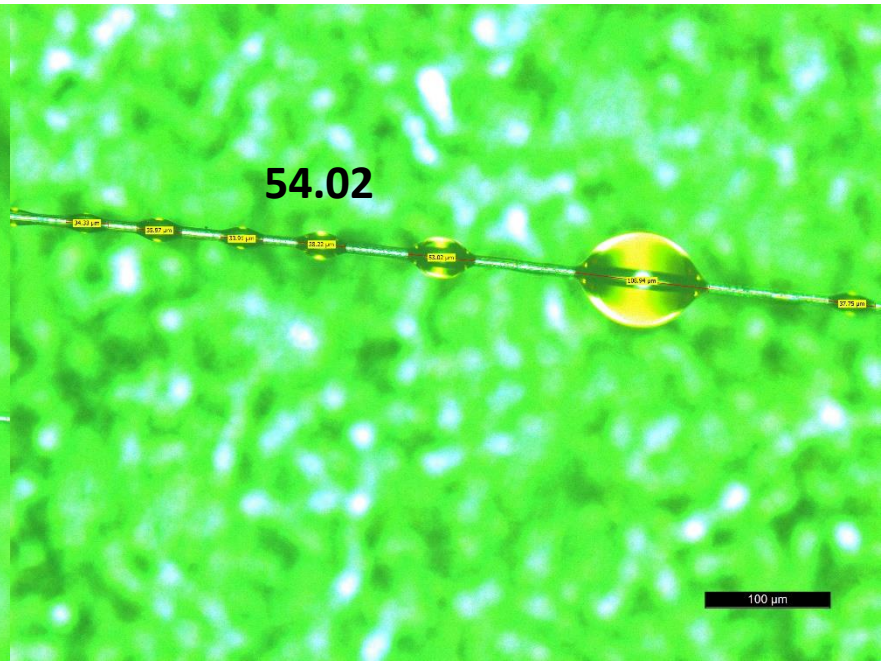

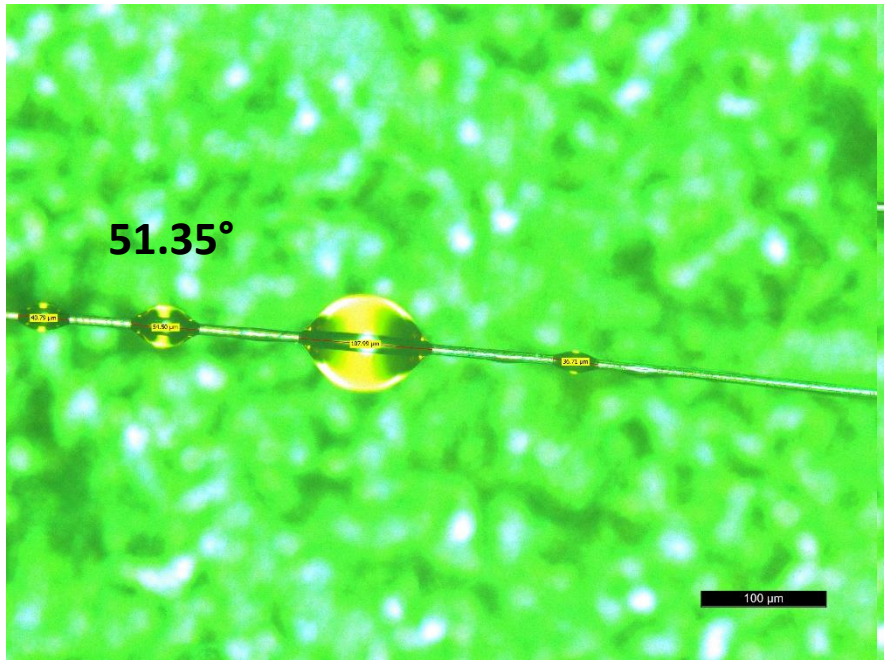

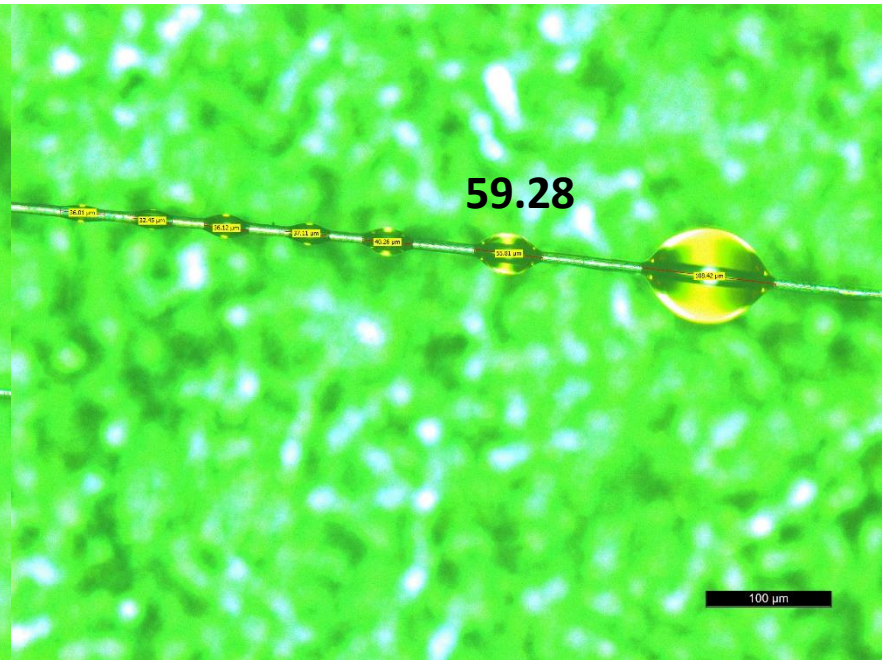

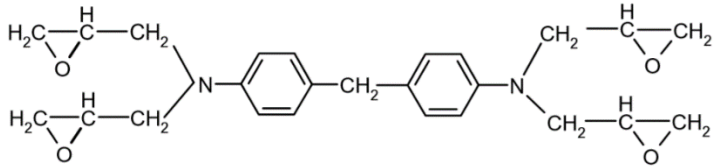

Chemical structure of AG 80
Epoxy resin

AG 80 is a new type of thermosetting matrix for advanced carbon/epoxy Composites

Contact angle (average) = 53.13°

Wettability of Carbon fibers (NX-100) with cyanate ester

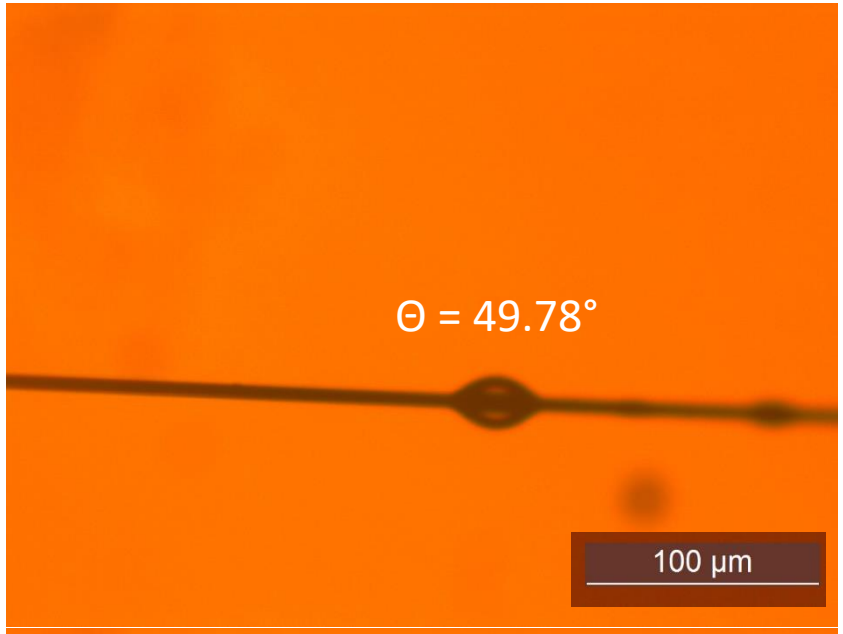

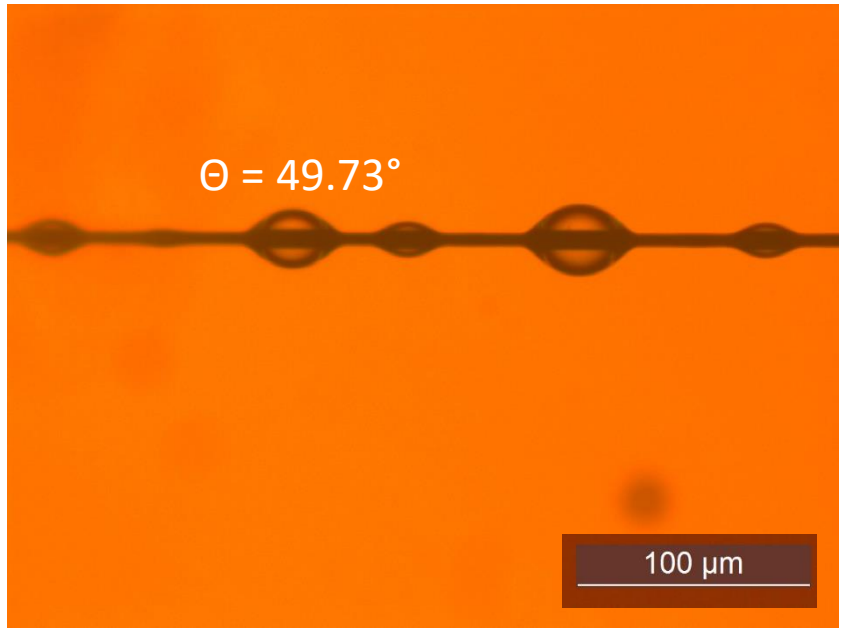

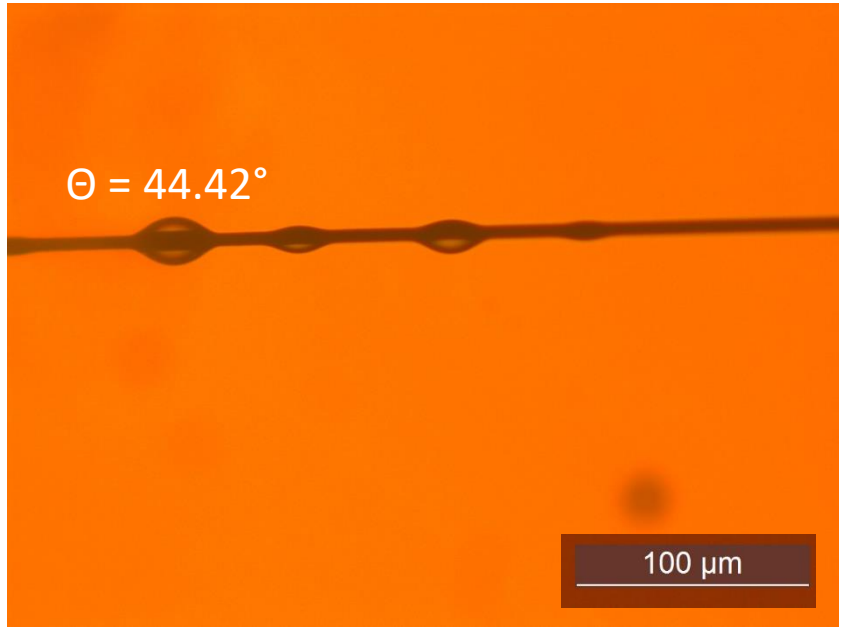

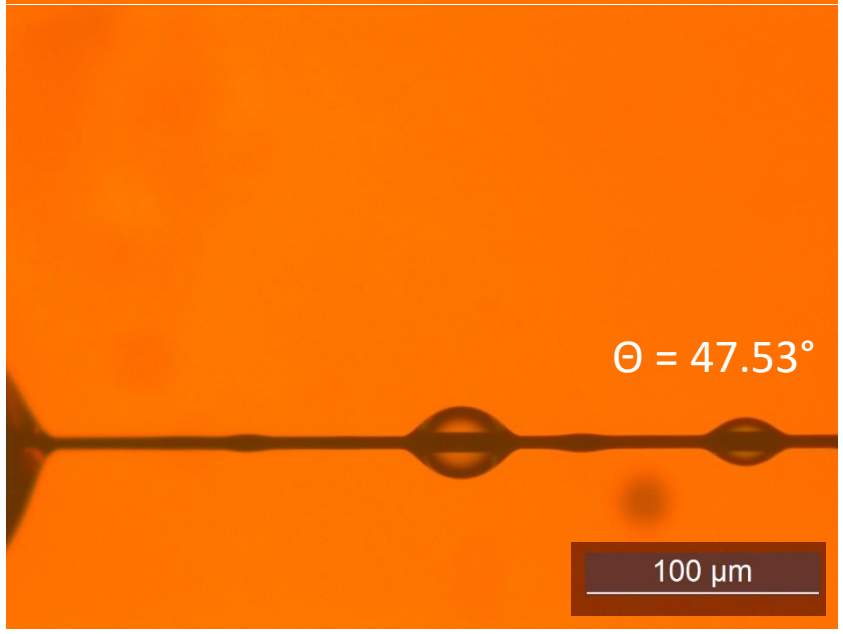

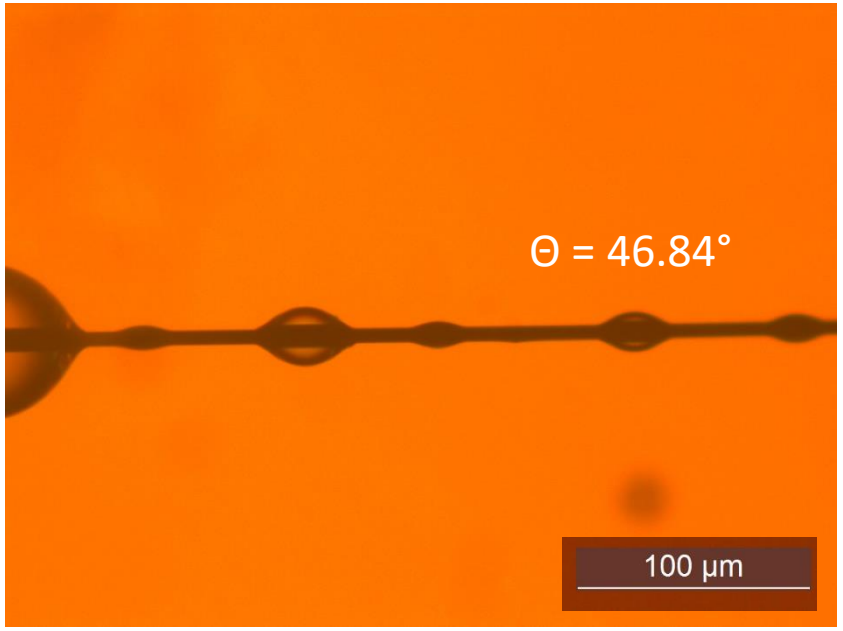

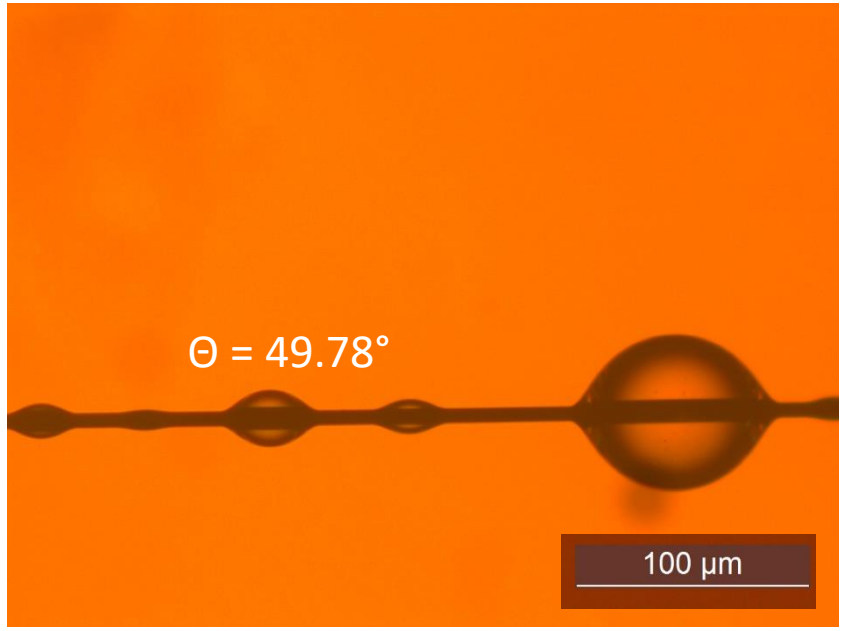

Curing conditions: 120 °C, 1 h; 180 °C, 3 h;

Contact angle (average) = 48.01°

Sizing of carbon fibers

Sizing means chemically modifying the surface of the CF to make the surface of CF more reactive chemically with the resin matrix facilitating stronger interface formation in the CFRP's.

Sizing process has commercial significance and so, much of the knowledge of sizing process, sizing agents used, sizing composition are often a subject of intellectual property and only limited knowledge is available in open literature

Sizing agent in Carbon fiber A from pitch

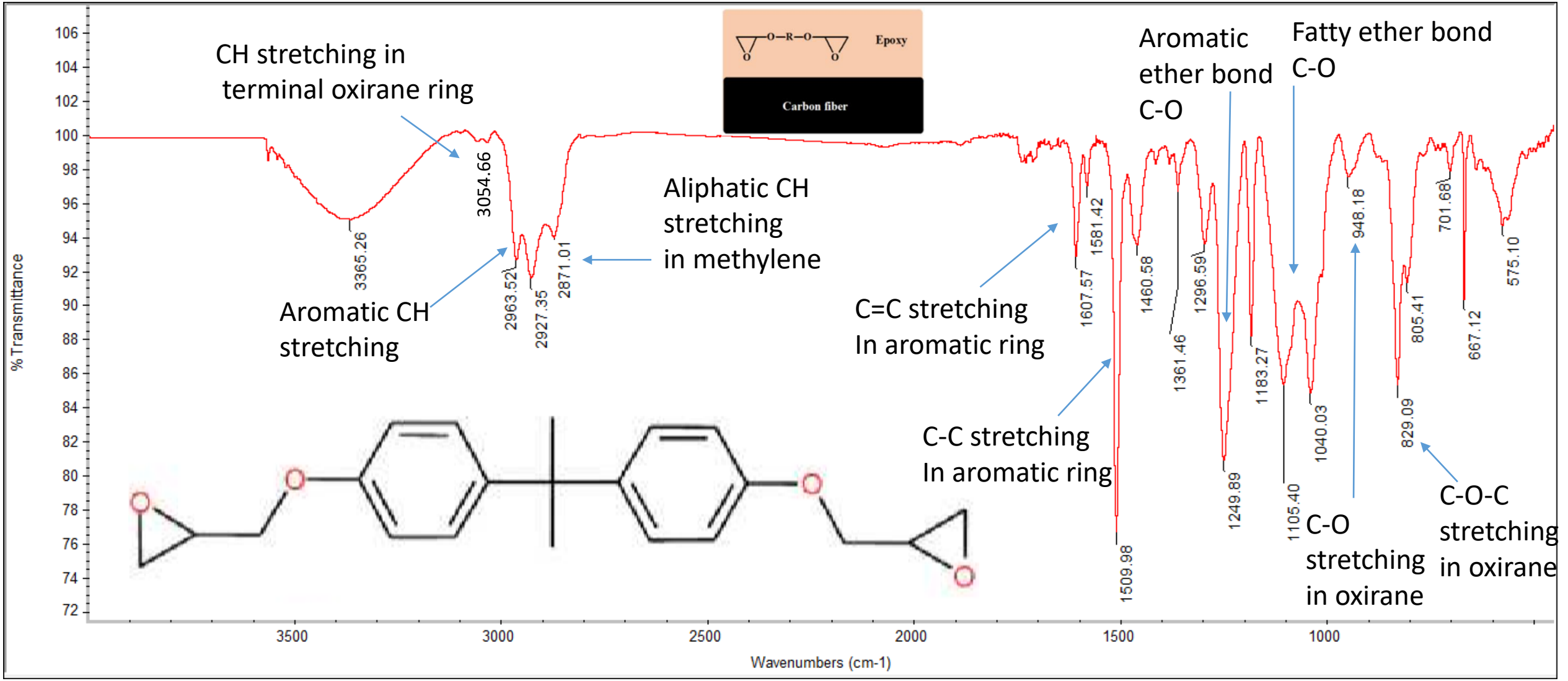

- Diglycedylether of bisphenol A is the sizing agent used for the surface modificaion of NX-100

FT-IR spectrum of DGEBA and its hydrogenated derivative

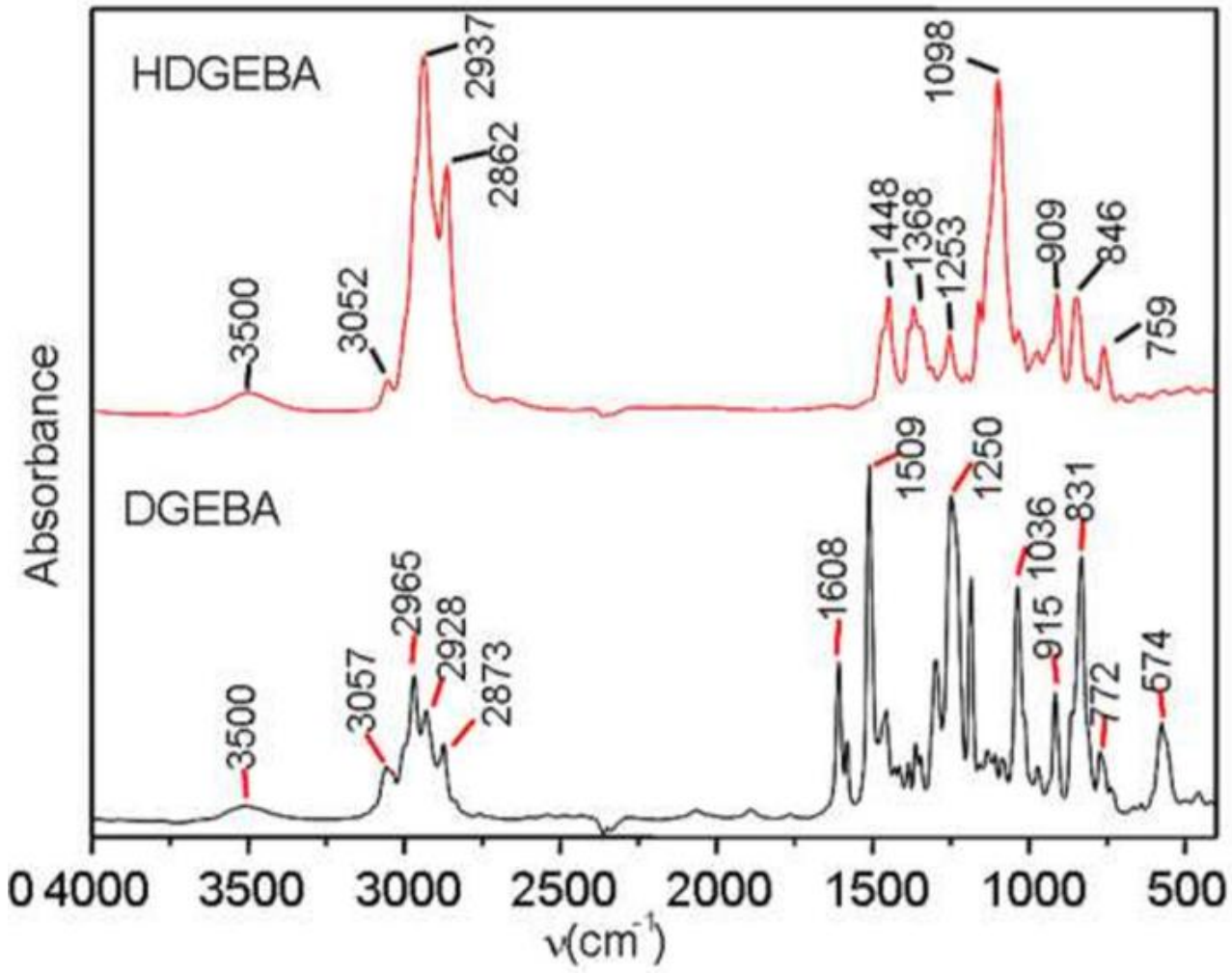

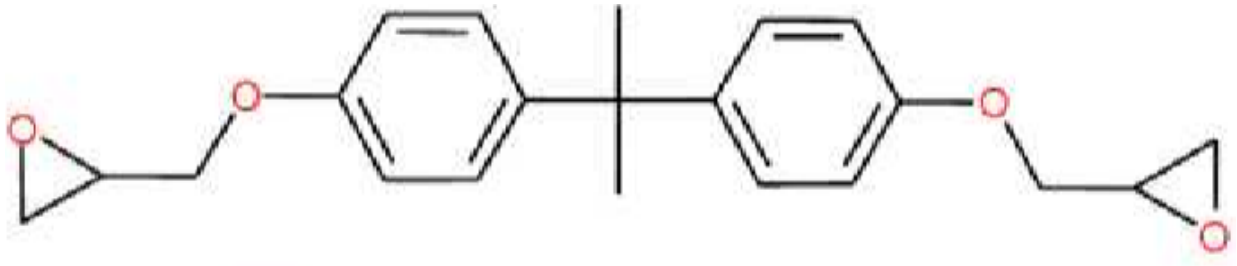

Diglycedylether of bisphenol A

Resin	Band (cm^{-1})	Assignment
DGEBA	≈ 3500	O-H stretching
	3057	Stretching of C-H of the oxirane ring
	2965- 2873	StretchingC-H of CH_2 and CH aromatic and aliphatic
	1608	Stretching C=C of aromatic rings
	1509	Stretching C-C of aromatic
	1036	Stretching C-O-C of ethers
	915	Stretching C-O of oxirane group
	831	Stretching C-O-C of oxirane group
	772	Rocking CH_2

María González González, Juan Carlos Cabanelas and Juan Baselga (2012). Applications of FTIR on Epoxy Resins - Identification, Monitoring the Curing Process, Phase Separation and Water Uptake, Infrared Spectroscopy - Materials Science, Engineering and Technology, Prof. Theophanides Theophile (Ed.),

Sizing agent in carbon fiber B from PAN

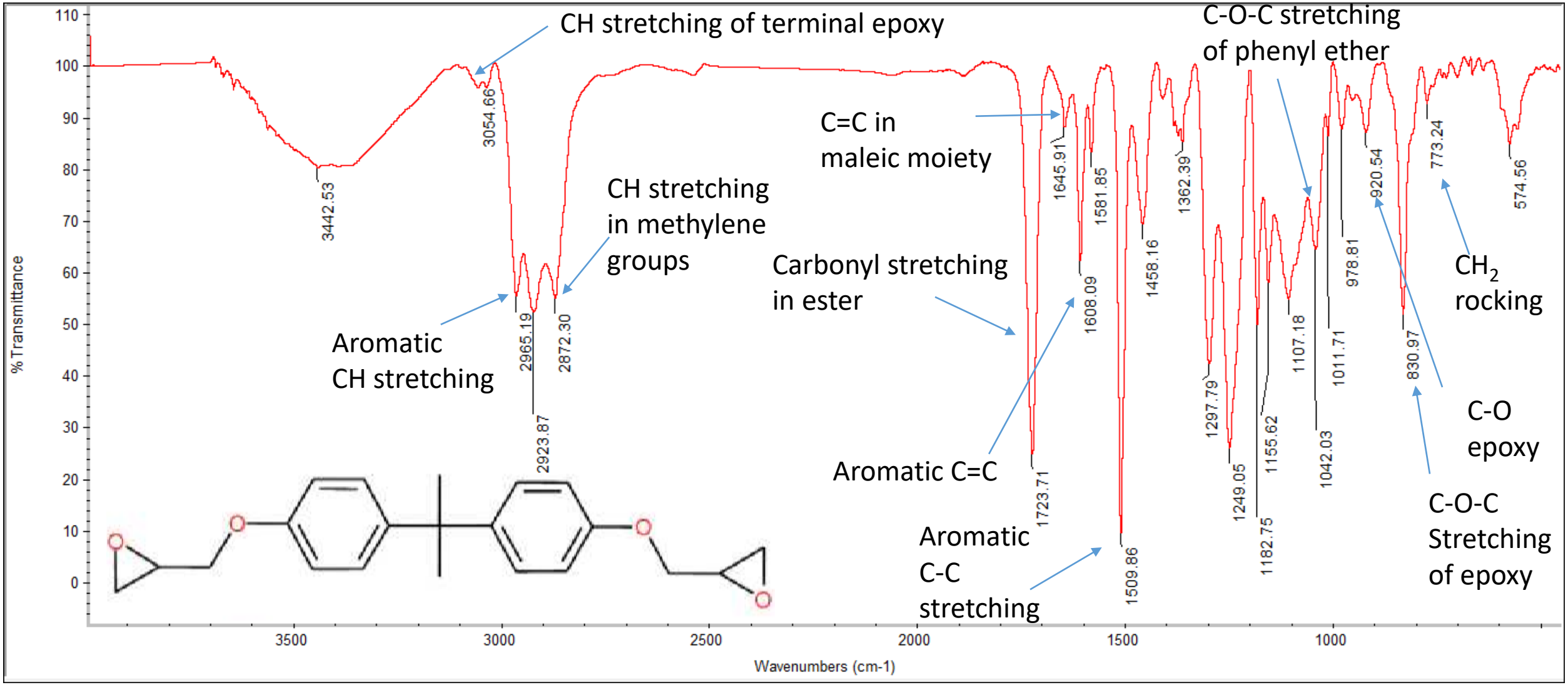

- **Epoxy resin, DGEBA with diluent such as maleate**
- **Brittleness of epoxy resin like DGEBA is reduced and made flexible by plasticizers and diluents like castor oil maleate**

Sizing agent in carbon fiber C from pitch

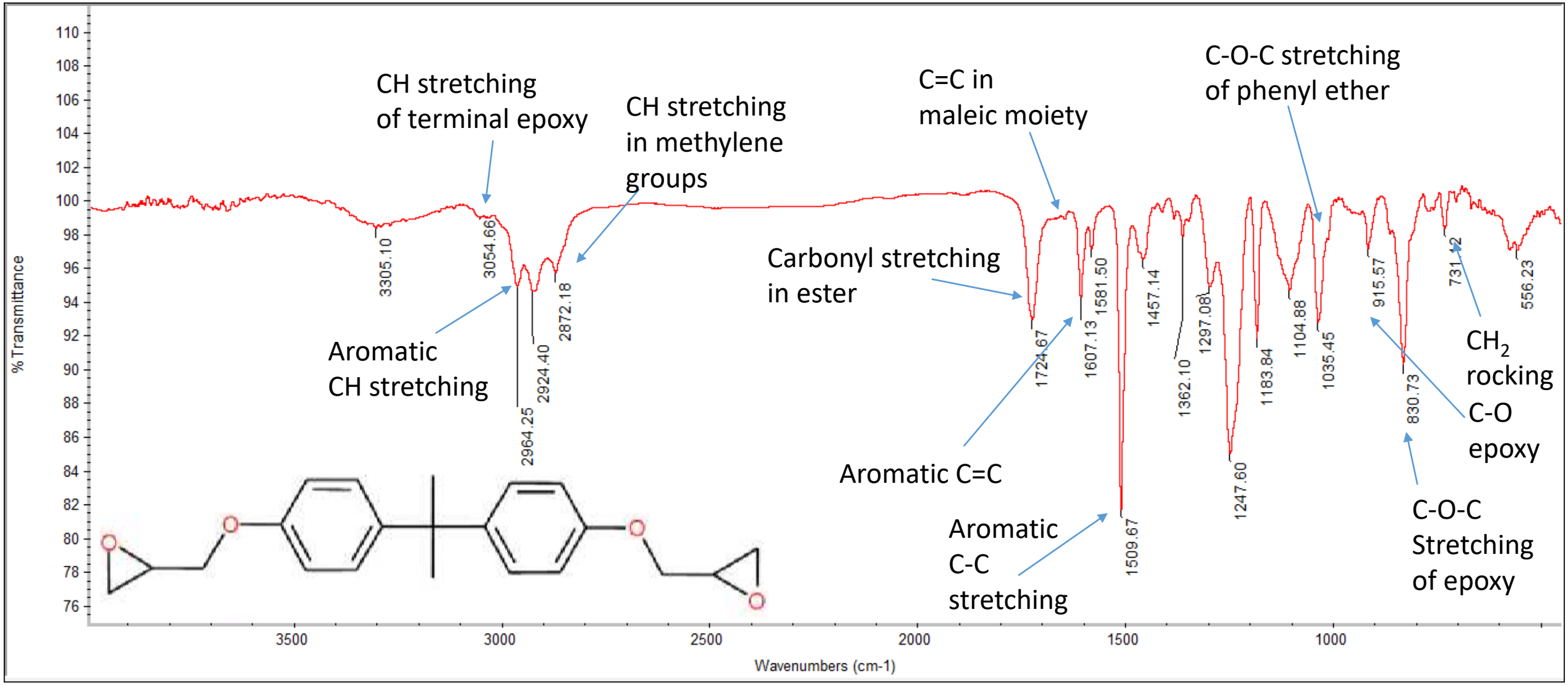

- **Epoxy resin, DGEBA with diluent such as maleate**
- **Brittleness of epoxy resin like DGEBA is reduced and made flexible by plasticizers and diluents like castor oil maleate**

Sizing agent in carbon fibers D from PAN

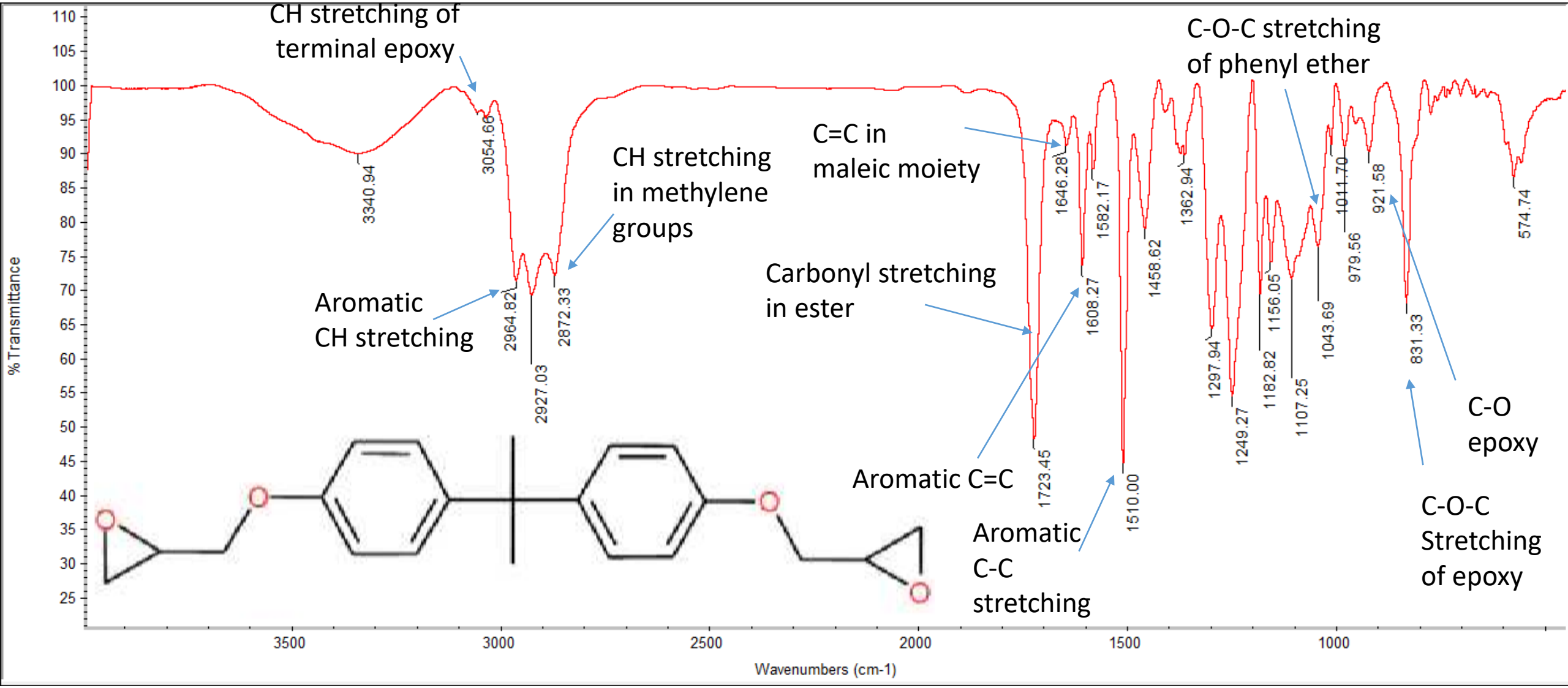

- **Epoxy resin, DGEBA with diluent such as maleate**
- **Brittleness of epoxy resin like DGEBA is reduced and made flexible by plasticizers and diluents like castor oil maleate**

FT-IR spectrum of sizing compound from CF E

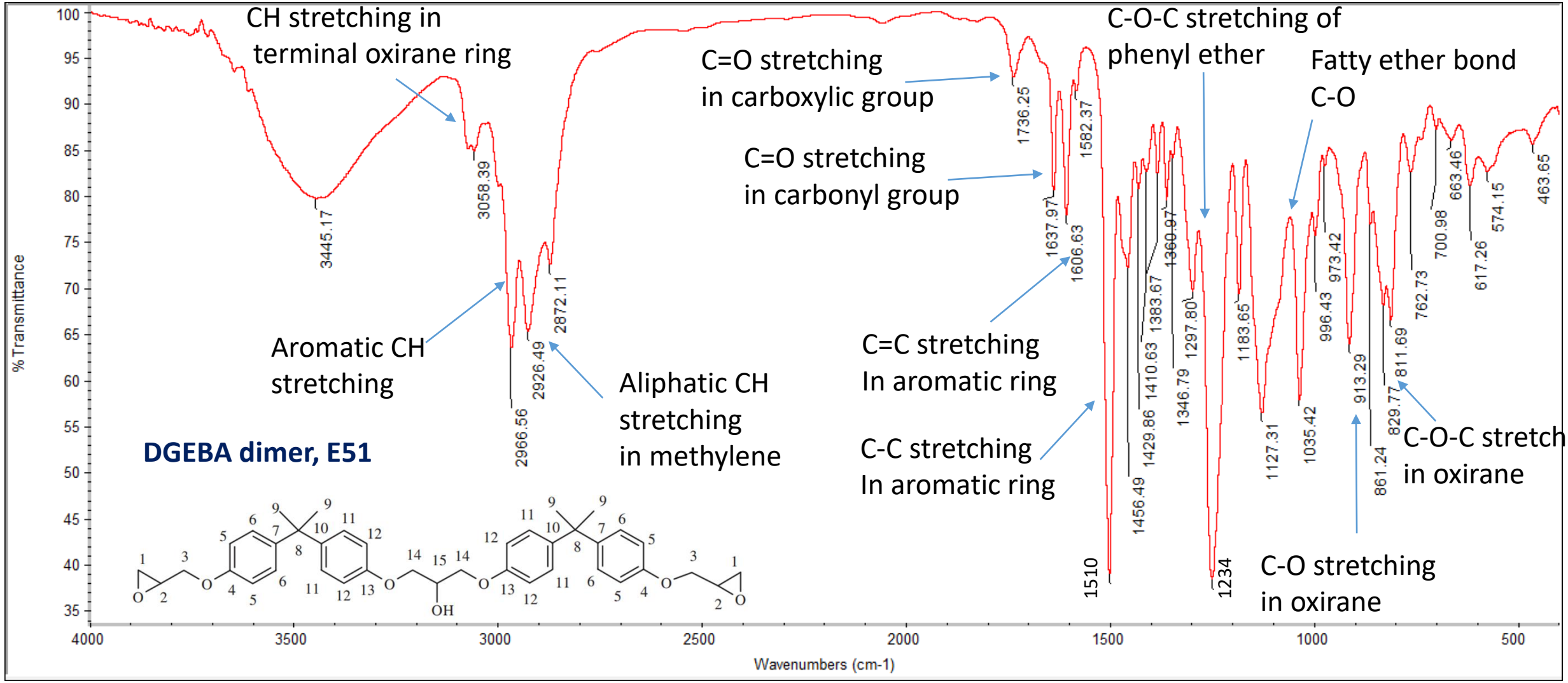

Sizing compound: DGEBA dimer E51, coated on oxidized CF (carboxylic and carbonyl C=O functionalized)

FT-IR spectrum of sizing compound from CF F

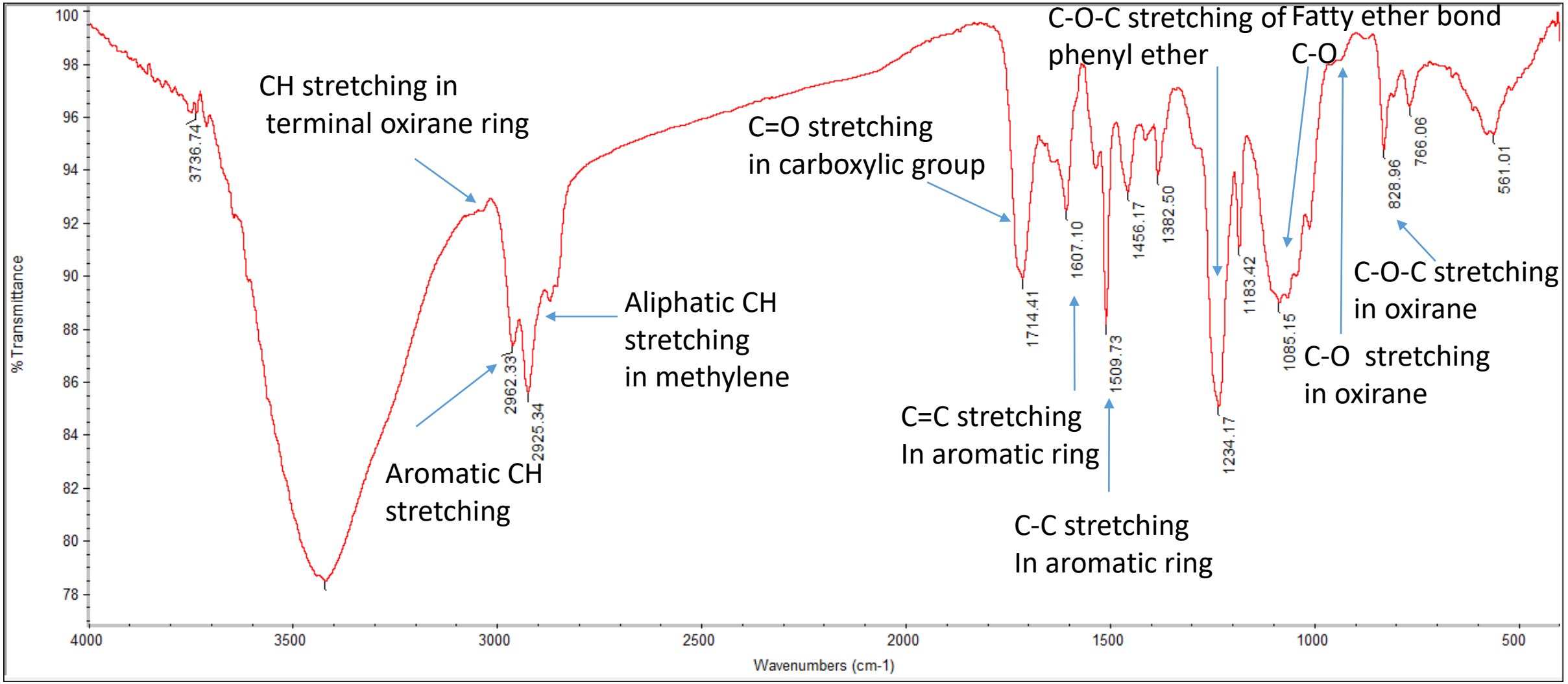

DGEBA dimer, E51

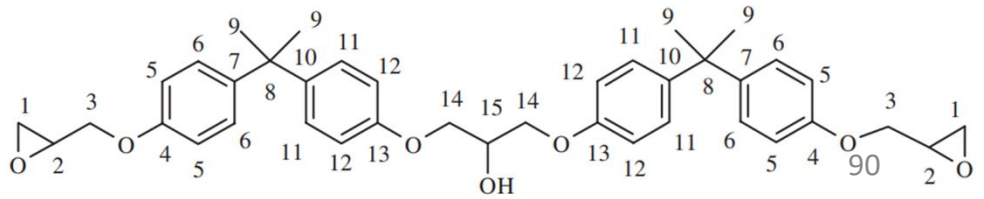

Sizing compound: DGEBA dimer E51, coated on oxidized CF (carboxylic and carbonyl C=O functionalized)

^{1}H NMR spectrum of DGEBA

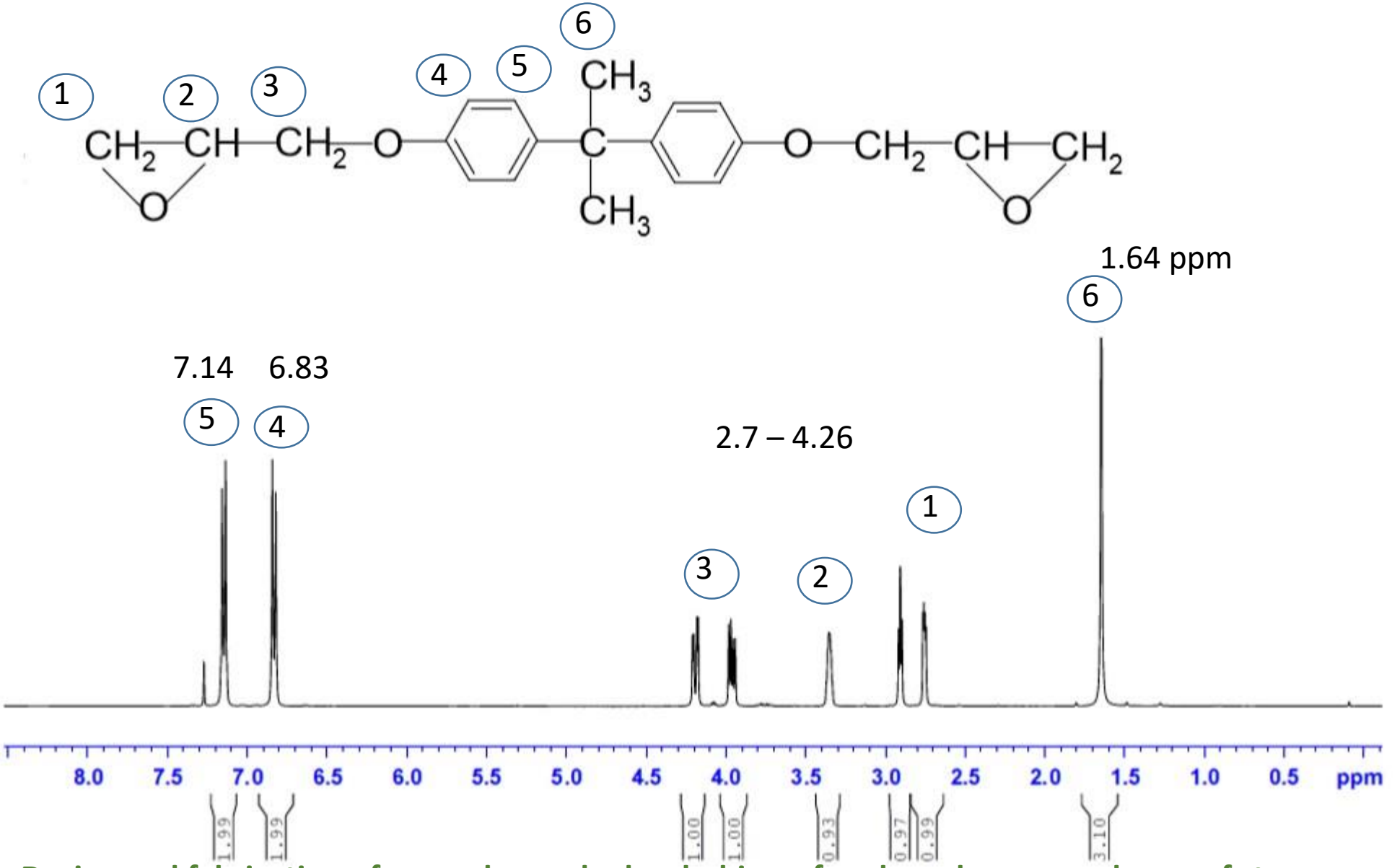

Liu et al., Design and fabrication of a novel superhydrophobic surface based on a copolymer of styrene and Bisphenol A diglycidyl ether monoacrylate, RSC Advances, 4, 2014, 18025-18032

Structure of sizing compound isolated from carbon fibers A

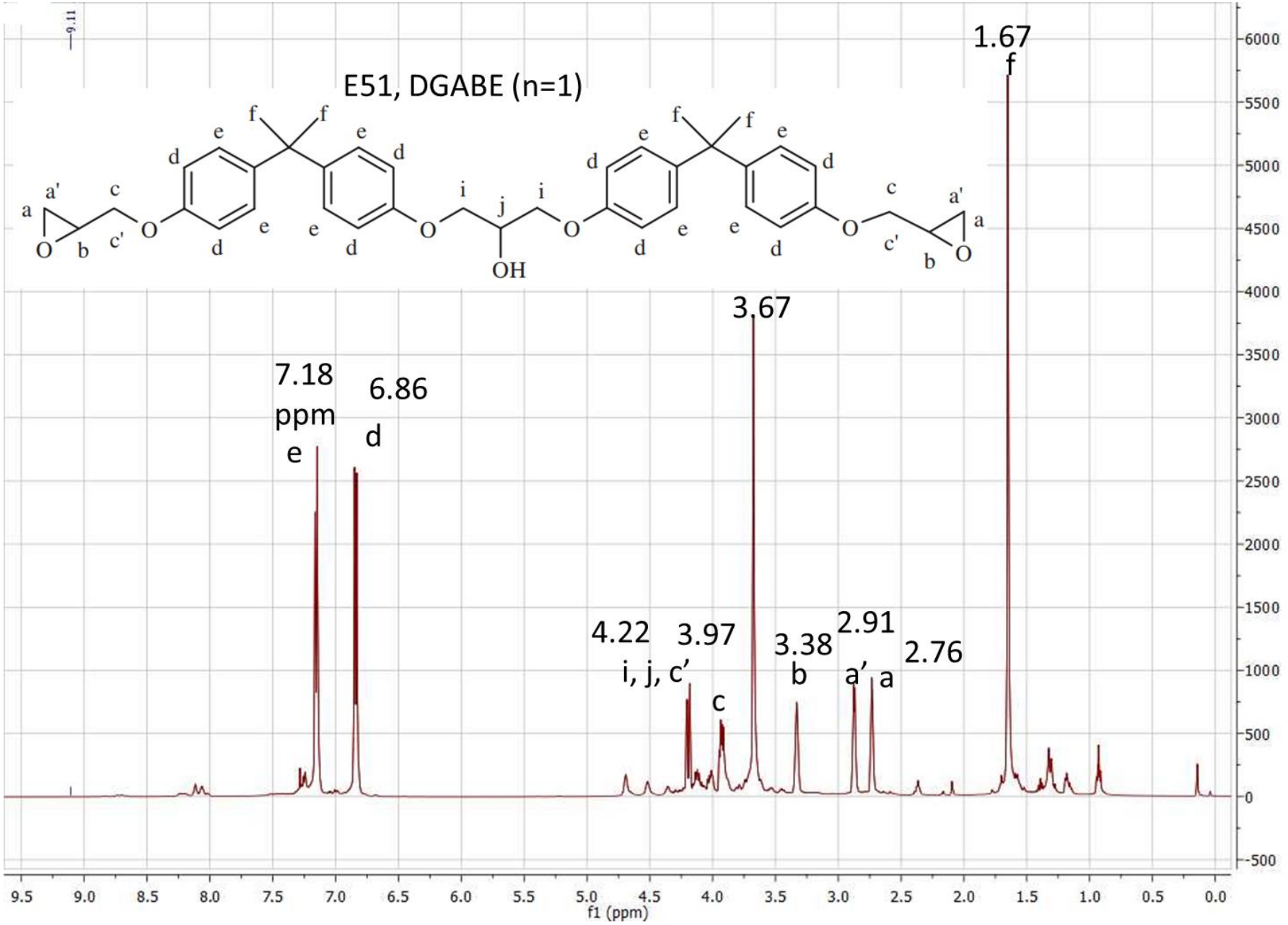

Structure of sizing compound isolated from carbon fibers A

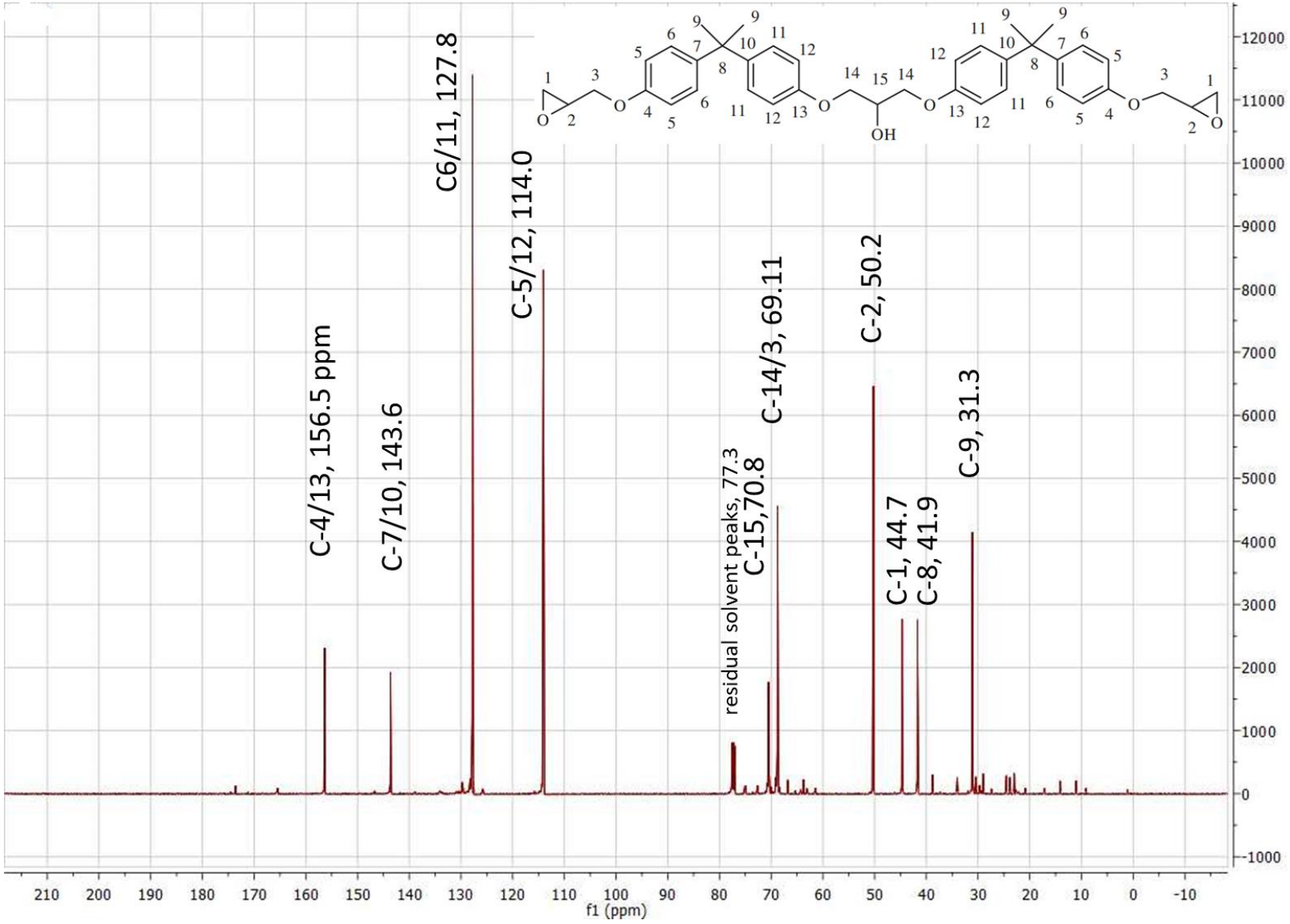

^{1}H NMR spectrum of commercial E51 resin

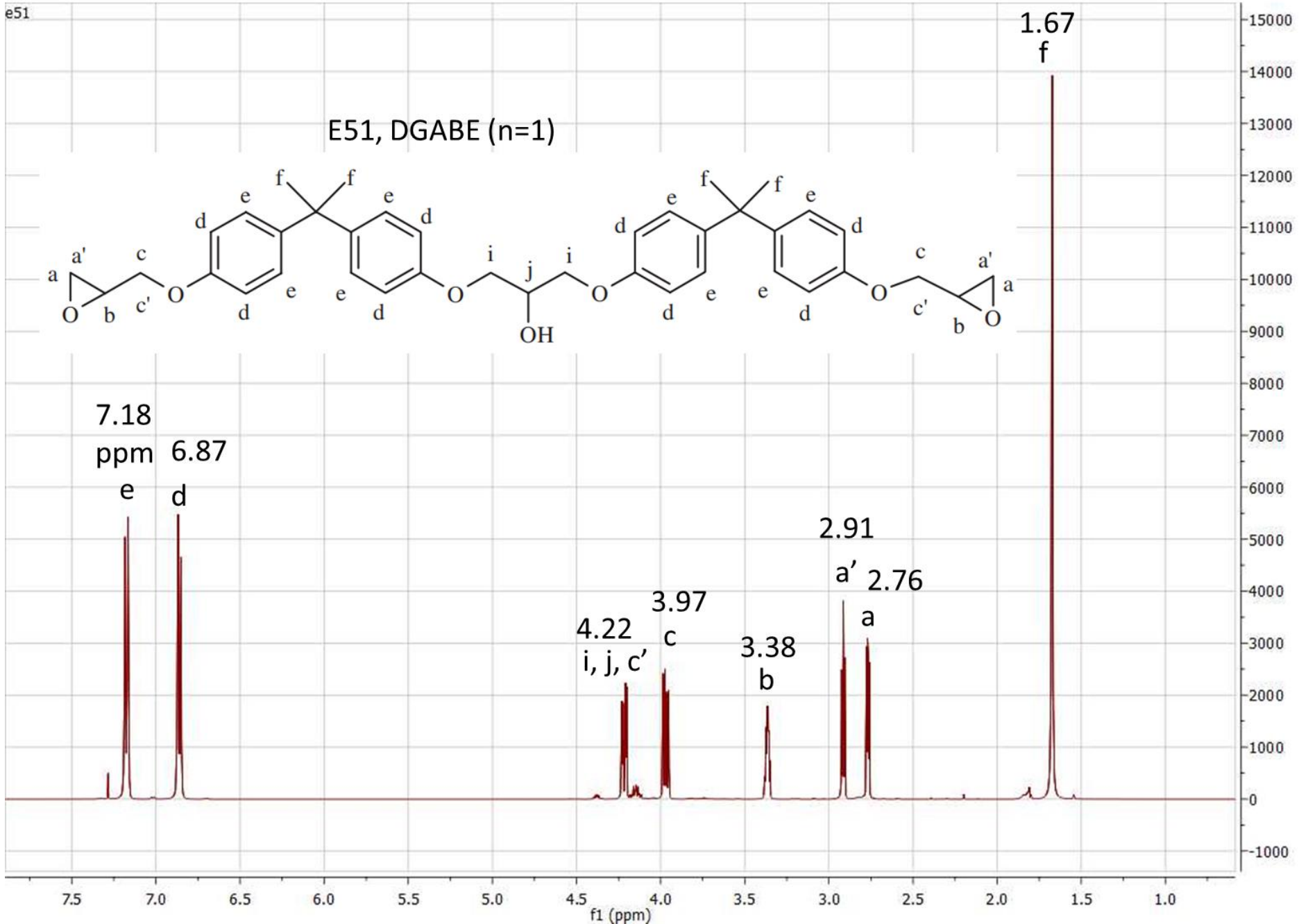

^{13}C NMR spectrum of commercial E51 resin

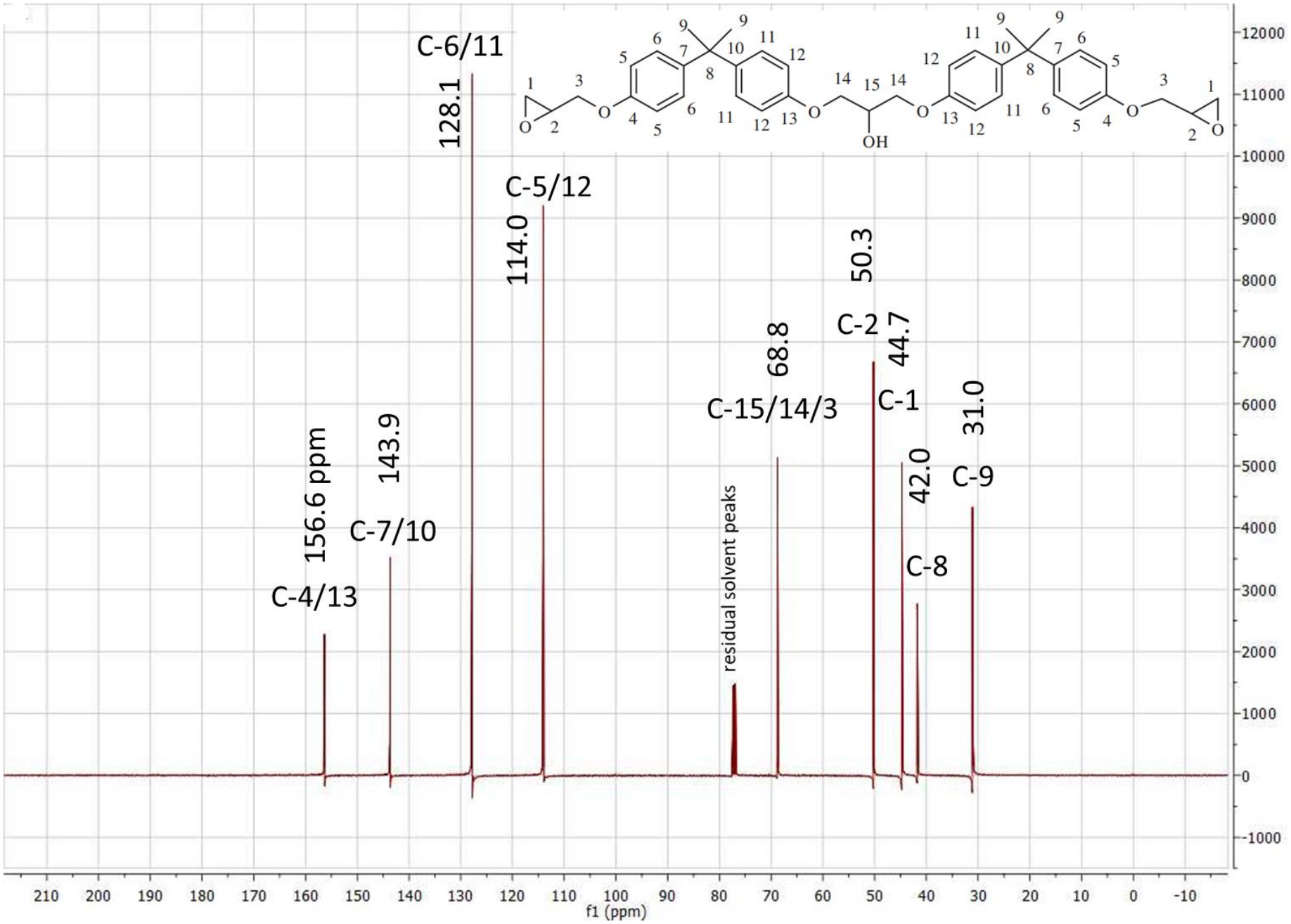

^{1}H NMR spectrum of sizing compound from CF E

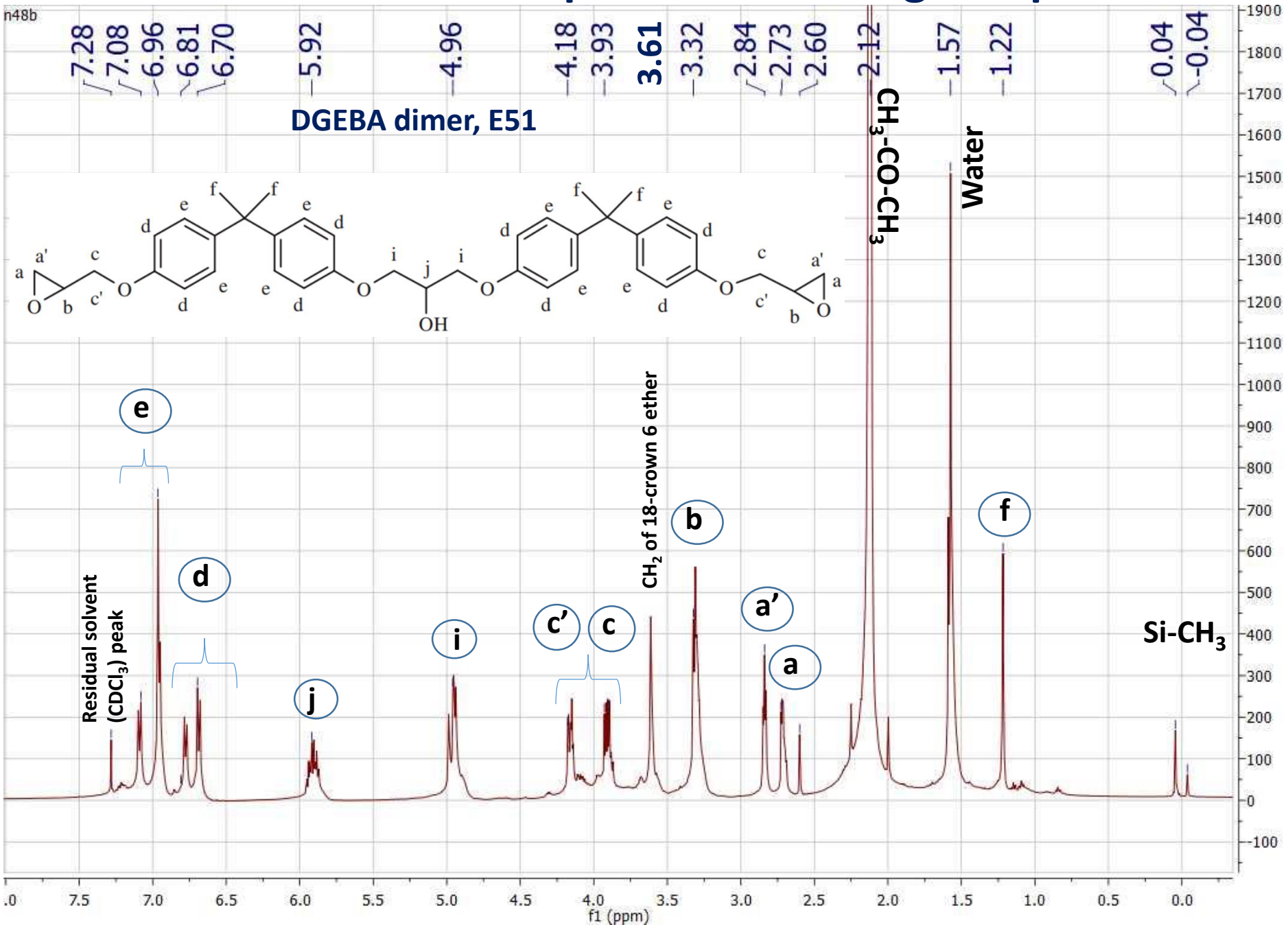

DGEBA dimer E51 is used as sizing agent for the surface modification of CF E

Coupling interaction between protons of CH_2 (i) and OH in $CDCl_3$ may result in the up field shift of resonance of CH_2 protons (i) and cause the signal to appear at 4.96 ppm

Protons of CH in propylene type species appear at 5.83 ppm in $CDCl_3$ solvent (Reference: ^{1}H NMR data)

Usually protons i, j and c' are supposed to resonate together at 4.22 ppm in the sizing (dimer of DGEBA, E51 compound) (^{1}H NMR of E51 epoxy resin)

Residual solvent peak of $CDCl_3$ is supposed to resonate at 7.23 ppm

CH_2 of 18 crown 6 ether resonates at 3.67 ppm

18 crown 6 improves fiber dispersion

Jiang et al.,

Chem Commun 53, 2017, 1498-1501

^{29}Si NMR spectrum of sizing compound from CF E

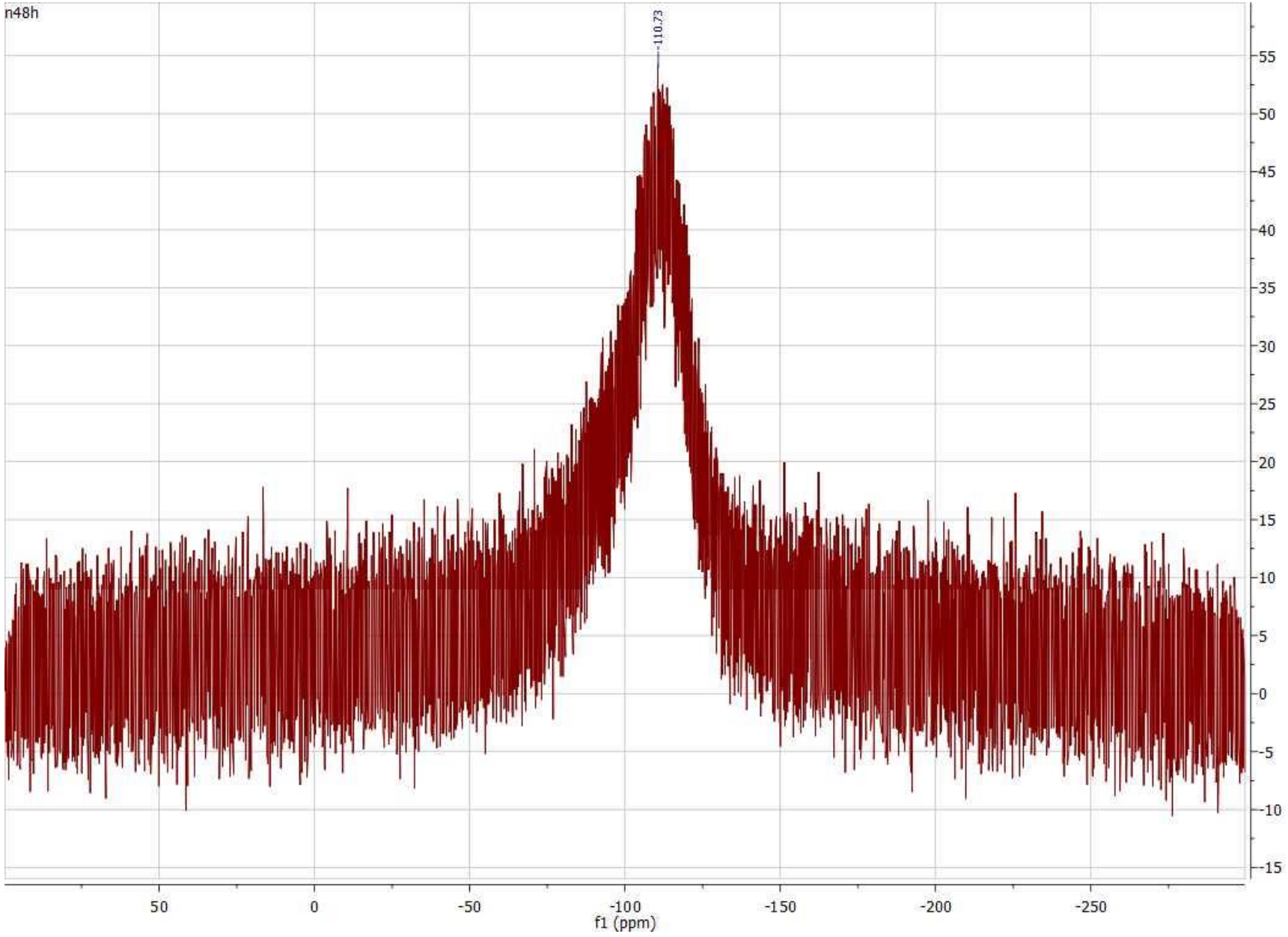

Presence of **Si** in the sizing composition of CF E
could be due to the use of **oil agent** in the production process of carbon fibers

^{13}C NMR spectrum of sizing compound from CF E

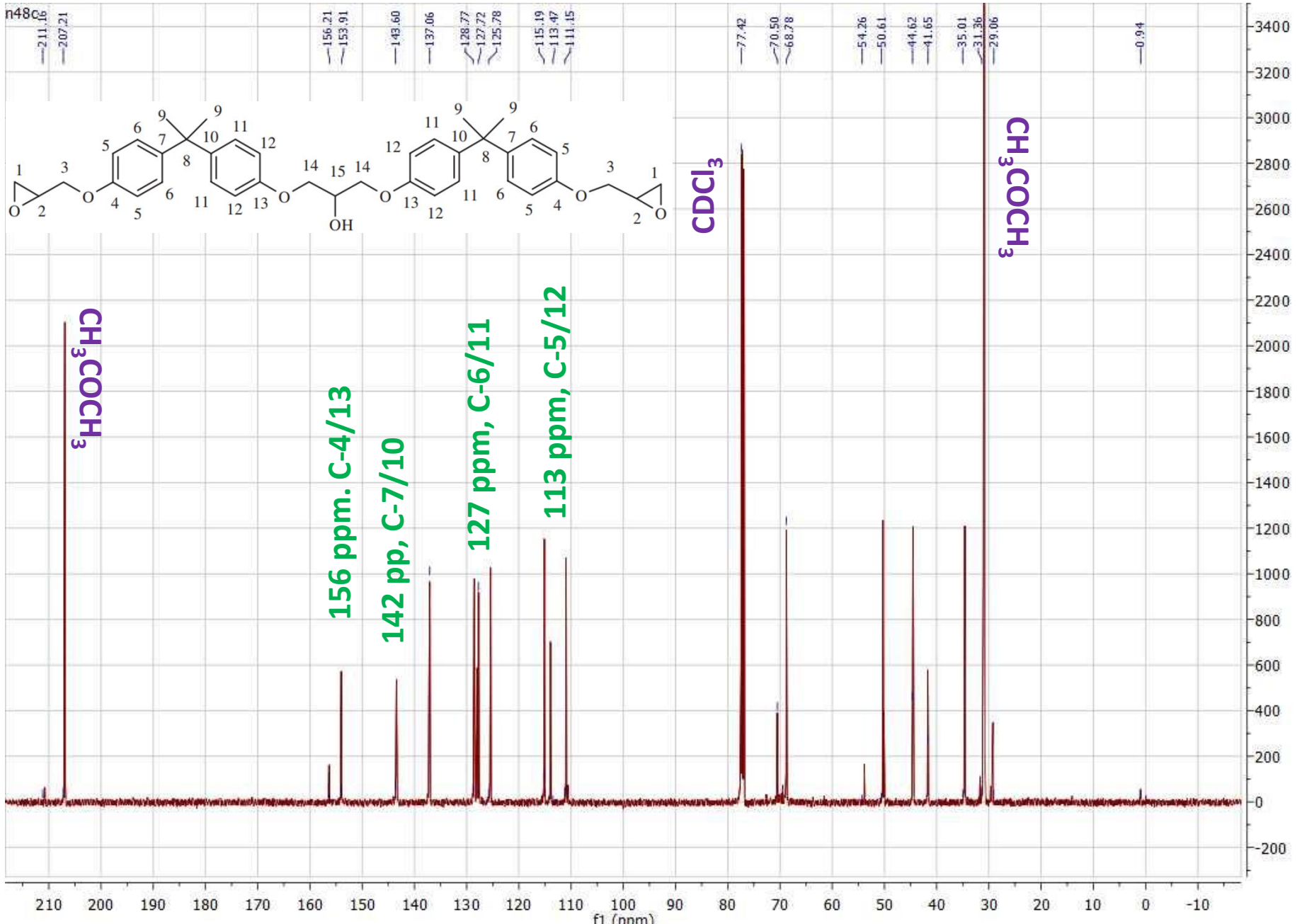

DGEBA dimer E51 is used as sizing agent for the surface modification of CF E

^{1}H NMR spectrum of sizing compound from Carbon fiber F

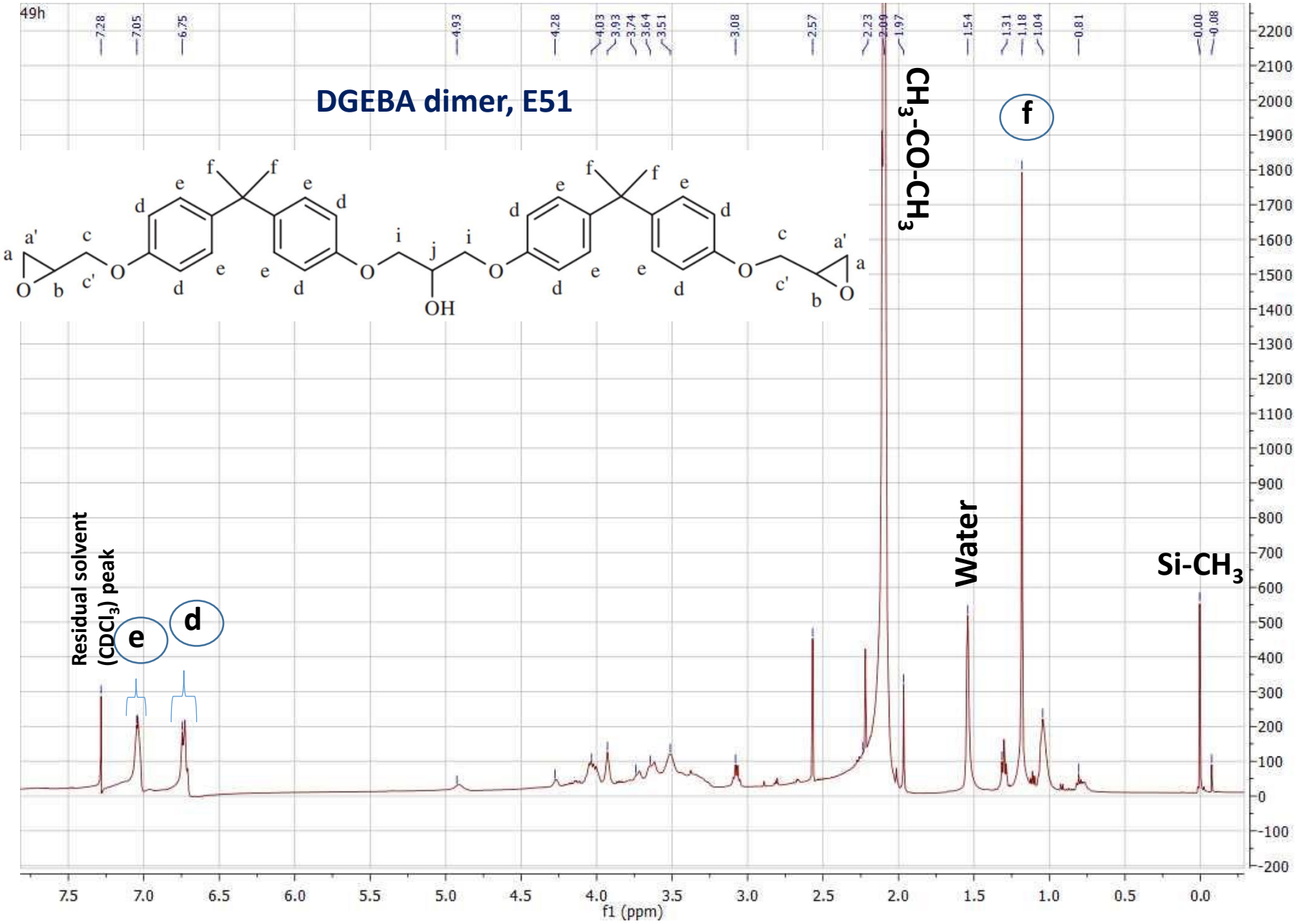

DGEBA dimer, E51 is used as sizing agent for the surface modification of T800 HB

^{29}Si NMR spectrum of sizing compound from CF F

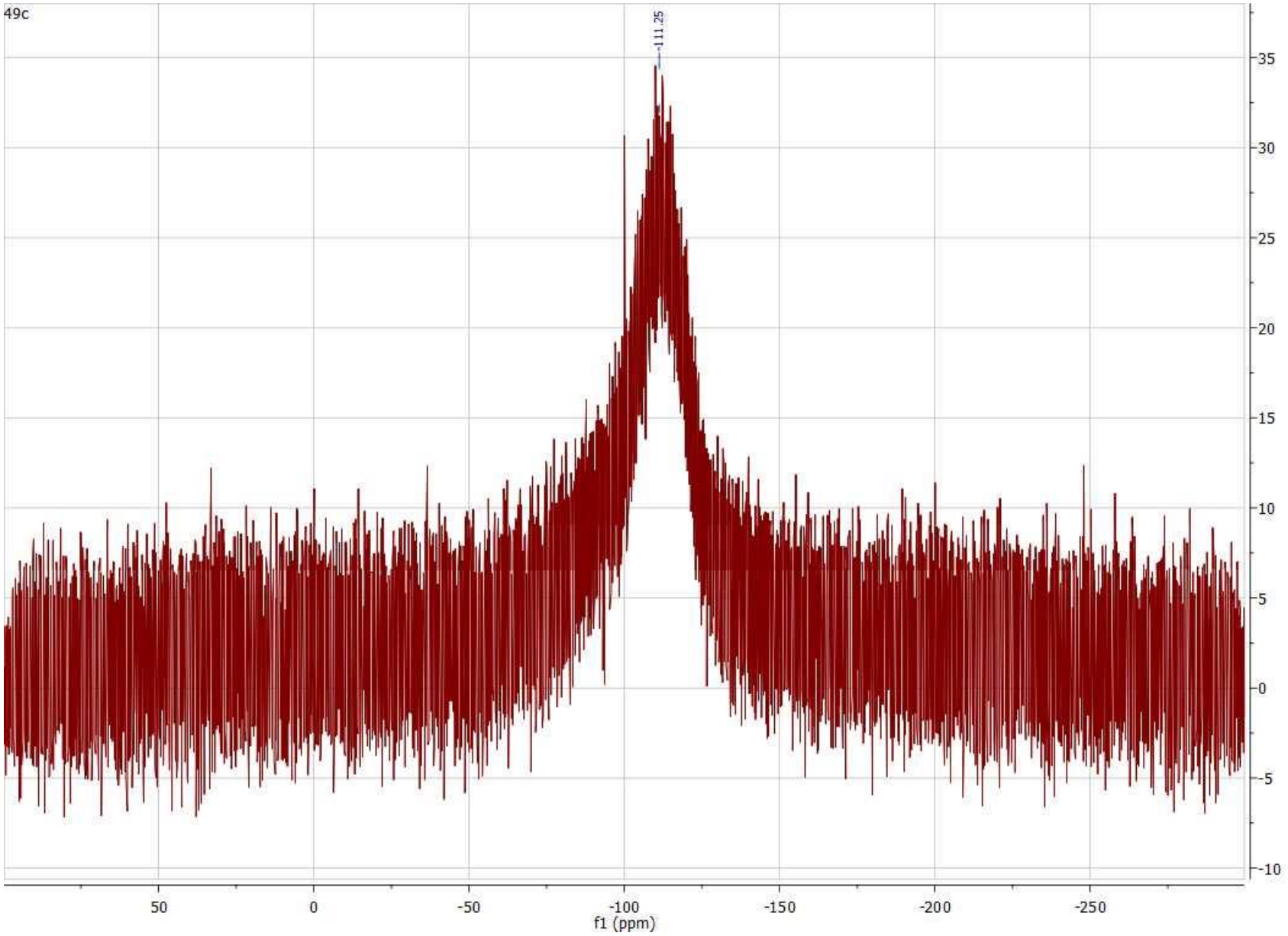

Presence of **Si** in the sizing composition of CF F
could be due to the use of **oil agent** in the production process of carbon fibers

^{13}C NMR spectrum of sizing compound from CF F

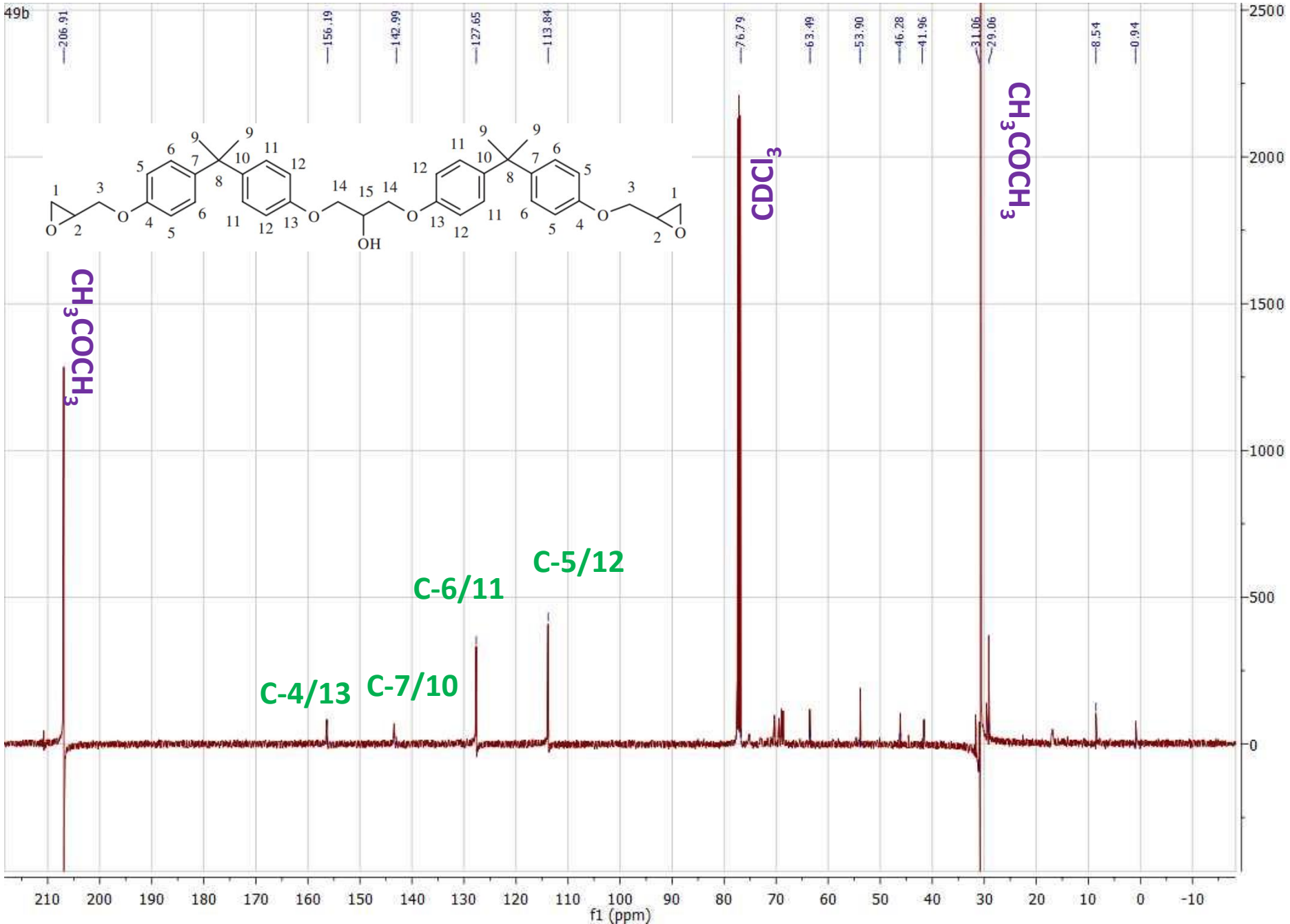

DGEBA dimer, E51 is used as sizing agent for the surface modification of T800 HB

LCMS spectra of the sizing compound from CF F

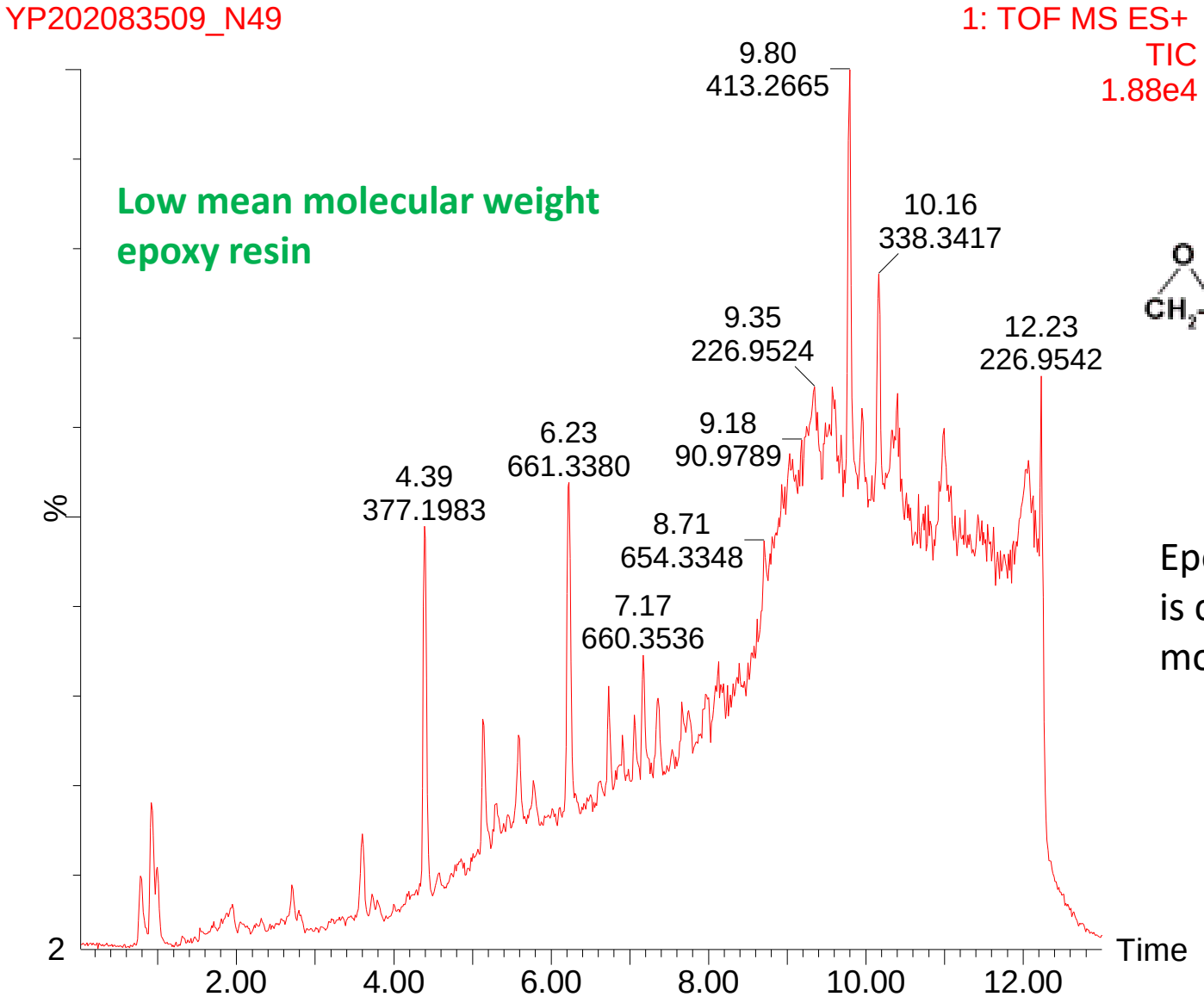

Low mean molecular weight epoxy resin

lowest molecular weight an epoxy resin of the DGEBA type can have is 340

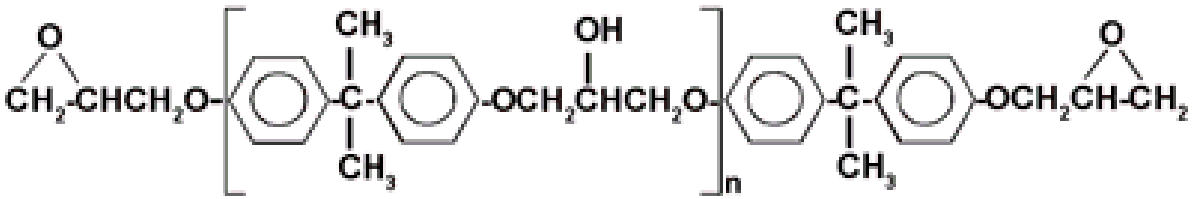

DGEBA epoxy resin

Epoxy resin with a mean molecular weight of over 700 is called high molecular, and epoxy resin with a mean molecular weight of under 700 low molecular.

http://www.nilsmalmgren.com/epoxy-chemistry/epoxy-plastics-general-chemical-and-physical-properties/

LCMS spectra of the sizing compound from CF F

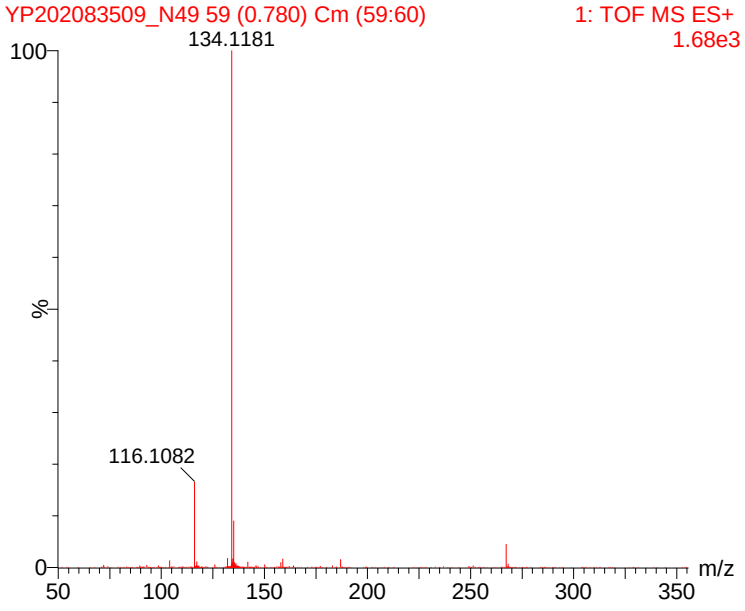

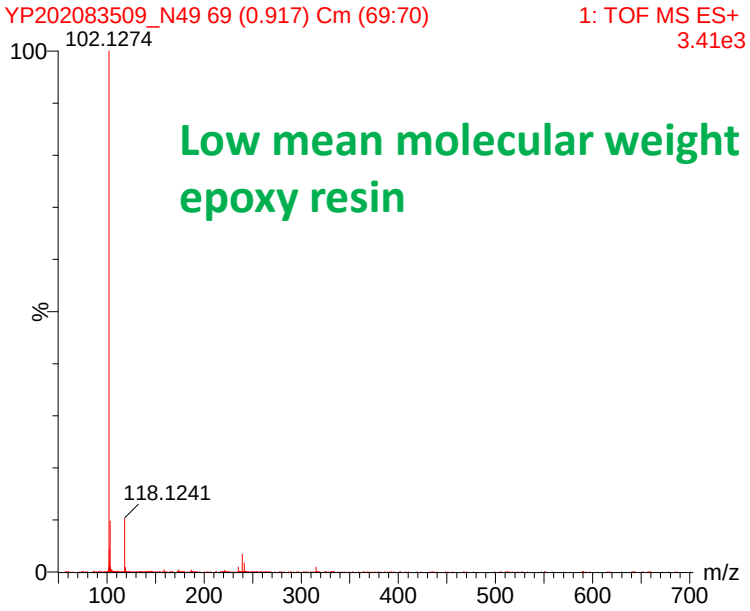

Low mean molecular weight epoxy resin

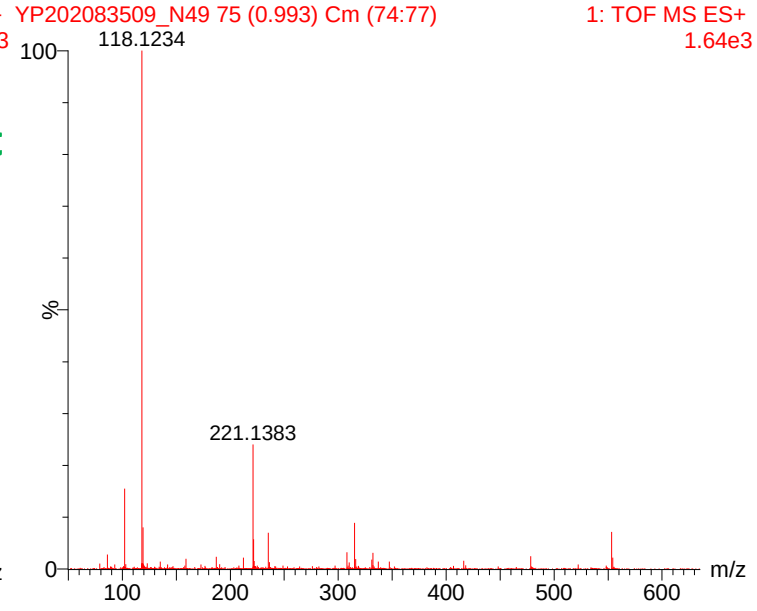

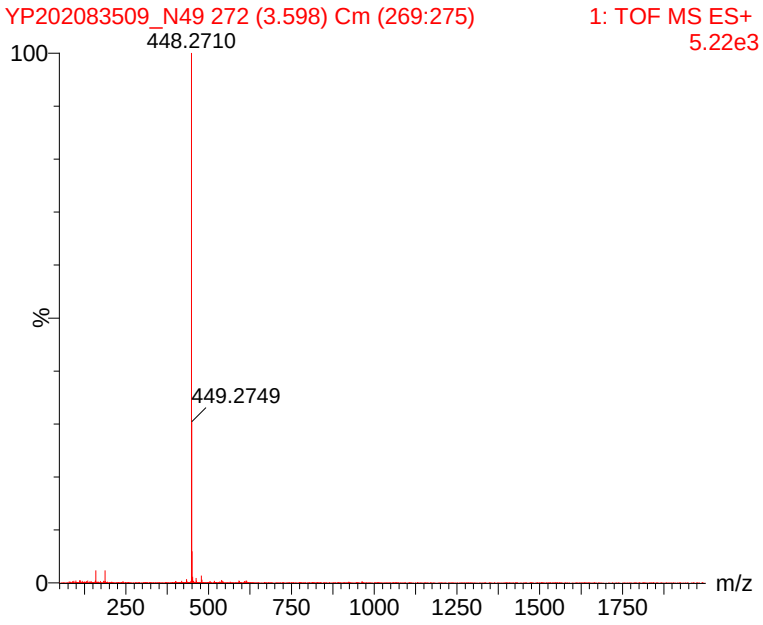

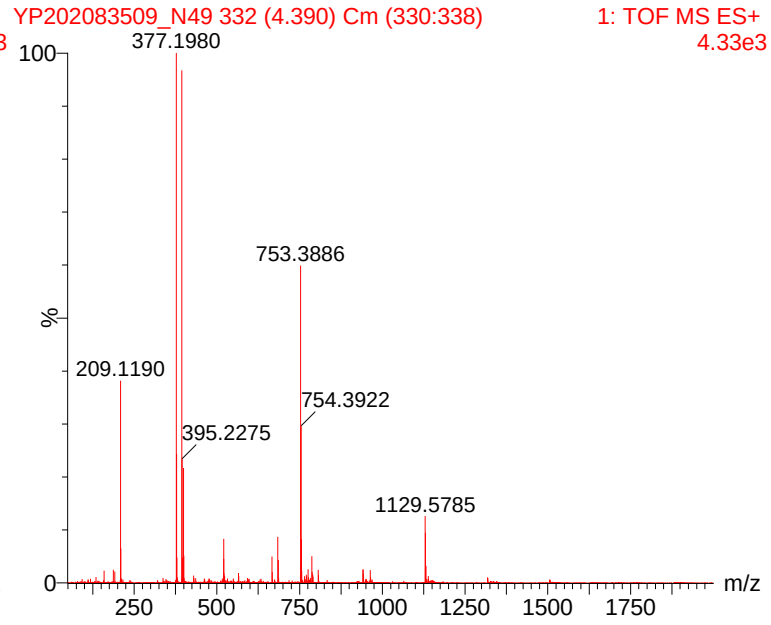

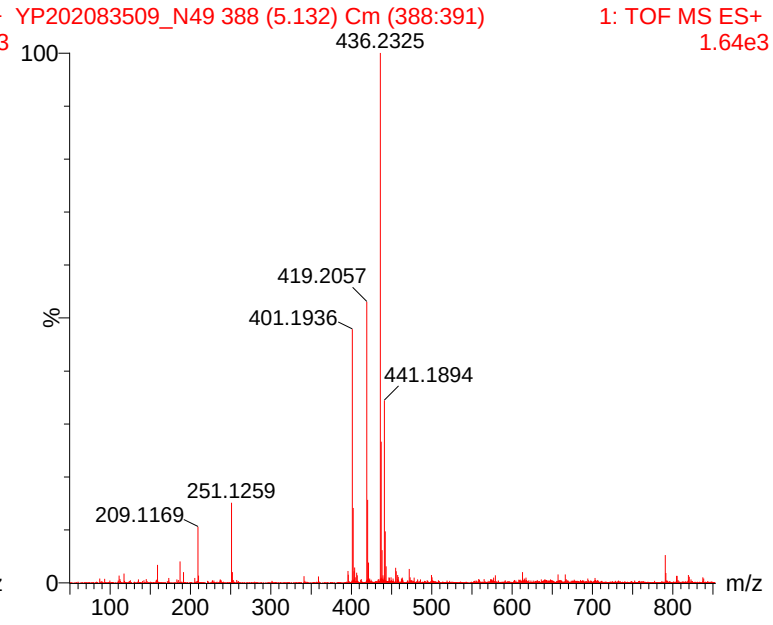

LCMS spectra of the sizing compound from CF F

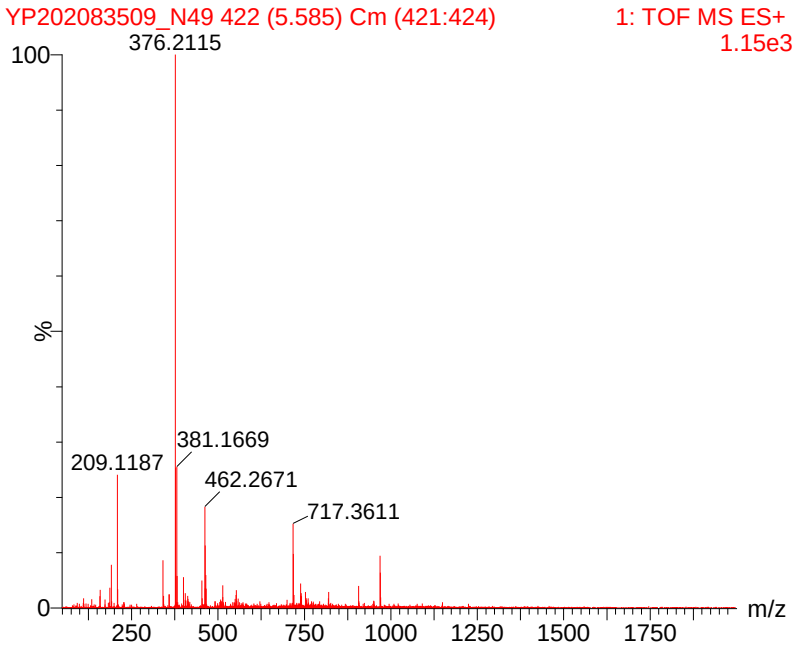

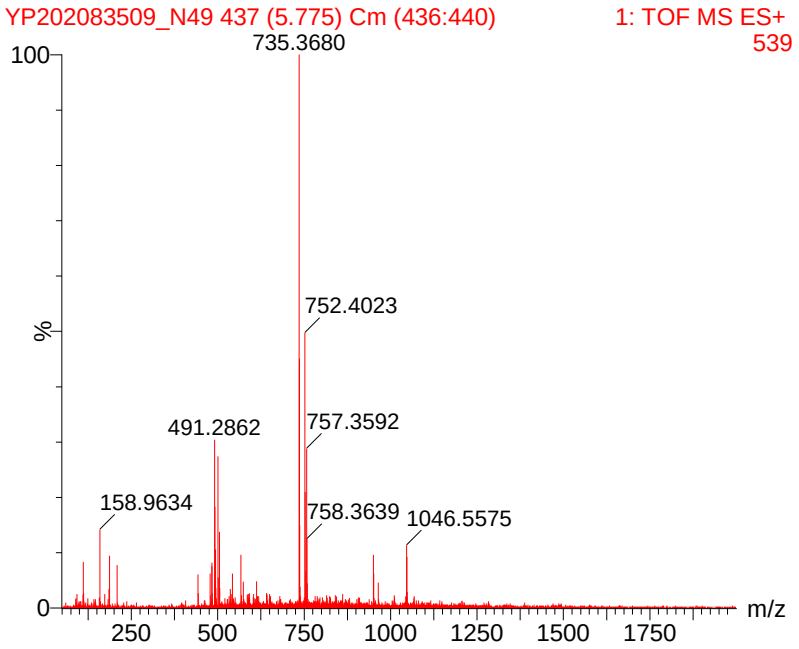

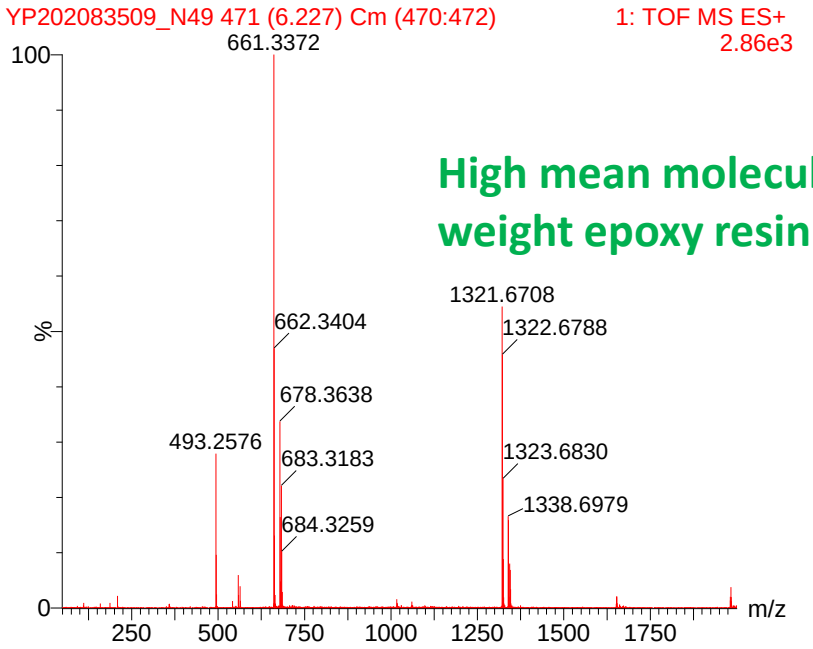

High mean molecular weight epoxy resin

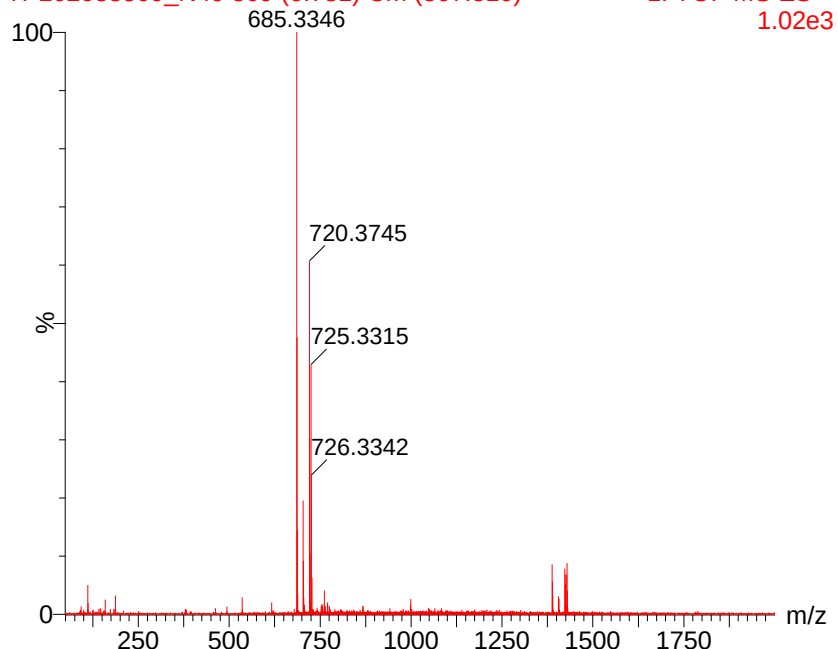

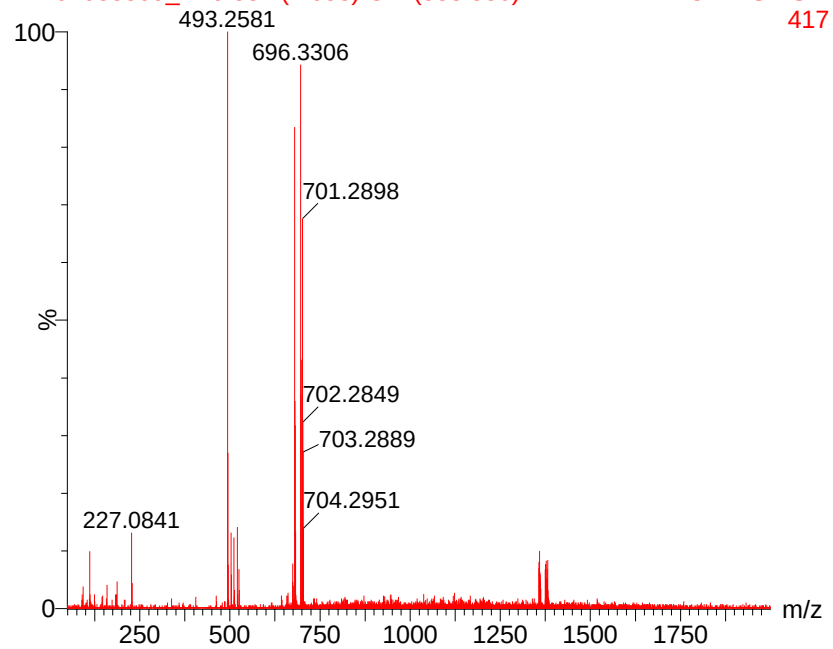

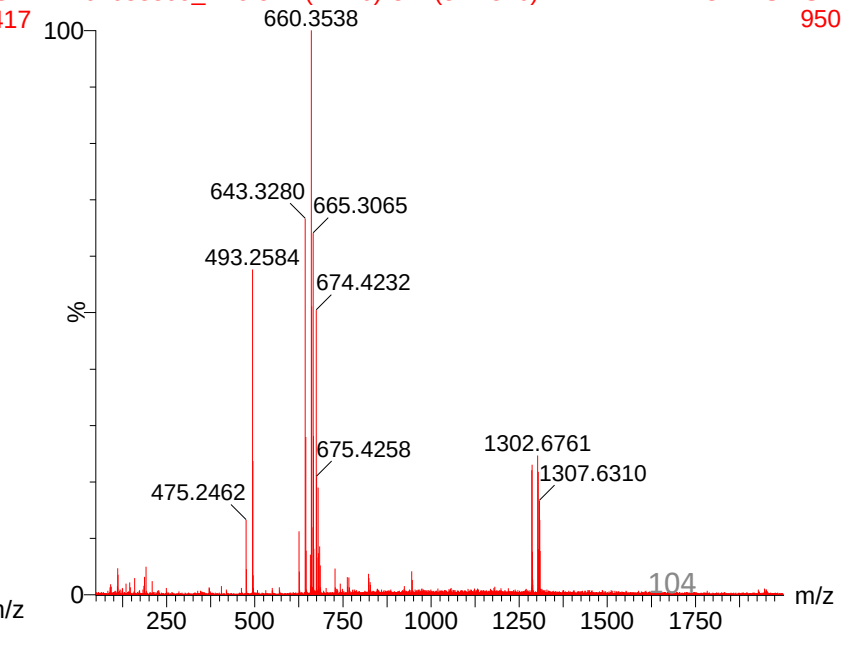

LCMS spectra of the sizing compound from CF F

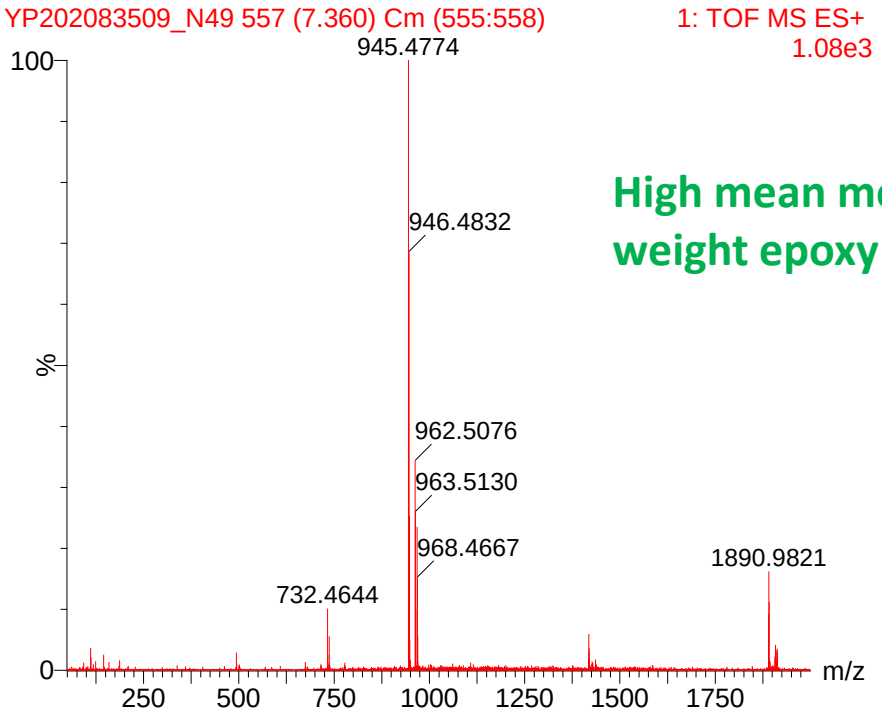

High mean molecular weight epoxy resin

Quantification of sizing compound in carbon fibers (E and F)

Carbon Fibers	Amount of sizing agent (Wt.%)		
	Gravimetry	Thermogravimetry	^{1}H NMR
CF E	1.64		
CF F	1.6		
CF A	2.26	0.96	1.35
CF B	1.21	-	0.635
CF C	0.27	1.24	0.47
CF D	3.84	2.32	1.92

There is plenty of room at the upcoming bio refinery and biochemical industries!

Carbon fiber based composites opened a new avenue in Materials Science!

The opportunities include CO_2 utilization for fuels and chemicals production and development of biomass based H_2 production.

Benefits include, as great as, nobel prize winning inventions like NH_3 synthesis process and elucidation of reaction mechanism for the formation of NH_3 in the hydrogenation of nitrogen.

The reliance on fossil energy for biorefinery operation, including heat and power requirements, should be completely avoided systematically.

This would make the bio refineries self-reliant, sustainable, competitive and environmentally friendly.

To achieve such a goal, innovation in nanoscience, especially, catalysis, is awaited for coupling the processing of unconventional feedstock (marine and fresh water algae, animal remains like glycogen and atmospheric CO_2) at the bio refinery facility with novel energy sources like solar energy.

Such a path ahead would lead to energy security and clean environment overcoming the problem of climate change.

Carbon fiber based composite materials revolutionize almost every sphere of human activity with amazing applications

Acknowledgement

Grateful thanks are due to Professor Aharon Gedanken, Israel for introducing the field of Biofuels and biochemicals

Grateful thanks are due to Professor Tae Hyun Kim, Republic of Korea, for introducing systematic methods of biomass characterization and conversion

Grateful thanks are due to Professor Xinling Wang, China for introducing the field of carbon fiber reinforced composites

Grateful thanks are due to Mr Yang Chongchong, Ph D scholar of Professor Wang's group for the motivation and guidance

Thanks are due to Dr Justin Masih, India, for the invitation to present the lecture in the Webiner

Thank You!